NAVAL POSTGRADUATE SCHOOL

MONTEREY, CALIFORNIA

THESIS

ENHANCEMENT OF THE DAYTIME GOES-BASED AIRCRAFT ICING POTENTIAL ALGORITHM USING MODIS

by

Jeremy B. Alexander

March 2005

Thesis Advisor: Philip Durkee

Approved for public release; distribution is unlimited.

THIS PAGE INTENTIONALLY LEFT BLANK

REPORT DOCUMENTATION PAGE			Form Approved OMB No. 0704-0188

1. AGENCY USE ONLY *(Leave blank)*	2. REPORT DATE March 2005	3. REPORT TYPE AND DATES COVERED Master's Thesis

4. TITLE AND SUBTITLE: Enhancement Of the Daytime GOES-Based Aircraft Icing Potential Algorithm Using MODIS	5. FUNDING NUMBERS
6. AUTHOR(S) Jeremy B. Alexander	
7. PERFORMING ORGANIZATION NAME(S) AND ADDRESS(ES) Naval Postgraduate School Monterey, CA 93943-5000	8. PERFORMING ORGANIZATION REPORT NUMBER
9. SPONSORING /MONITORING AGENCY NAME(S) AND ADDRESS(ES) N/A	10. SPONSORING/MONITORING AGENCY REPORT NUMBER

11. SUPPLEMENTARY NOTES The views expressed in this thesis are those of the author and do not reflect the official policy or position of the Department of Defense or the U.S. Government.

12a. DISTRIBUTION / AVAILABILITY STATEMENT Approved for public release; distribution is unlimited.	12b. DISTRIBUTION CODE A

13. ABSTRACT (maximum 200 words)

In this thesis, a fuzzy logic algorithm is developed for the detection of potential aircraft icing conditions using the Moderate-Resolution Imaging Spectroradiometer (MODIS). The fuzzy MODIS algorithm is developed in a manner similar to the cloud mask currently used to process MODIS imagery. The MODIS icing potential detection algorithm uses thresholds for 8 channels in a series of 12 tests to determine the probability of icing conditions being present within a cloud. The MODIS algorithm results were compared to results of the GOES icing potential detection algorithm run on MODIS imagery for 4 cases. When compared to positive and icing pilot reports for the cases, the MODIS algorithm identified regions where icing was encountered more effectively than the GOES algorithm. Furthermore, the use of fuzzy thresholds on MODIS rather than the hard thresholds of the GOES algorithm allowed for less restrictive coverage of potential icing conditions, making the MODIS algorithm more reasonable in assessing all cloud regions for icing potential. The results found here are preliminary, as further statistical analysis with a larger validation dataset would be more effective. Algorithm details are provided in the appendix for reference.

14. SUBJECT TERMS MODIS, aircraft icing, multispectral satellite analysis, cloud thermodynamic phase	15. NUMBER OF PAGES 106
	16. PRICE CODE

17. SECURITY CLASSIFICATION OF REPORT	18. SECURITY CLASSIFICATION OF THIS PAGE	19. SECURITY CLASSIFICATION OF ABSTRACT	20. LIMITATION OF ABSTRACT
Unclassified	Unclassified	Unclassified	UL

NSN 7540-01-280-5500 Standard Form 298 (Rev. 2-89)
Prescribed by ANSI Std. 239-18

THIS PAGE INTENTIONALLY LEFT BLANK

Approved for public release; distribution is unlimited.

ENHANCEMENT OF THE DAYTIME GOES-BASED AIRCRAFT ICING POTENTIAL ALGORITHM USING MODIS

Jeremy B. Alexander
Captain, United States Air Force
B.S., United States Air Force Academy, 1999

Submitted in partial fulfillment of the
requirements for the degree of

MASTER OF SCIENCE IN METEOROLOGY

from the

NAVAL POSTGRADUATE SCHOOL
MARCH 2005

Author: Jeremy Brandon Alexander

Approved by: Philip A. Durkee
Thesis Advisor

Mr. Thomas Lee
Second Reader, Naval Research Laboratory

Philip A. Durkee
Chairman, Department of Meteorology

THIS PAGE INTENTIONALLY LEFT BLANK

ABSTRACT

In this thesis, a fuzzy logic algorithm is developed for the detection of potential aircraft icing conditions using the Moderate-Resolution Imaging Spectroradiometer (MODIS). The fuzzy MODIS algorithm is developed in a manner similar to the cloud mask currently used to process MODIS imagery. The MODIS icing potential detection algorithm uses thresholds for 8 channels in a series of 12 tests to determine the probability of icing conditions being present within a cloud. The MODIS algorithm results were compared to results of the GOES icing potential detection algorithm run on MODIS imagery for 4 cases. When compared to positive and icing pilot reports for the cases, the MODIS algorithm identified regions where icing was encountered more effectively than the GOES algorithm. Furthermore, the use of fuzzy thresholds on MODIS rather than the hard thresholds of the GOES algorithm allowed for less restrictive coverage of potential icing conditions, making the MODIS algorithm more reasonable in assessing all cloud regions for icing potential. The results here are preliminary, as further statistical analysis with a larger validation dataset would be more effective. Algorithm details are provided in the appendix for reference.

THIS PAGE INTENTIONALLY LEFT BLANK

TABLE OF CONTENTS

THIS PAGE INTENTIONALLY LEFT BLANK

LIST OF FIGURES

THIS PAGE INTENTIONALLY LEFT BLANK

LIST OF TABLES

THIS PAGE INTENTIONALLY LEFT BLANK

LIST OF SYMBOLS, ACRONYMS AND ABBREVIATIONS

AFCCC	AF Combat Climatology Center
AFSC	Air Force Safety Center
AIRS-II	Alliance Icing Research Study - II
ASF	Air Safety Foundation
ATReC	Atlantic THORpex Regional Campaign
AWS	Air Weather Service
CIRA	Cooperative Institute for Research in the Atmosphere
CSU	Colorado State University
ECLIPS	Experimental Cloud Lidar Pilot Study
FAA	Federal Aviation Administration
GOES	Geostationary Earth Observing Satellite
IDEA	Interactive Digital Environmental Laboratory
IIDA	Integrated Icing Diagnostic Algorithm
MODIS	Moderate Resolution Imaging Spectroradiometer
NASA	National Aeronautical and Space Administration
NCAR	National Center for Atmospheric Research
NOGAPS	Navy Operational Global Atmospheric Prediction System
NPS	Naval Postgraduate School
RAL	Research Applications Laboratory
USAF	United States Air Force
BTD	Brightness Temperature Difference
EM	Electromagnetic
ICN	Ice Crystal Nuclei
IR	Infrared
IWC	Ice Water Content
NIR	Near-Infrared
SLD	Super-cooled Liquid Drops
SNR	Signal-to-Noise Ratio
km	Kilometers
mb	Millibars
μm	Micrometers or Microns

THIS PAGE INTENTIONALLY LEFT BLANK

ACKNOWLEDGMENTS

The author would like to thank Professor Phil Durkee for his thorough guidance and patience through the research process. Tom Lee provided initial brainstorming and background information that helped bring the thesis topic and goal into view. Professor Mary Jordan was instrumental in editing and writing the MATLAB programs to process the algorithm, none of which would have been possible if not for the amazing set of MODIS MATLAB programming that had previously been accomplished by Dr. Shaima Nasiri. Kurt Nielsen provided endless support in the gathering and processing of MODIS and GOES imagery during the preparatory stages of research.

From the National Center for Atmospheric Research, thanks to Greg Thompson for providing the initial GOES algorithm and for suggesting fuzzy set theory as a possible improvement to the algorithm. Julie Haggarty was always quick to provide assistance and guidance as needed throughout the process. Marcia Politovich, Jothiram Vivekanandan, and Merritt Deeter were especially helpful during discussions of the MODIS channel selection process. Their guidance and expertise allowed for greater focus on the proper channels from the beginning of the thesis process.

From the Naval Research Laboratory, thanks to Joe Turk, Steve Miller, and Jeff Hawkins, who provided much needed input into discussion of the channel properties for the GOES and MODIS platforms.

The author extends special thanks to his wonderful bride for her love, patience, encouragement, and understanding throughout the 18-month master's program.

THIS PAGE INTENTIONALLY LEFT BLANK

I. INTRODUCTION

A. BACKGROUND

As aircraft use increases in both civilian and military operations, weather hazards continue to be a critical planning factor. Among the major weather flight hazards, aircraft icing ranks near the top of most lists in terms of costliness, fatalities, and occurrence. As seen in Figure 1, icing accretion increases aircraft drag and weight while decreasing lift and thrust, making the aircraft less able to sustain flight (USAF 1997). As a result, even the most experienced pilots can fall victim to aircraft icing once it is encountered and ice buildup begins. According the Federal Aviation Administration's Air Safety Foundation (ASF), one in eight weather-related aircraft accidents in the 1990's resulted from aircraft icing with 67 percent involving highly-experienced pilots and 27 percent involving fatalities (ASF 2002).

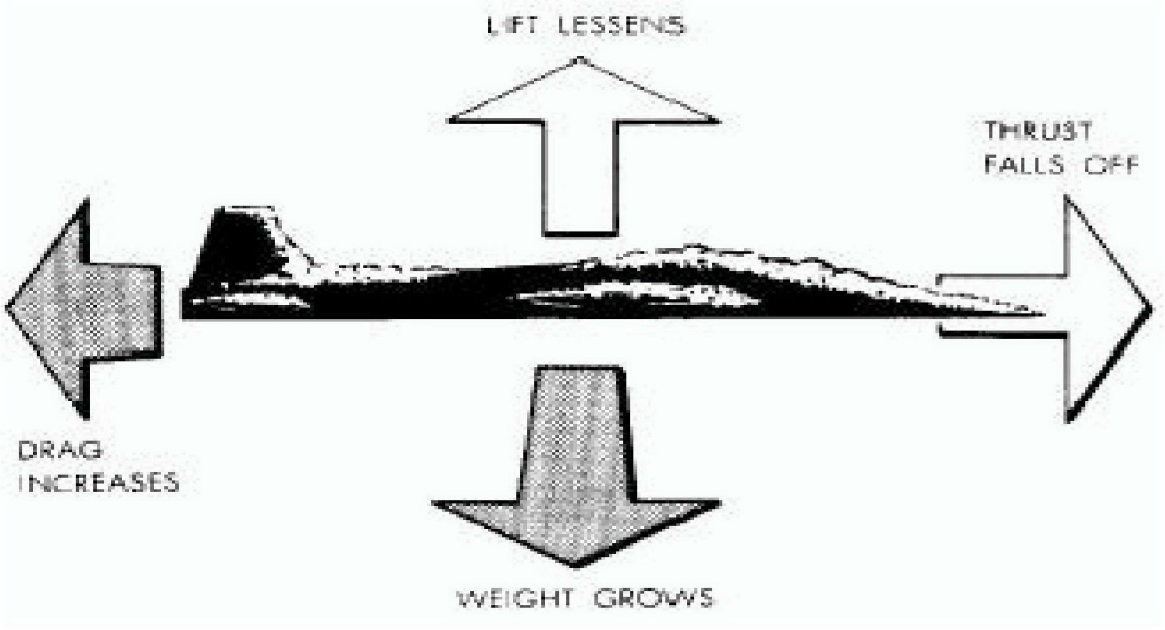

Figure 1. Effects of aircraft icing on flight (from USAF 1997).

B. MOTIVATION

The United States Air Force (USAF) has managed to keep icing-related losses relatively low – only about $400,000 and no fatalities since 2000 according to the Air Force Safety Center (AFSC 2004) – by strictly avoiding any forecasted icing regions (USAF 1997). This policy requires precise knowledge of where to expect icing conditions. However, Air Force meteorologists generally use very spatially broad model output maps of atmospheric moisture and temperatures as the only tools to create icing forecasts. If these products suggest clouds with temperatures within the thresholds set for potential icing, the large majority of forecasters are trained to use them without viewing other data. Thompson et al. (1997) found the areas covered by model-based icing forecasts to be more than twice as large as necessary for an aircraft to avoid icing conditions. The only other information available for icing avoidance are pilot reports, which are ineffective due to lack of coverage, detail, accuracy, and timeliness (Erickson 1997).

Though these conservative criteria lead to the Air Force's very low icing accident rate by creating a large avoidance cushion around actual icing areas, such expansive forecasts undoubtedly result in excessive fuel consumption, protracted flights, and unnecessary wear on aircrafts and aircrews. This method also bases icing detection, solely on model output without adequate confirmation that expected icing conditions actually exist. Thompson et al. (1997) found that the Navy Operational Global Atmospheric Prediction System (NOGAPS) icing forecasts generally

captured only 70 percent of icing encounters by aircraft, leaving a large margin for error.

C. PURPOSE

The goals of any effort to remotely sense in-flight icing conditions are the increased flight safety, military readiness, and aircraft utilization while decreasing flight delays (Ryerson 2000). Thompson et al. (1997) showed that the objective use of satellite data to detect icing conditions can reduce the spatial extent of model-forecasted icing regions by nearly 50 percent with a minimal loss in forecast accuracy of only a few percent. Using the Advanced Very-High Resolution Radiometer, they showed that 3 of the 5 channels on the Geostationary Earth Observing Satellite (GOES) platform can be used to develop a multispectral algorithm to detect potential icing conditions based on temperature thresholds, cloud optical properties, and reflectance and differential emittance properties of water and ice particles in clouds. The resulting product is available operationally online by selecting "Icing Product" and clicking "Contiguous US" at http://www.rap.ucar.edu/weather/satellite/. An example of this product is shown in Figure 2. It is likely that better multispectral products can be developed as stand-alone detection methods.

The GOES algorithm, like other icing detection techniques, has several limitations that are discussed in Section II. In an effort to make up for these limitations, the GOES algorithm is currently used along with model outputs, radar mosaics, and surface observations as part of the NCAR Integrated Icing Diagnostic Algorithm (IIDA) product in the capacity described by Thompson et al (1997)

and Bernstein et al (2000). Improvements made in sensor-based icing potential detection techniques would in turn lead to the enhancement of products such as IIDA.

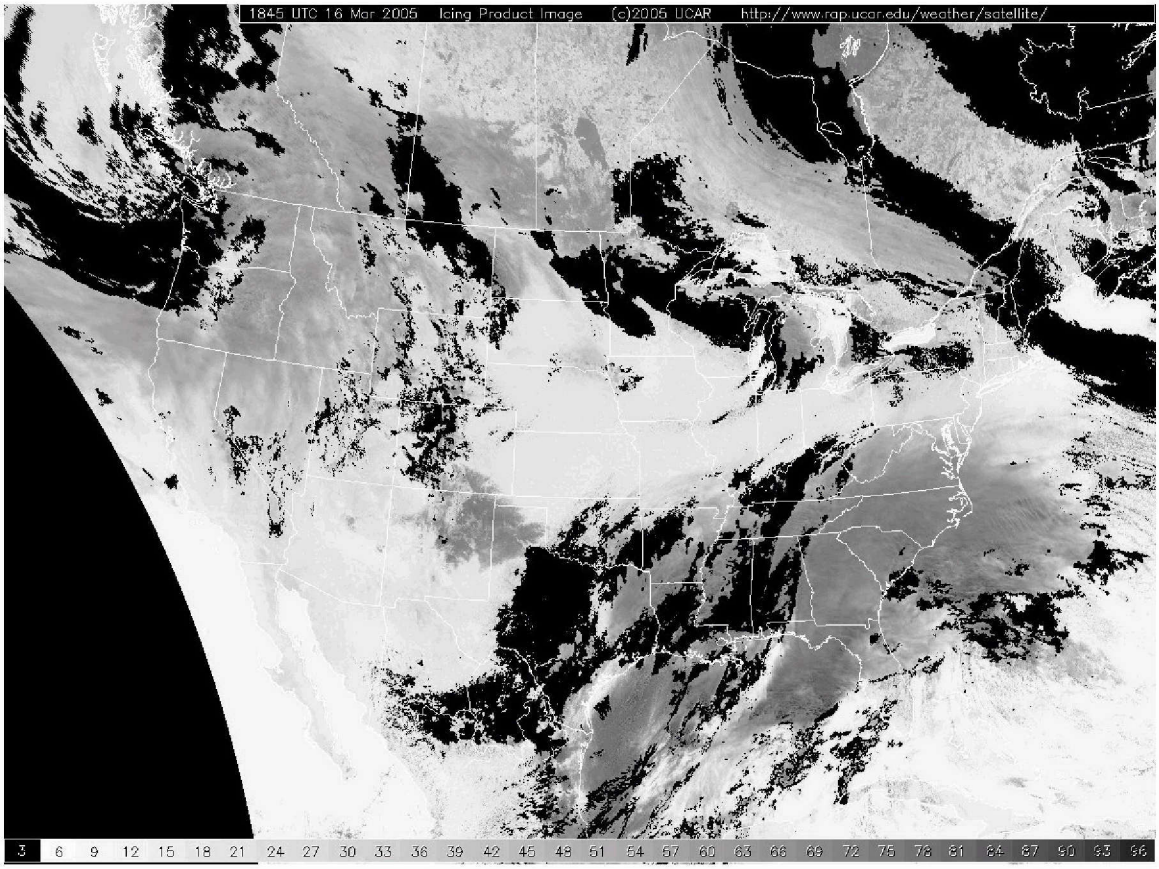

Figure 2. Example of NCAR's GOES icing potential detection product. Icing regions appear in black.

Since its launch in 1999, much research has gone into investigating the capabilities and usefulness of the Moderate Resolution Imaging Spectroradiometer (MODIS). With 36 available wavelengths, superior spatial resolution, and global coverage, MODIS provides an opportunity to improve the 3-channel, GOES-based icing potential detection algorithm currently being used. Several channels have shown the capability to detect a wide variety of cloud properties that would assist in satellite-based icing potential detection. Many of the channels currently used

on MODIS will also be chosen for the next generation of GOES satellites.

D. THESIS PLAN

The 36 MODIS channels are researched to determine which channels provide potentially useful information for detecting icing conditions, specifically cloud-top temperature, cloud optical depth, thermodynamic phase, and effective particle radius. The applicable channels are tested either individually or in concert with other channels to develop a fuzzy algorithm that provides icing probability within a given cloud scene. Aircraft icing and channel selection theory are discussed in Chapter II. Chapter III explains the data, investigation and verification procedures used, followed by results in Chapter IV and concluding remarks in Chapter V.

THIS PAGE INTENTIONALLY LEFT BLANK

II. THEORY

A. ICING OVERVIEW

Aircraft icing cannot be detected directly via remote sensing methods. Relevant detection techniques applied to determine icing potential must therefore focus on detecting ideal atmospheric conditions that generally result in icing, the most pertinent of which are air temperature, cloud phase, and drop size. Icing occurs when large (diameter > 30μm), liquid water drops freeze upon contact with the surface of an aircraft, causing the accretion of ice on the airframe. Because the aircraft's surface temperature must be below freezing, these drops – referred to as super-cooled liquid drops (SLD) – must exist in temperatures below freezing while remaining in the liquid phase (AWS 1980).

Water droplets smaller than 5μm in diameter spontaneously freeze at about −40°C in the absence of ice crystal nuclei (ICN) or a frozen surface, while larger droplets may freeze at slightly warmer temperatures. This is different from the bulk water freezing point of 0°C because the distribution of cloud water mass among a large quantity of individual drops limits the surface area available for homogeneous nucleation. Statistical research shows that due to heterogeneous nucleation caused by the presence of ICN in the atmosphere, clouds generally consist of an appreciable number of ice crystals below −15°C (Rogers 1989). Earlier research showed that clouds generally consist of ice crystals below −20°C, (Sand 1984). Pruppacher (1995) combined data from several previous investigations of super-cooled water drops in clouds with

his own data collection, shown in Figure 3, to demonstrate that no cloud with cloud-top temperatures less than –20°C contain only water drops. Furthermore, he found that fewer than 10 percent of clouds with cloud-top temperatures between –25°C and –40°C may partially consist of super-cooled liquid drops. Young et al. (2000) further substantiated these results using ground-based lidar measurements during the Experimental Cloud Lidar Pilot Study (ECLIPS), finding no water droplets in mid-level clouds below -25°C, as indicated in Table 1.

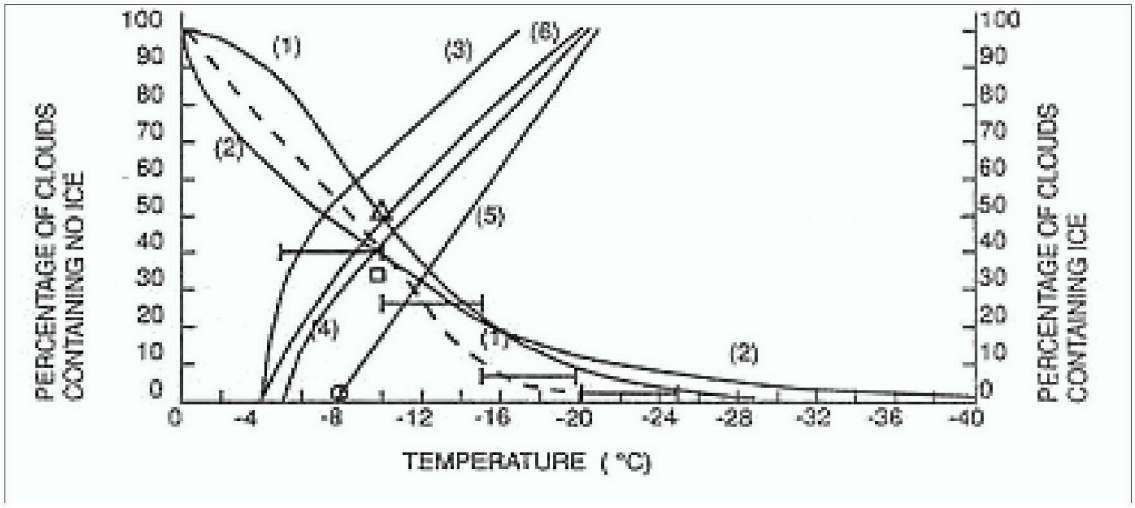

Figure 3. Percentage of clouds containing no ice (1 & 2) and clouds containing ice (3-6) with respect to cloud-top temperature. (From Pruppacher 1995)

Table 1. Frequency and duration of detection of ice and water in clouds during ECLIPS (after Young et al 2000).

Temperature Interval	Frequency of detection (%)		Duration of detection (minutes)	
(°C)	Water	Ice	Water	Ice
-30 to -25	0	100	0	15
-25 to -20	21	79	20	75
-20 to -15	56	44	79	61
-15 to -10	33	67	61	122
-10 to -5	41	59	30	44
-5 to 0	92	8	170	14
0 to 5	100	0	96	0

Heterogeneous nucleation caused by the presence of ice crystals and ICN quickly depletes liquid water drops in mixed phase clouds, as water generally freezes when it comes into contact with any particle in sub-freezing temperatures. Because the saturation vapor pressure of ice is lower than that of liquid water, once ice crystals begin to form liquid water attrition occurs very rapidly (Rogers 1989). Any remaining liquid water existing below -25°C is generally below the 30μm threshold for SLD, decreasing the potential for significant aircraft icing in ice clouds to near zero (AWS 1980). This operationally restricts the potential for icing to clouds containing super-cooled liquid drops with temperatures between 0°C and -25°C.

B. GOES-BASED ICING POTENTIAL DETECTION ALGORITHM

The current algorithm used by the National Center for Atmospheric Research - Research Applications Laboratory (NCAR-RAL 1994) uses 3 of the 5 channels available on the GOES satellite imager to detect possible icing conditions. The algorithm was originally developed as a tool to reduce the spatial coverage of forecasted icing conditions created by models, which tend to overforecast aircraft icing potential regions. The 3 GOES channels (0.65μm, 3.9μm, and 10.7μm) are applied to detect the presence of clouds, their thermodynamic phase, and the temperature of the cloud top (NCAR 1994). The molecular structure of water drops and ice crystals affect how they absorb, scatter, and emit electromagnetic (EM) energy at a given wavelength. Differential properties of ice and water particles make it possible to distinguish ice cloud from water cloud, as well as determine properties such as particle size and cloud thickness. To assess cloud phrase, the current algorithm employed at NCAR uses the 0.65μm, 3.9μm, and 11μm channels.

1. Channel 1 (0.65μm)

GOES Channel 1 is centered at 0.65μm and detects the amount of visible solar energy reflected by the earth's surface and clouds back into space. This wavelength falls within a window region in atmospheric transmittance, where solar radiation peaks and the earth's atmosphere is virtually transparent to incident visible energy (Figure 4). This leads to a direct correlation between incident and reflected visible energy (Kidder 1995). The amount of energy reflected by a cloud is a function of sun-satellite geometry and cloud optical depth. Once corrected for satellite viewing angle and solar incident angle, cloud reflectance can be measured directly as the percentage of energy incident energy reflected toward the satellite (Allen 1987).

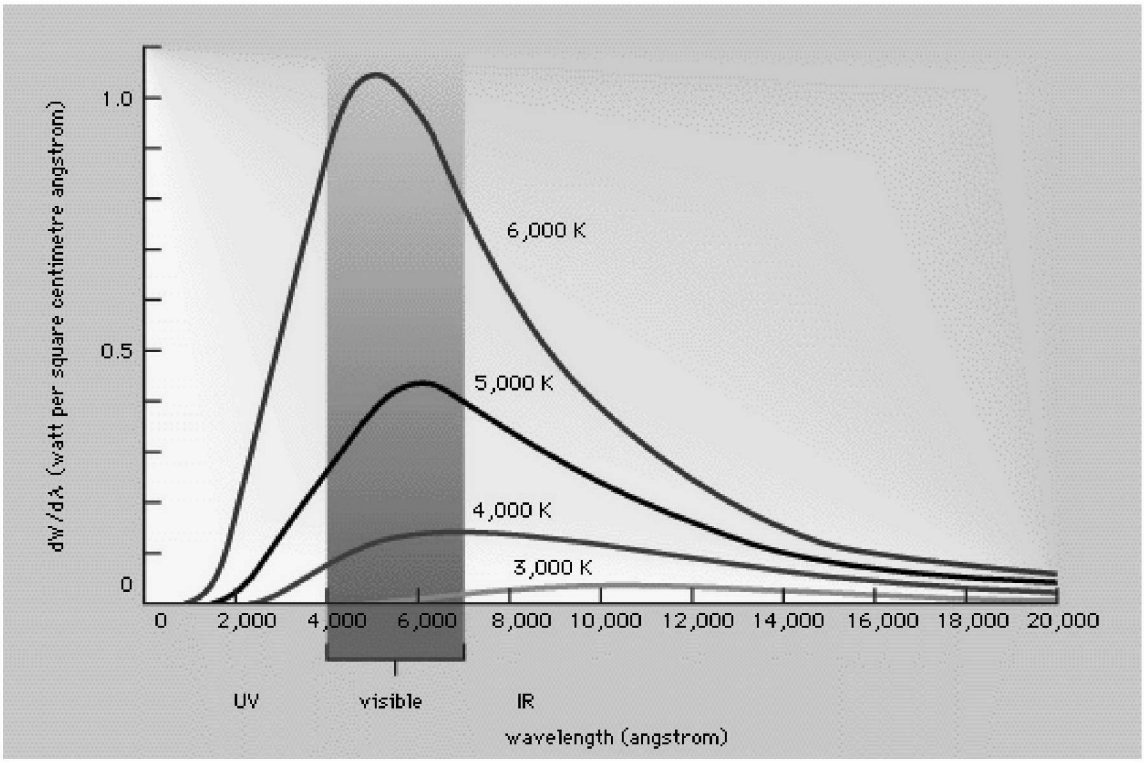

Figure 4. Spectral irradiance (dW/dλ). The sun's radiative temperature is 6000°K. (from Encyclopaedia Britannica 2005)

The sole remaining determinant of reflectance is cloud optical depth, which is a function of particle size and cloud thickness. Cloud particles, with an average radius of approximately 10μm, act as geometric scatterers when visible radiation impinges on them. This suggests that a cloud must only be a few dozen meters thick to scatter all incident visible radiation (Kidder 1995). A generally accepted study of cloud radiative properties calculated that a 2-km thick stratus cloud scattered approximately 80 percent of incident visible energy out of the top of the cloud toward space and only absorbed about 0.3 percent, which is in effect negligible (Welch 1980). Therefore, clouds with a thickness greater than about 2-km will have relatively large reflectance values when compared thin clouds or land and ocean surfaces, regardless of the thermodynamic phase of the cloud particles.

Often a thick cloud may contain few water droplets and ice crystals, while a thin cloud may lack of coverage but have a high water or ice content. In both cases, the cloud is optically thick and reflects most of the incident energy at this wavelength. Only snow-covered land surfaces and deserts have similar reflectance values as clouds. Snow cover has similar characteristics as atmospheric ice crystals in the visible channel and must be distinguished by using the near-infrared (NIR) wavelength. Deserts are distinguished by thresholds for brightness temperature. The GOES-based icing detection algorithm uses Channel 1 reflectance values greater than 25 percent to delineate regions where clouds with high water content, i.e. clouds containing SLD drops or ice crystals may exist (NCAR 1994).

2. Channel 2 (3.9μm)

GOES Channel 2 is perhaps the most complex window region used in satellite remote sensing. Centered at a wavelength of 3.9μm, this channel lies within the crossover region between incoming solar and outgoing terrestrial radiation (Figure 5). Therefore, the radiance values sensed by the satellite at this wavelength will have nearly equal contributions from the incident solar energy and average emitted terrestrial energy. In order to determine the magnitude of one energy source, the other source must be filtered or removed from the scene. In this case, a cloud's reflectance at 3.9μm can only be determined by removing the cloud's emittance. The removal of emittance is complicated by radiative variability caused by atmospheric transmittance, emissivity, optical depth, cloud effective radius, and blackbody emission temperature. Typically, assumptions are made to remove variability caused by the first three factors, such that atmospheric transmittance is 1.0, cloud emissivity is 1.0, and clouds are optically thick (Allen 1987). Cloud effective radius can be idealized as well, leaving all radiance variability to be a result of blackbody emission temperature. Accounting for this blackbody temperature is critical in retrieving information about cloud thermodynamic phase using 3.9μm reflectance.

Allen et al. (1987) developed a method to determine the reflected radiance of clouds at 3.9μm by estimating and removing of the emitted EM energy. First, the Planck blackbody emission temperature of a given pixel is assumed to be equal to that measured by GOES Channel 4. Using this temperature, an idealized Planck function curve is used to

determine the expected emittance of the pixel at 3.9μm. This value is then subtracted from retrieved GOES Channel 3 radiance, with incident solar radiation and sun-satellite geometry taken into account, to determine the reflectance value (Allen 1987). Based on the real index of refraction of water (Figure 6), clouds made up of water droplets reflect more energy at this wavelength than ice clouds. This is enhanced by the fact that water clouds tend to be made up of smaller particles than ice clouds, and smaller particles scatter more solar energy because their radii are close to solar wavelengths (CIRA-CSU 2005). The GOES icing algorithm uses Channel 3 reflectance values greater than 6 percent to delineate water clouds (NCAR 1994).

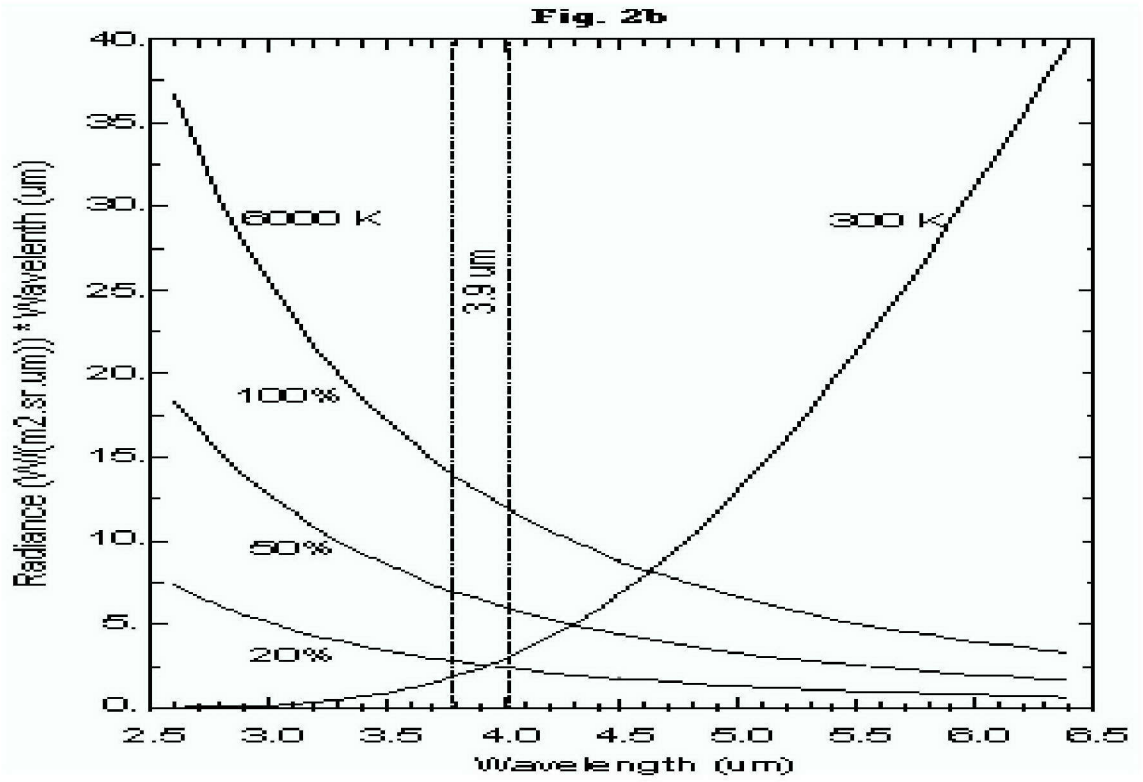

Figure 5. Terrestrial Planck curve with crossover region of solar Planck curve. (CIRA-CSU 2005)

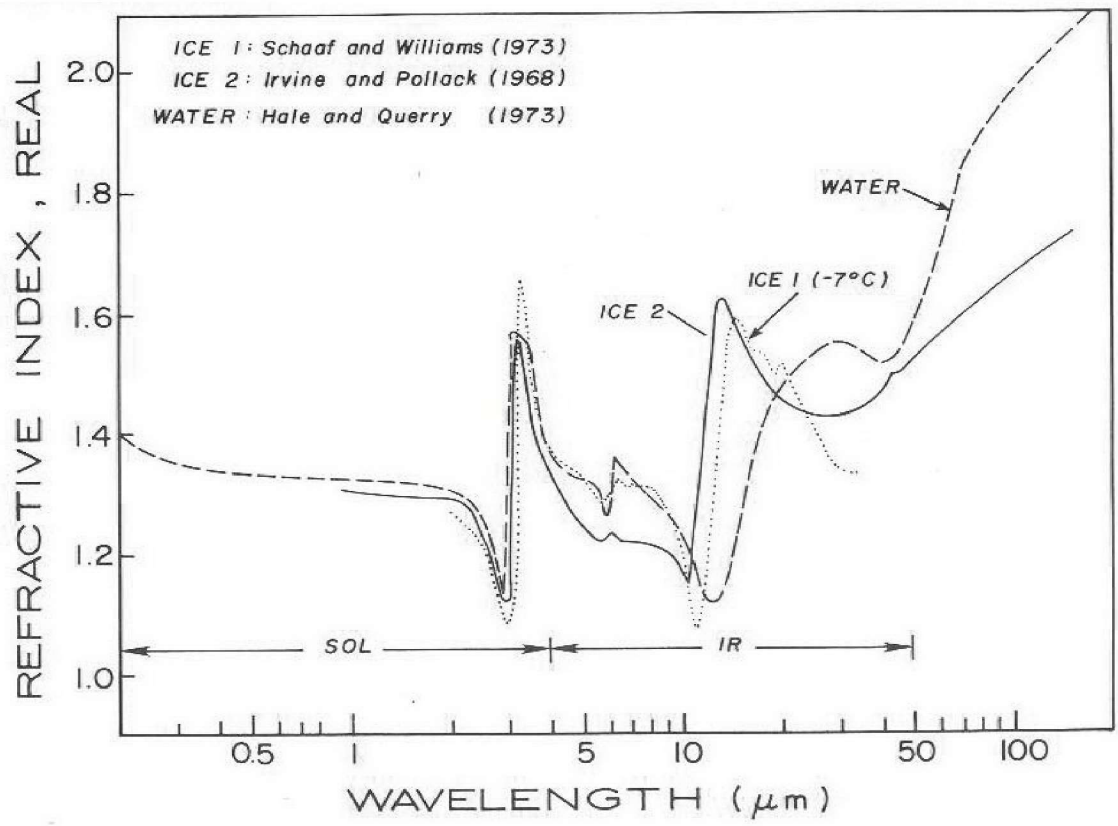

Figure 6. Real index of refraction for ice and water particles. (From Hobbs and Deepak 1981)

3. Channel 4 (11μm)

GOES Channel 4, centered at 10.7μm, provides the typical infrared imagery used for the depiction of clouds at night. The earth's blackbody emission peaks near this wavelength as it radiates EM energy out to space (Figure 7). This peak coincides with a relative minimum in atmospheric interference because atmospheric transmittance at this wavelength is greater than 0.8 (Kidder 1995). Utilizing Mie scattering theory, the imaginary index of refraction (Figure 8) of both ice and water is large in this spectral region, signifying that ice and water clouds are strong absorbers, and thus strong emitters at 10.7μm (Hobbs 1981). Due to these optical characteristics, the radiance detected at this wavelength indicates the true

radiance emitted by ice and water clouds, which can then be converted to cloud temperature via Schwarzchild's equation.

Energy detected from a cloud at 10.7μm will only be emitted by the top few meters of a cloud, given that the cloud is not optically thin (Kidder 1995). Therefore, passive satellite measurements can only measure the temperature of cloud tops. Thompson et al. (1997) showed that while this is not ideal, cloud top temperature is a valuable tool in determining whether temperatures within a cloud region are favorable for icing (Thompson 1997). This allows the GOES algorithm to use Channel 4 brightness temperature to determine whether cloud tops detected within a scene have temperatures within the 0°C to -25°C threshold determined to be most favorable for the existence of SLD drops, and therefore potential aircraft icing (NCAR 1994).

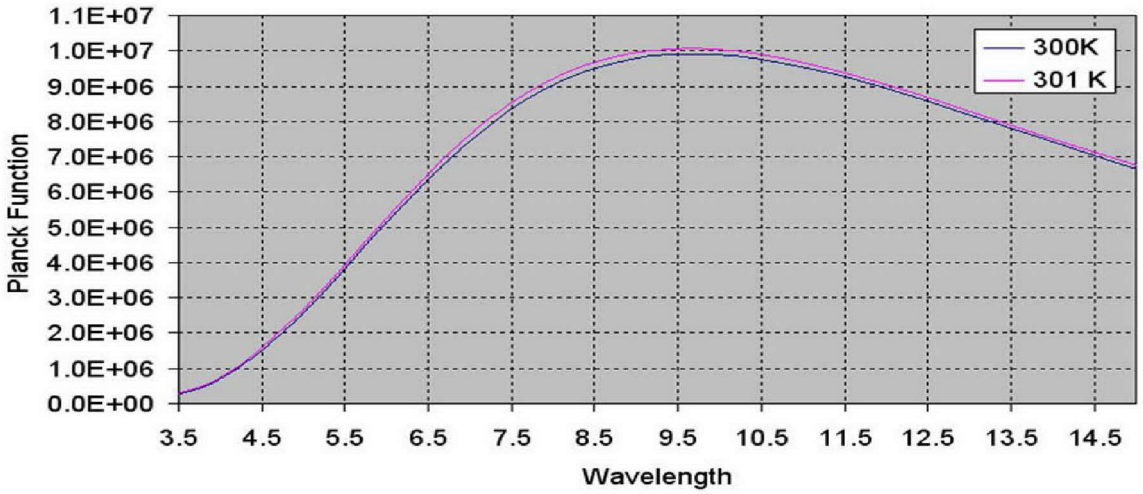

Figure 7. Thermal radiation Planck function at 300°K and 301°K, given in units of W/m^2.

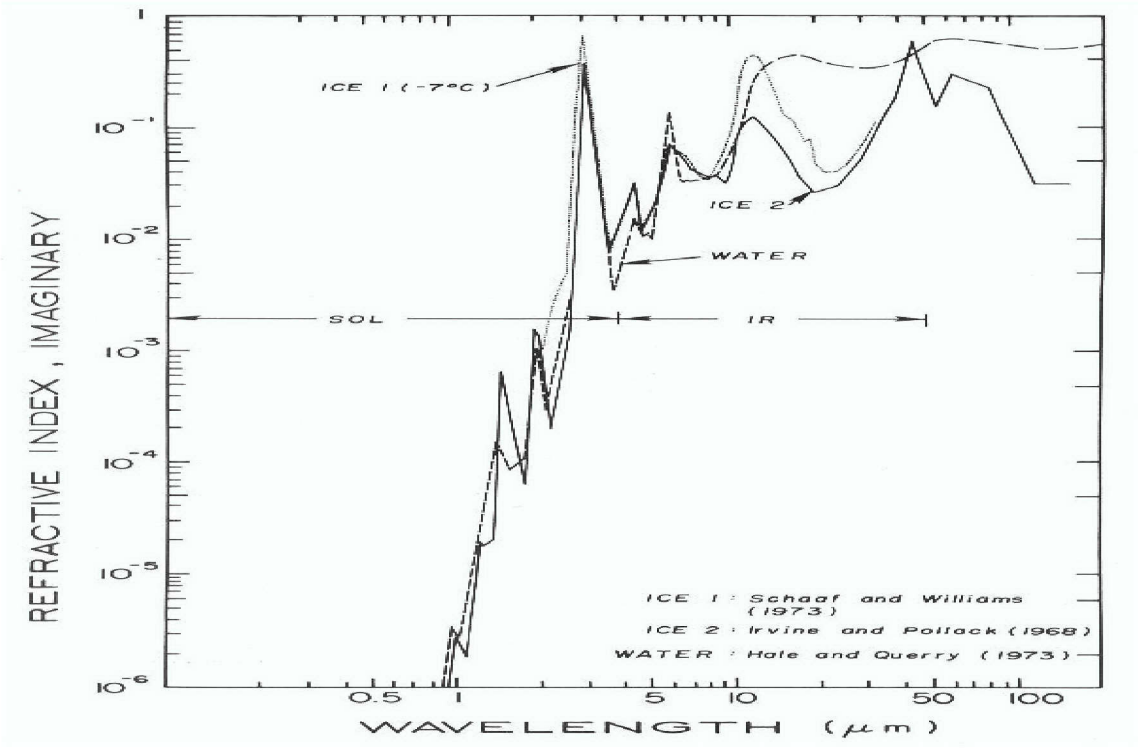

Figure 8. Imaginary index of refraction for water and ice, which determines emittance of EM energy. (from Hobbs and Deepak 1981)

4. Channel 2 – Channel 4 Difference (3.9-11μm)

The final piece of the GOES-based icing potential detection algorithm is the difference between the Channel 2 and Channel 4 brightness temperatures (referred to as 2-4BTD). As discussed previously, an object considered to be a blackbody has an idealized Planck curve based on its temperature. This curve was used to determine Channel 2 reflectance; however, this reflectance value is only available during daylight hours. The 2-4BTD may be used to assist in determining the thermodynamic phase of clouds, regardless of the presence of reflected solar radiation.

At night, differences sensed between water clouds and ice clouds are solely based on emission. As NCAR (2005) explains water drops emit less energy at 3.9μm than at 11μm

while emissions at the two wavelengths are nearly the same for ice particles. The 2-4BTD produces negative values for water clouds and near-zero values for ice clouds (NCAR 2005). Therefore, the GOES icing algorithm uses 2-4BTD values less than -2°C to denote water clouds (NCAR 1994).

In daytime imagery, both reflected and emitted energy contributes to the 3.9μm brightness temperature. As mentioned above in Section 2, water clouds are much more reflective at this wavelength than ice clouds. The amount of energy emitted by clouds at 3.9μm is roughly 20 percent of the amount available to be reflected (Figure 4). The increased spectral radiance causes the sensed brightness temperature of water clouds to appear much warmer at 3.9um than at 11um due to the reflected solar energy. As discussed in Section 2, ice crystals reflect much less energy at 3.9μm than water clouds (Hobbs 1981). The nighttime 2-4BTD has already shown that the emittance difference between 3.9μm and 11μm for ice crystals is nearly zero (NCAR 2005). The daytime 2-4BTD product will thus have near zero values for ice crystals and large positive values for water clouds. Therefore, the GOES algorithm uses a 2-4BTD greater than 10°C during daylight hours to delineate water clouds (NCAR 1994).

C. APPLICABLE MODIS CHANNELS

The first MODIS was launched in 1999 as one of five instruments aboard NASA's Terra satellite. The satellite has a sun-synchronous, polar orbit with a descending-pass equator crossing of 10:30 local. Though its time resolution only allows it to see the same general area once per day, MODIS afford the opportunity to view the bulk of the earth's surface on a daily basis at up to 16 times the

spatial resolution of GOES. MODIS also has the added value of 36 channels from 0.4μm to 14.4μm, listed in Table 2, fine-tuned to view a vast array of land, ocean, and atmospheric phenomena (NASA 1999a). Distinctive cloud properties can be detected using each of the 36 MODIS channels either individually or using various multispectral techniques. This opens up a wide range of research opportunities that are currently unavailable using the GOES platform.

Any effort to improve the GOES-based icing potential detection algorithm must be built on the foundation of the original algorithm. Therefore, the MODIS channels corresponding to the GOES channels described in section B will be used exactly as above, except where described in Section III. The GOES-equivalent channels available on MODIS are listed in Table 3. Beyond these channels, MODIS channels 6, 7, 26, 29, and 32 have been shown in prior research to have applications in the detection of potential icing conditions.

Table 2. Characteristics of the 36 channels available on the MODIS platform. (after MODIS Web 2004).

Primary Use	Band	Bandwidth[1]	Spectral Radiance[2]	Required SNR[3]
Land/Cloud/Aerosols Boundaries	1	0.62 – 0.67	21.8	128
	2	0.841 – 0.876	24.7	201
Land/Cloud/Aerosols Properties	3	0.459 – 0.479	35.3	243
	4	0.545 – 0.565	29.0	228
	5	1.23 – 1.25	5.4	74
	6	1.628 – 1.652	7.3	275
	7	2.105 – 2.155	1.0	110
Ocean Color/ Phytoplankton/ Biogeochemistry	8	0.405 – 0.420	44.9	880
	9	0.438 – 0.448	41.9	838
	10	0.483 – 0.493	32.1	802
	11	0.526 – 0.536	27.9	754
	12	0.546 – 0.556	21.0	750
	13	0.662 – 0.672	9.5	910
	14	0.673 – 0.683	8.7	1087
	15	0.743 – 0.753	10.2	586
	16	0.862 – 0.877	6.2	516
Atmospheric Water Vapor	17	0.89 – 0.92	10.0	167
	18	0.931 – 0.941	3.6	57
	19	0.915 – 0.965	15.0	250
Surface/Cloud Temperature	20	3.66 – 3.84	0.45(300K)	0.05
	21	3.929 – 3.989	2.38(335K)	2.00
	22	3.929 – 3.989	0.67(300K)	0.07
	23	4.02 – 4.08	0.79(300K)	0.07
Atmospheric Temperature	24	4.433 – 4.498	0.17(250K)	0.25
	25	4.482 – 4.549	0.59(275K)	0.25
Cirrus Clouds Water Vapor	26	1.36 – 1.39	6.00	150(SNR)
	27	6.535 – 6.895	1.16(240K)	0.25
	28	7.175 – 7.475	2.18(250K)	0.25
Cloud Properties	29	8.4 – 8.7	9.58(300K)	0.05
Ozone	30	9.58 – 9.88	3.69(250K)	0.25
Surface/Cloud Temperature	31	10.78 – 11.28	9.55(300K)	0.05
	32	11.77 – 12.27	8.94(300K)	0.05
Cloud Top Altitude	33	13.185 – 13.485	4.52(260K)	0.25
	34	13.485 – 13.785	3.76(250K)	0.25
	35	13.785 – 14.085	3.11(240K)	0.25
	36	14.085 – 14.385	2.08(220K)	0.35

[1] Bands are in μm
[2] Spectral Radiance values are (W/m^2 -μm-sr)
[3] SNR = Signal-to-noise ratio
[4] NE(delta)T = Noise-equivalent temperature difference
Note: Performance goal is 30-40% better than required

Table 3. GOES channels used in the current icing detection algorithm and the equivalent channels available on the MODIS platform.

GOES Channel	Wavelength (μm)	MODIS Channel
1	0.65	1
2	3.9	22
4	10.7	31

1. Reflectance Tests

Cloud particles interact readily with solar wavelengths due to their small size. This makes the wavelengths between 0.4μm and 4.0μm very useful in identifying cloud cover over the earth's surface. In general, clouds reflect or scatter most of the solar energy that impinge upon their surfaces regardless of phase. However, there are scattering property differences between ice and water at several wavelengths in the solar spectrum that allow for phase discrimination of cloud tops. The GOES algorithm makes use of just two wavelengths within this window, 0.65μm and 3.9μm, of which only 3.9μm provides information about cloud phase. MODIS provides both of these channels within the solar spectrum, as well as 21 additional channels between 0.4μm and 4.0μm. Of these, 3 channels show great promise in assisting in the problem of icing potential detection: Channels 6 (1.6μm), 7 (2.1μm), and 26 (1.38μm).

a. Channel 6 (1.6μm)

Though limited to daytime, 1.6μm exhibits radiative properties that are extremely valuable in distinguishing cloud thermodynamic phase. The real index of refraction near 1.6μm, which drives scattering

properties, is fairly similar for ice and water. However, Figure 9 shows that the imaginary index of refraction for ice is nearly an order of magnitude larger than that of water. This causes the ice to absorb 40 percent more incident energy than water at this wavelength. Therefore, water clouds will usually be more reflective than ice clouds (Baum et al 2000).

Particle size also factors into reflectance by ice and water clouds. Baum et al. (2000) found that single-scatter albedo for water was larger than that of ice for a given effective particle size. However, as water droplet radius grew, reflectance values decreased anywhere from 5 percent for optically thin clouds to 60 percent for optically thick clouds. Similar reflectance decreases were measured for increasing ice particle effective size. This sharp decrease with increasing particle or droplet size makes it possible for a large water drop to have reflectance values equal to that of smaller ice particles.

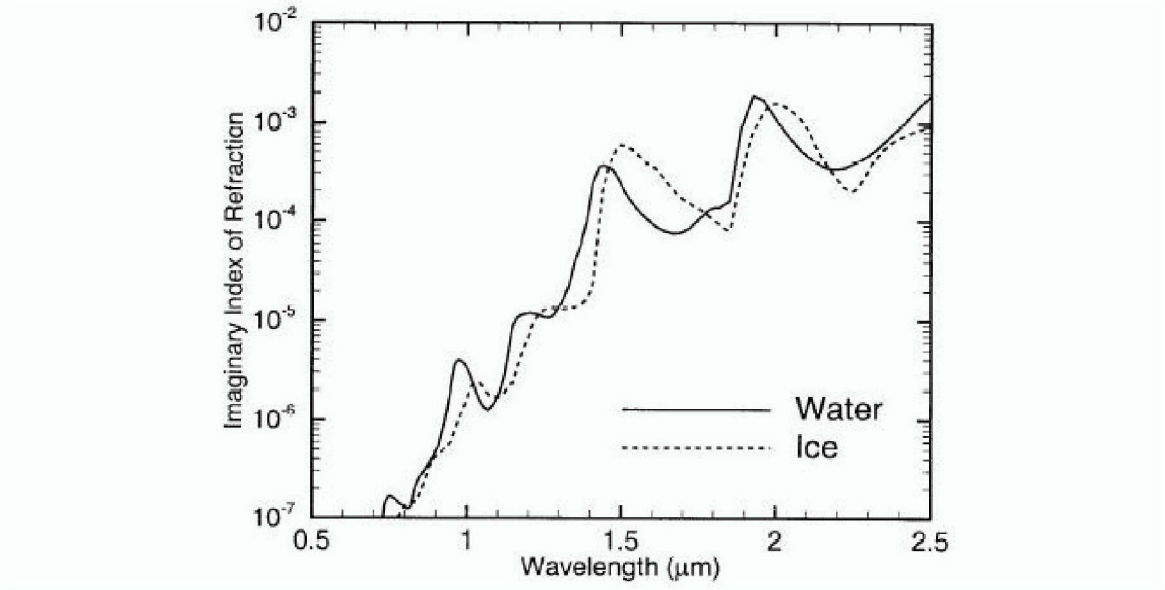

Figure 9. Imaginary index of refraction for ice and water between 0.5μm and 2.5μm (Baum et al. 2000).

Earlier research indicates that it may be possible to eliminate some of the reflectance crossover between large water droplets and small ice crystals. Heymsfield and Platt (1984) found a nearly direct correlation between temperature, ice water content (IWC) and maximum ice particle size, summarized in Table 4 and Figure 10. As temperature increases, both IWC and the maximum dimensions of the ice particle increase. This is probably due to the existence of larger SLD, which makes it possible for ice crystals to grow faster and larger than at lower temperatures. Therefore, the largest ice particles will tend to reside in air temperatures necessary for high icing potential. Any cloud region where small ice particles are present will tend to be much colder than the -25°C threshold required for icing potential. An appropriate test to screen out low cloud-top temperature would significantly decrease the probability of misidentifying icing potential for such clouds. This test makes it possible to lower the reflectance threshold for detecting water clouds to as low as 0.2 since clouds containing the smallest ice particle size will have already been screened out (Baum et al 2000). The 0.5 reflectance value will be applied here as an initial threshold.

Table 4. Ice water content and maximum particle dimensions for given temperature ranges (after Heymsfield and Platt 1984).

Temperature Range	**Maximum Particle Dimensions**	**Range of IWC**
(°C)	*(mm)*	*(g m^{-3})*
-20 → -25	2.6	0.001-0.063
-25 → -30	1.8	0.001-0.066
-30 → -35	2.4	0.008-0.043
-35 → -40	2.0	0.009-0.025
-40 → -45	1.8	0.0004-0.008
-45 → -50	1.2	0.0002-0.008
-50 → -55	1.6	0.0002-0.004
-55 → -60	1.0	0.0002-0.0018

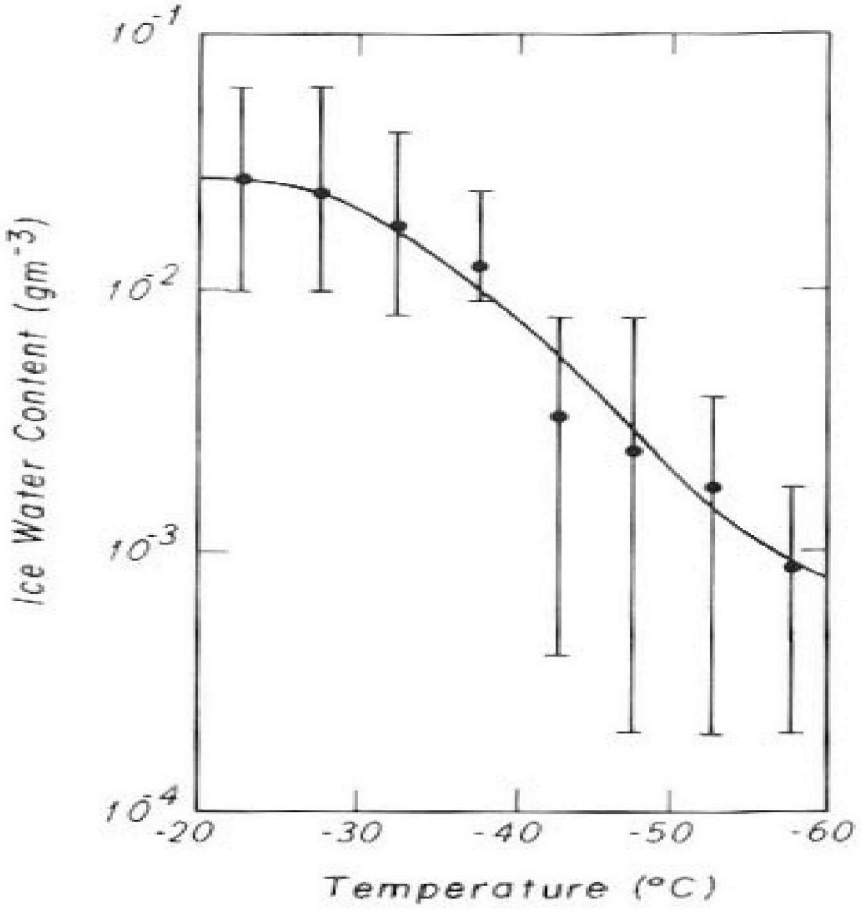

Figure 10. Mean ice water content for clouds found at temperatures between -20°C and -60°C (Liou 1992).

b. Channel 7 (2.1μm)

The bulk scattering properties of ice and water at 2.1μm are similar to those discussed for Channel 6. As is the case for 1.6μm, the real index of refraction is nearly identical for ice and water. The imaginary index of refraction for ice is larger than that of water, making ice less reflective at this wavelength, as well. However, 2.1μm has many subtle differences from 1.6μm that are worth noting.

The imaginary index of refraction is larger at 2.1μm than at 1.6μm, causing increased absorption that reduces the reflectance of both ice and water clouds at 2.1μm. The increase in the imaginary refractive index of water is much greater than that of ice. Therefore, the difference between the imaginary refractive indices is only half that of the difference at 1.6μm, reducing the ability of 2.1μm to distinguish between ice and water (Liou 1992). Nonetheless, Baum et al. (2000) found that a reflectance threshold of 0.4 can be used to distinguish water clouds from ice clouds at 2.1μm.

Increases in effective particle size also cause 2.1μm reflectance to decrease for both ice and water, as was the case for 1.6μm reflectance. Furthermore, the same research discussed for Channel 6 with regards to particle size, IWC, and temperature can be applied to 2.1μm. Smaller ice particles are generally found at temperatures much lower (higher altitudes) than those where icing potential is high (Heymsfield and Platt 1984). Cloud-top temperature tests will greatly screen out higher clouds characterized by high 2.1μm reflectance. The screened-out pixels probably contain either large water droplets or

small ice particles. By eliminating the high reflectance values caused by just the smallest ice particle effective size from Baum et al. (2000), the threshold for determining water clouds can be lowered to 0.25 with a negligible possibility of mistaking ice crystals for water droplets. However, the given threshold of 0.4 will be used here.

c. Channel 26 (1.38μm)

Unlike the other NIR wavelengths presented here, water and ice clouds have nearly identical radiative properties at 1.38μm. Both water and ice are highly reflective at this wavelength due to absorption (Bunting 1984). What makes this wavelength useful to this problem is that it is strongly absorbed by the presence of water vapor in the atmosphere. Many studies have shown the usefulness of the 1.38μm band in detecting cirrus clouds, and therefore regions where no icing would be expected.

More than 90 percent of the atmosphere's water vapor is found in the troposphere below 7 kilometers (km). Cirrus clouds generally reside above 400 millibars (mb), which equates to roughly 7 km. The use of this level as a threshold for icing potential of clouds was validated by Curry and Liu (1992). Their statistical analyses of January 1979 North Atlantic temperature fields obtained from the European Centre for Medium-Range Weather Forecasts (ECMWF), shown in Table 5, indicated that the warmest temperature found at 7 km is about -25°C, which is the lower limit given for aircraft icing potential.

Water vapor's strong absorption of EM energy at 1.38μm allows very little energy reflected by the earth's surface or clouds below 7 km to reach the top of the atmosphere. However, most of the energy reflected by

clouds near or above 7 km would be transmitted to a satellite sensor, as two-way atmospheric transmittance is about 0.6 above 7 km. An additional benefit of using this channel is that the strong absorption energy reflected by low-level surfaces creates a uniform background that causes thin cirrus to be detected 40 times better than possible with IR emission techniques such as the 11-12μm brightness temperature difference technique discussed in section 3 below (Gao and Kaufman 1995). Gao et al. (2003) later determined that 1.38μm reflectance values greater than 0.02 denote high clouds so long as the atmosphere is not dry (i.e. having more than 0.4 cm of column precipitable water vapor). However, Gao's threshold was developed to include all possible pixels containing cirrus clouds, whereas the goal here is to exclude cirrus clouds. Pavolonis and Heidinger (2004) used a threshold of 0.08 to determine when to use multilayered cloud tests to eliminate regions where thick cirrus obscured the scene. Based on previous discussions on the low likelihood that clouds above 7 km have temperatures above -25°C, a lower limit of 0.08 is used here to detect regions where icing potential is negligible.

Table 5. January 1979 temperature statistics obtained from ECMWF analyses (from Curry and Liu 1992).

Pressure Level	**Average Height**	**Mean Temperature**	**Maximum Temperature**	**Minimum Temperature**	**Standard Deviation**
(mb)	*(m)*	*(°C)*	*(°C)*	*(°C)*	*(°C)*
1000	115	3.3	18.4	-10.7	4.47
850	1419	-2.9	11.8	-21.6	5.65
700	2937	-10.1	4.4	-32.2	6.38
500	5457	-24.0	-12.5	-46.3	6.38
400	7038	-37.2	-24.9	-55.9	5.50
300	8974	-49.8	-39.2	-61.4	3.63
200	11557	-58.9	-43.0	-70.1	5.06

2. Reflectance Ratio Tests

While much can be gleaned from using reflectance values at 1.6μm and 2.1μm, these two wavelengths can provide even more significant information when compared to the reflectance at 0.65μm for a given scene. Reflectance values for both Channel 6 and Channel 7 will tend to be less than visible reflectance for all clouds, but will be larger for water clouds than ice clouds. When taking a ratio of either channel versus Channel 1 reflectance, large values will tend to be water clouds, while lower values will be ice clouds or background features. The only exception to this is vegetated surfaces, which are more reflective in Channels 6 and 7 than in Channel 1, causing the ratios described to be greater than zero. Therefore, large values of this ratio on a scale between 0 and 1 will indicate clouds with high icing potential. These ratios

have been used by King et al. (2002) in their final thermodynamic phase determination on the MODIS platform.

3. Infrared Difference Tests

The tests recommended to this point have focused on wavelengths located in the solar portion of the EM spectrum. This limits retrievals to imagery gathered during daytime. IR tests can extend the usefulness of the icing potential detection algorithm to nighttime, providing 24-hour data availability while roughly doubling the number of useful passes made by a polar orbiting satellite over a given location. Both GOES and MODIS algorithms need 3.9μm and 11μm. However, there is a high possibility of ambiguity in 3.9μm values because the wavelength is located in the crossover region of the solar and terrestrial blackbody emission curves. Furthermore, the radiance values in this channel are quite low when compared to 11μm, so small errors can have a large impact on 3.9μm retrieved properties.

Strabala et al (1994) showed that the atmospheric window region between 8μm and 13μm located near the peak of the terrestrial radiation curve maintains useful differences in the absorption/emission properties of ice and water particles (Figure 6). The imaginary index of refraction for both ice and water are relatively low between 8μm and 10μm, then increases sharply toward 12μm (Figure 8). The absorption coefficient for ice and water closely follows the shape of the imaginary index of refraction. However, ice absorption between 10μm and 12μm increases by more than two times that of water, such that various BTD calculations taken within this window region yield divergent values for ice crystals and water droplets.

Applicable BTD measurements include 8μm minus 11μm (8-11BTD), 11μm minus 12μm (11-12BTD), and the difference between the 8-11BTD and 11-12BTD tests (trispectral BTD).

a. Channel 29 – Channel 31 (8.5-11μm)

Strabala et al. (1994) showed that as wavelength increases from 8.5μm to 11μm, the imaginary index of refraction for both ice and water increases. The absorption coefficient, seen in Figure 11, is directly proportional to the imaginary index of refraction and therefore also increases between 8.5μm and 11μm for ice and water. Absorption by ice particles increases more than water droplets of the same size when the particle size is less than 30μm, which is true for most water droplets in cloud tops since droplets larger than 30μm tend to reside below cloud top (Liou 1992). Clouds are assumed to have the properties of a blackbody at these wavelengths, and thus ice clouds will emit better than water clouds based on the absorption efficiency. The combination of these effects results in a positive 8.5-11BTD for relatively opaque (optical thickness > 1) ice clouds, while opaque water clouds will have negative 8.5-11BTD values (Strabala et al 1994). Because water clouds generally reside lower in the atmosphere, the tendency for increased water vapor absorption above water clouds will further separate ice and water clouds by causing lower water clouds to have more negative values (Platnick 2003).

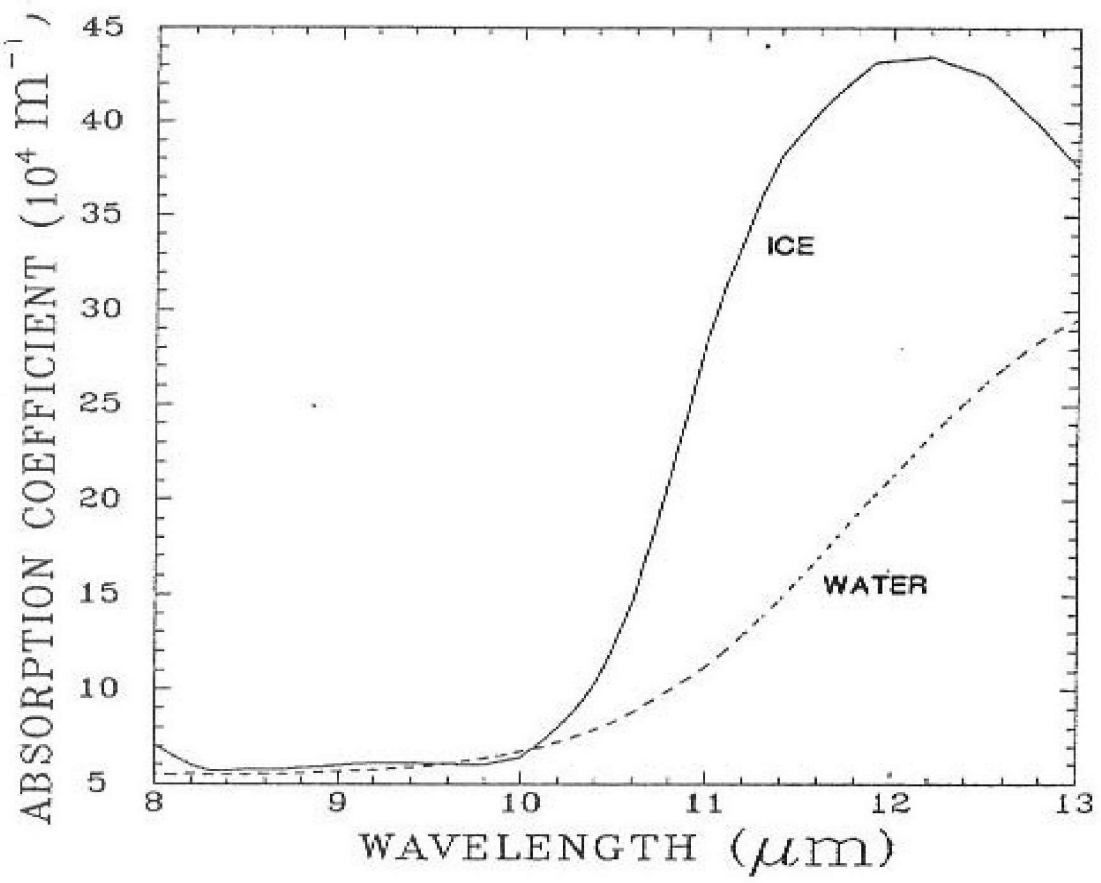

Figure 11. Absorption coefficient, 8-13μm (from Ackerman 1990).

b. Channel 31 – Channel 32 (11-12μm)

This test can be somewhat difficult to use because the 11-12BTD tends to be positive for all land and ocean backgrounds as well as all cloud types (Ackerman 1990). Yet subtle differences in the imaginary index of refraction for ice and water are present and can help distinguish ice and water clouds. The imaginary index of refraction – and thus the absorption coefficient for both ice and water particles is increasing from 11μm to 12μm (Figure 10). This means that clouds will be more absorptive, i.e. emit at a colder temperature at 12μm, causing the generally positive 11-12BTD. However, Inoue

(1987) showed that while thick cirrus clouds have an 11-12BTD similar to water clouds, thin cirrus clouds have BTD values greater than about 1°K. Building on Inoue's research, Wieman (1990) found that while cloud-free and multi-layered cloud scenes have an 11-12BTD less than 0.8°K, cirrus clouds have an 11-12BTD greater than 0.81°K, with thin cirrus being greater than 1.51°K. Therefore, this test may be helpful in identifying some ambiguous thin cirrus.

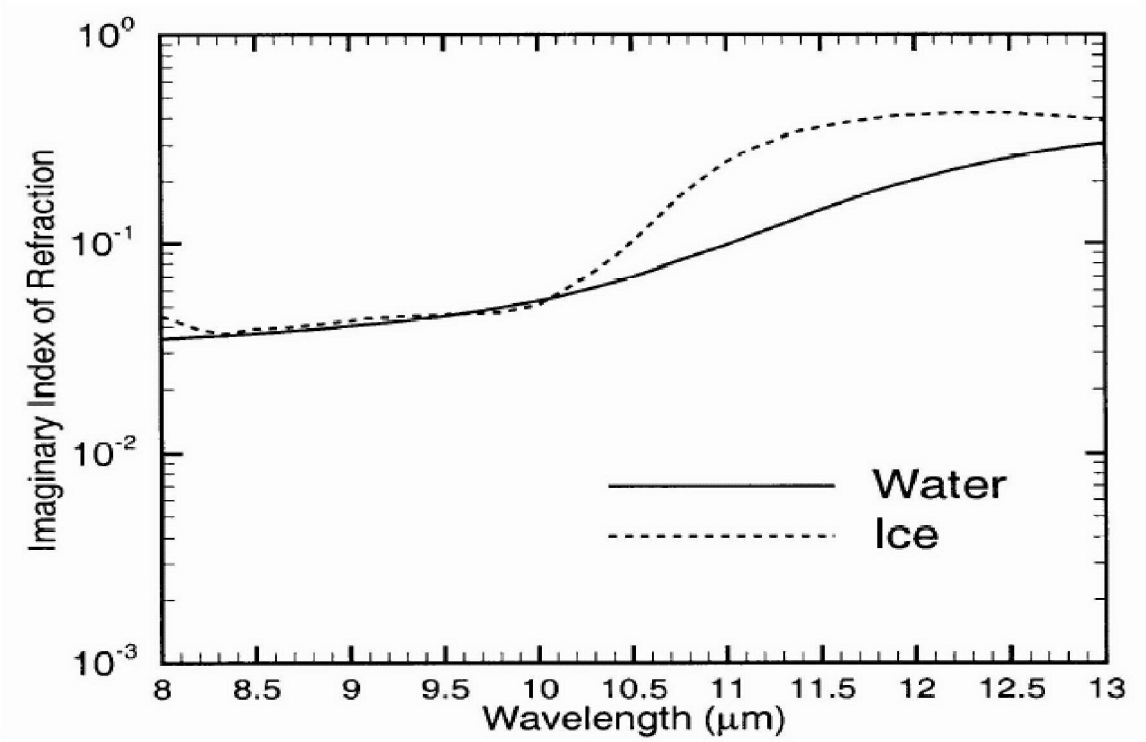

Figure 12. Imaginary index of refraction for water and ice in the 8-13μm window region (from Baum et al 2000).

c. Trispectral - Channels 29-31 vs. 31-32 (8.5-11μm vs. 11-12μm)

Strabala et al. (1994) demonstrated that it can be very beneficial to combine 8.5-11BTD and 11-12BTD data using either a scatter plot test or a difference between the 8.5-11BTD and 11-12BTD (trispectral BTD). Water

droplet absorption increases more between 11 and 12μm than between 8.5 and 11μm, such that the 11-12BTD for water clouds are larger than the 8.5-11BTD. The opposite is true for ice particle absorption. Because water clouds tend to have a negative 8.5-11BTD and a larger, positive 11-12BTD, the trispectral BTD for water clouds will tend to be negative. In a scatter diagram comparing 8.5-11BTD to 11-12BTD, pixels containing water clouds will cluster together along a line with slope less than 1. Ice clouds, on the other hand, will generally have a positive trispectral BTD, and will cluster along a line with slope greater than 1 in the 8.5-11BTD vs. 11-12BTD scatter diagram. Mixed-phase clouds or pixels containing both ice and water clouds will cluster near the unity line between water and ice clouds. For the purpose of the icing potential detection algorithm, the difference between 8.5-11BTD and 11-12BTD is calculated. The thresholds used to discriminate between water and ice clouds are the same as the 8.5-11BTD thresholds. Large negative values (below -2°C) are generally water clouds, while large positive values (above 3°C) denote ice clouds.

III. PROCEDURES

MODIS imagery was gathered for November 11, 24, 28, and 30, 2003, over the northeastern U.S. and southeastern Canada (40-50°N, 65-85°W). These coincide with the dates and operating area of the 2003 Atlantic THORpex Regional Campaign / Alliance Icing Research Study II (ATReC/AIRS-II) conducted by NASA's Langley Flight Ops Center in Bangor, Maine. ATReC/AIRS-II personnel focused their research on mid-latitude cyclones passing through the region on these dates in which icing conditions were forecasted as likely (ATReC 2005). GOES imagery was not used to eliminate error induced by spatial and spectral resolution differences (Ellrod and Bachmaier 2003, Chavez et al. 2002), allowing a direct comparison of algorithm performance rather than the satellite platforms.

A. INVESTIGATION

Initial imagery analysis was conducted to exhibit a confidence in using the thresholds suggested in Section II. Image processing was performed using Terascan at the Naval Postgraduate School (NPS) Interactive Digital Environmental Analysis (IDEA) Laboratory. 5 sub-regions were selected in the November 24 image based on the satellite interpretation of images:

1. Ice clouds located within a thick cirrus shield.
2. Low-level water clouds with above-freezing temperatures to ensure the absence of ice crystals.
3. Mixed clouds where differentiation of cloud composition and phase was difficult using conventional satellite analysis techniques.
4. Cloud-free land background.
5. Cloud-free ocean background.

Channel data for the pixels within each sub-region were ingested into Microsoft Excel and analyzed for cloud phase discrimination trends similar to those discussed in Section II. Regions 1, 2, and 3 were used to settle on channel radiance tendencies that indicate the transition from ice clouds to water clouds, while regions 4 and 5 provided each channel's threshold to separate clouds from background surfaces.

The test thresholds suggested by previous research are listed in column 3 of Table 6. Each of the 12 tests were placed into one of 4 groups: reflectance tests (Group I), reflectance ratio tests (Group II); brightness temperature test (Group III), and brightness temperature difference tests (Group IV). For all tests, the differentiation of ice, water, and mixed cloud regions from one another and from land and ocean backgrounds matched very closely with the previously discussed thresholds, though minor changes were implemented and are listed in column 4 of Table 6.

Table 6. MODIS icing tests, with test group and thresholds.

Test Group	***Test (no units unless noted)***	***Old Icing Thresholds***	***New Icing Thresholds***
I	0.65µm Reflectance (P01)	> 0.25	Min < 0.10 Max > 0.25
I	1.63µm Reflectance (P06)	> 0.5	Same
I	2.1µm Reflectance (P07)	> 0.4	Same
I	3.9µm Reflectance (P22)	> 0.06	Same
I	Cirrus Reflectance (P26)	< 0.08	Same
II	1.63µm Ratio (P61)	> 0.75	Min < 0.2 Max > 0.9
II	2.1µm Ratio (P71)	> 0.65	Min < 0.15 Max < 0.65
III	Temperature (°C) (P31)	<-25 & < 0	Min > 0 & <-40 Max @ -10
IV	3.9-11µm BTD (°C) (BTD1)	> 10 (Day)	same
IV	8-11µm BTD (°C) (BTD2)	< 0	Min > 3 Max < -2
IV	11-12µm BTD (°C) (BTD3)	< -0.5 & > 4.5	same
IV	Trispectral BTD (°C) (BTD4)	< 0	Same as 8-11 BTD

Eleven of the tests are straightforward linear scales, as shown by the example using visible reflectance in Figure 13. However, the cloud top temperature test based on Channel 31 BT is somewhat more involved based on research by Sand et al. (1984). Their research found that the chance of icing conditions peaks near -10°C, drops significantly through -25°C to about 5 percent, and tails off to 0 percent by -40°C, rather than decreasing linearly from 0°C to -40°C. The Channel 31 BT test is designed to incorporate their results, and is illustrated in Figure 14.

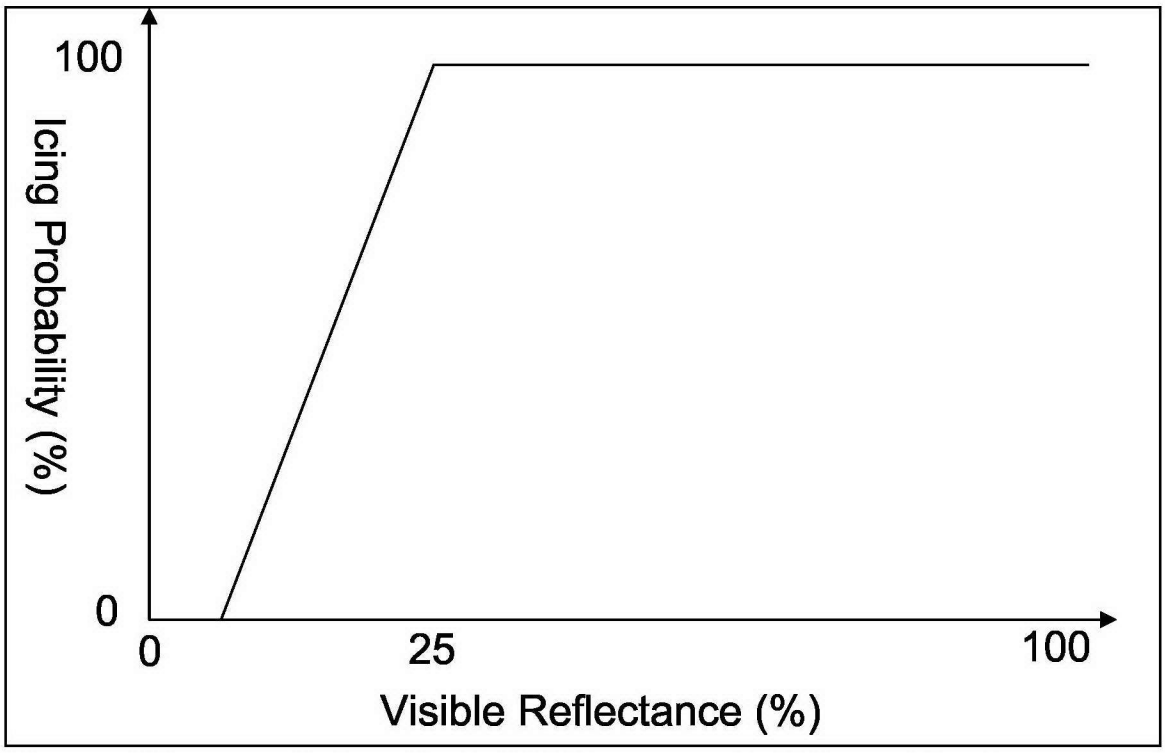

Figure 13. Icing Probability vs. visible reflectance for MODIS Channel 1.

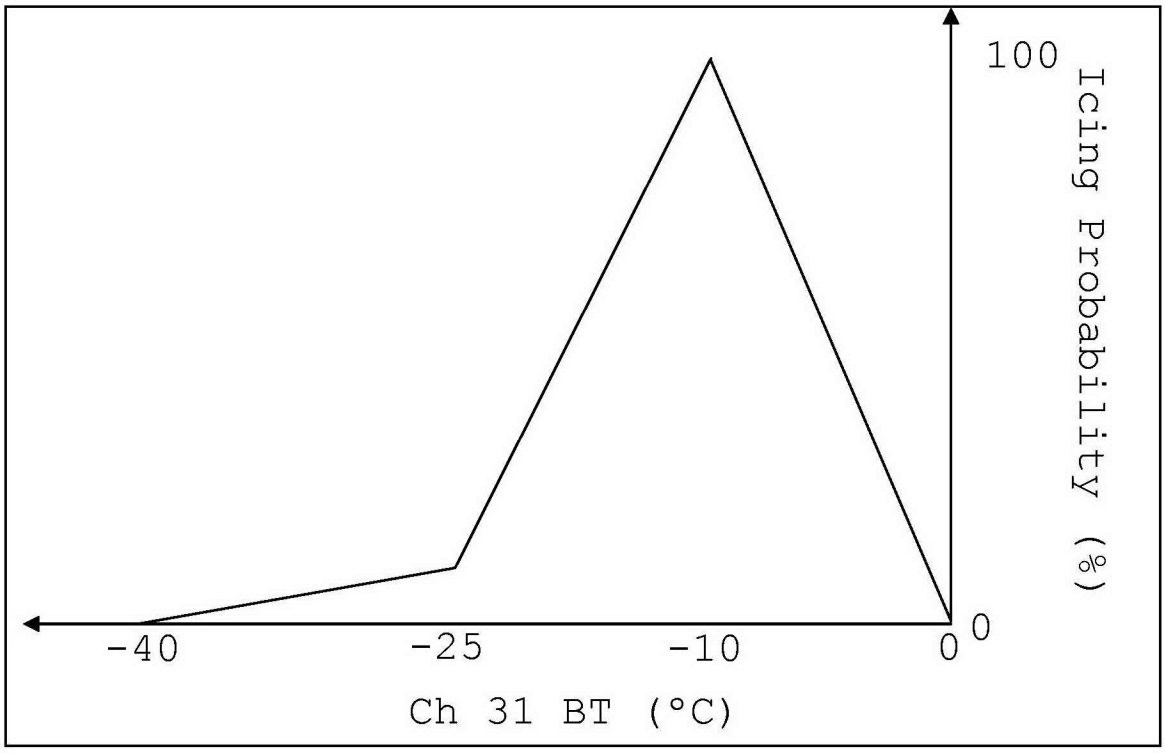

Figure 14. Icing probability test for MODIS Channel 31 brightness temperature.

Using these thresholds as a baseline value and the region analysis as guidance, a range of values for each channel was selected to allow for a linear scaling test based on fuzzy set theory to determine the likelihood of icing conditions for each pixel. This method allows the algorithm to derive a probability of icing based on the combination of several tests, rather than hard, on/off thresholds for each pixel that can be dominated by a single test or measurement. Hard thresholds are currently applied in the GOES icing potential algorithm such that icing conditions are only detected when all of the tests are true, i.e. that icing detection criteria for that channel are met. A similar threshold algorithm for MODIS would only add to the number of tests that must be true, which mathematically could only restrict the number of pixels flagged for potential icing conditions. A fuzzy algorithm would still flag the pixels meeting given thresholds as having high icing potential, but also allow many of the pixels that do not meet the desired thresholds to be given a degree of uncertainty based on the distance of test values from the required criteria (Lai and Hwang 1992). This method also provides the advantage of adding new testing techniques as well as removing those found to be untrustworthy by future research.

The fuzzy method of calculating each pixel's icing probability is similar to the calculation of the MODIS cloud mask confidence score described in Ackerman et al. (1998) and later in Memmen (2000). Each pixel was given an icing probability score based on each of the 12 tests. The maximum test scores from each group were multiplied, and the fourth root of the product yielded the overall icing

probability. The use of the maximum test score in each group biases the algorithm toward higher icing potential scores, imparting a conservative, safety-minded slant to the algorithm. This parallels the MODIS cloud mask, which is biased toward a higher likelihood of cloudiness, i.e. the mask is more likely to determine a pixel to be cloudy than clear (Ackerman et al. 1998). Furthermore, the Channel 31 BT test, being the sole member of Group III, will tend to have more weight on the results than the other individual tests. This is useful for the overall test, because air temperature is a driving force behind whether or not icing conditions exists within a given cloud. Decision tree diagrams illustrating the 12 tests can be viewed in Appendix I.

B. VERIFICATION

Once the MODIS algorithm was created, the raw MODIS files for each scene were processed using MATLAB. Several steps of the MODIS processing were performed using a series of program files created by Dr. Shaima Nasiri and used in research at CIMSS at the University of Wisconsin (Nasiri 2005). The GOES algorithm was also converted for use with MODIS imagery using MATLAB. Forty-six pilot reports (PIREPs) containing either positive (39) or negative (7) icing reports, provided by the Air Force Combat Climatology Center (AFCCC), were collected for the 4 selected dates within the 40-50°N, 65-85°W test region. PIREPS were used for verification because they are the only current measure of actual icing events. However, as discussed by Brown (1996), there are several biases and limitations of PIREPs that reduce their statistical usefulness, such that false alarm rate and bias are not considered completely reliable.

Three statistical tests recommended by Brown (1996) and Brown et al. (1997) to compare the accuracy of icing algorithms were used here: the probability of detection (POD), probability of correct null (POD-no) and area efficiency (AE). POD determines the percentage of icing encounters correctly detected by the algorithm (correct positive icing reports detected per total number of positive icing reports), POD-no determines the percentage of negative icing reports correctly detected by the algorithm (correct negative icing reports detected per total number of negative icing reports), and AE determines how much area was covered by the algorithm in order to achieve its POD score (POD per unit area). For example, if an algorithm obtains an extremely high POD by labeling an enormous area as having high icing potential, the algorithm will have a low AE because the algorithm needed a broad coverage to achieve its high POD. While these tests were not ideal to assess the accuracy of each algorithm individually, they were appropriate for algorithm comparisons, as was the goal here.

Pixels within 2500 square miles of each PIREP were used to compute each algorithm's POD and POD-no for comparison, as illustrated in Figure 15. The 25-mile radius used to obtain the 2500 square mile region was selected based on AF regulations, which state that weather personnel must notify aircrews of weather hazards occurring within 25 miles of the expected flight path (USAF 2004). Then the POD was divided by the total area of detected icing within the entire 40-50°N, 65-85°W region to establish AE. For each PIREP-centered region, the mean and median icing probability scores were calculated for the

MODIS algorithm, and the percentage of the region determined by the GOES algorithm to contain icing was calculated. For verification purposes, the algorithm was said to have high icing probability, and thus detected positive icing conditions, if the MODIS mean or median was greater than 50 percent, meaning that the MODIS algorithm concluded that the region likely contained icing. Areas with MODIS mean and median values below 50 percent were said to have detected negative icing conditions. For the GOES algorithm, if the percentage of the PIREP-centered area covered by icing was above 50 percent, the region was said to have detected positive icing conditions, while percentages below 50 percent were considered to be negative icing conditions. The MODIS mean and median, and the GOES percentages were compared to positive and negative PIREPS to determine POD, POD-no, and AE for all PIREPS on each day, those within 3 hours of the MODIS image time, and those within 1 hour of MODIS image time.

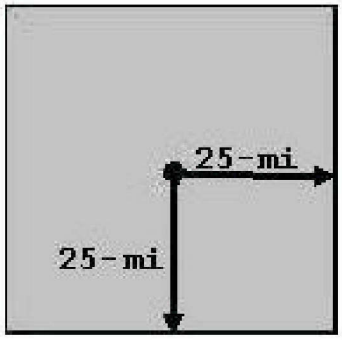

Figure 15. Depiction of PIREP-region used for algorithm comparison and verification.

IV. RESULTS

Verification results for the MODIS and GOES icing potential detection algorithms are compared here. Data from November 24, 2003, is used as a case study to examine the merits of each test in the MODIS algorithm. The 24 November case will be followed by overall statistics for the two algorithms.

The MODIS visible and IR images from the November 24 16:25 UTC descending pass over the northeast U.S. and southeast Canada are shown in Figure 16(a) and (b), respectively. A cold front is positioned over the Great Lakes, moving toward New England with icing conditions anticipated in the vicinity of the front based on model forecasts at the time (ATReC 2005). A cirrus shield is present along the front, with an area of cumulus clouds over Michigan, and a wedge of clearing ahead of the front covering much of New England. A mixed cloud region is present from Maine into eastern Quebec, with an area of stratus over central Pennsylvania and fog off the Massachusetts coast.

This particular case is useful for analysis because the scene contains many varying cloud features associated with a passing extratropical cyclone: warm and cold cloud tops, liquid and ice clouds, thin and thick cloud decks, and cloud-free regions with varying backgrounds. This variability can help to illustrate some of the strengths and weaknesses of the tests used by the MODIS algorithm. The location of the verification PIREPS are superimposed on the IR image in Figure 16(b) for reference.

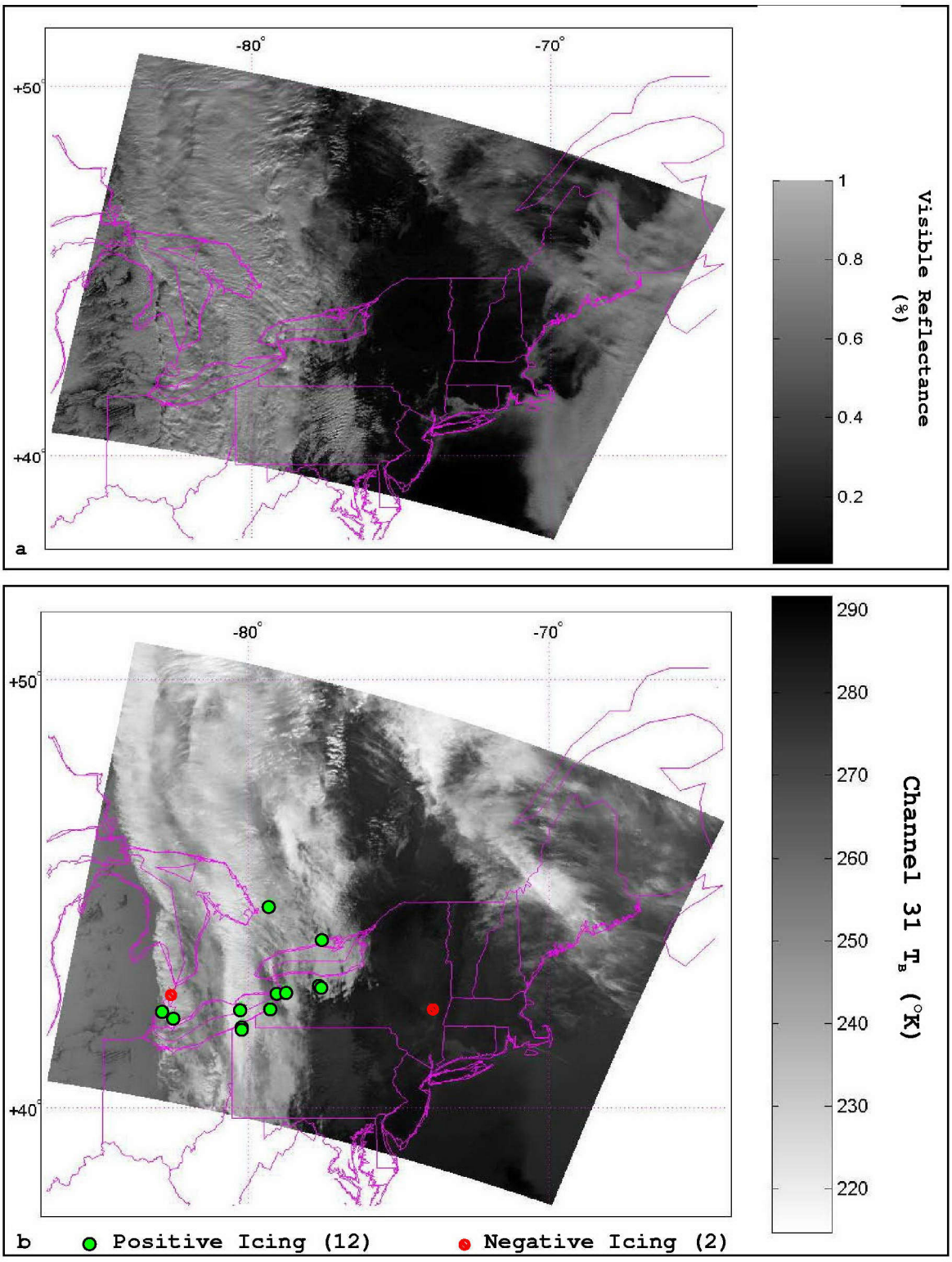

Figure 16. (a) Visible MODIS image for 16:25Z on 24 November, 2003. (b) Matching IR MODIS image with verification PIREPS overlaid.

A. GROUP I RESULTS

The Channel 1 reflectance (P01) test detects regions where highly reflective clouds are present. The test gives pixels with reflectance greater than 25 percent a score of 1, and decreases the score linearly for reflectance values below 25 percent. In Figure 17, bright areas are those with visible reflectance near or greater than 25 percent. It is evident that while high LWC clouds which may contain icing conditions have higher scores for P01, this test cannot discriminate between optically thick water clouds and optically thick cirrus clouds, evident in the multi-level clouds over the eastern Great Lakes, as well as the mid-level clouds and fog in the Atlantic Ocean.

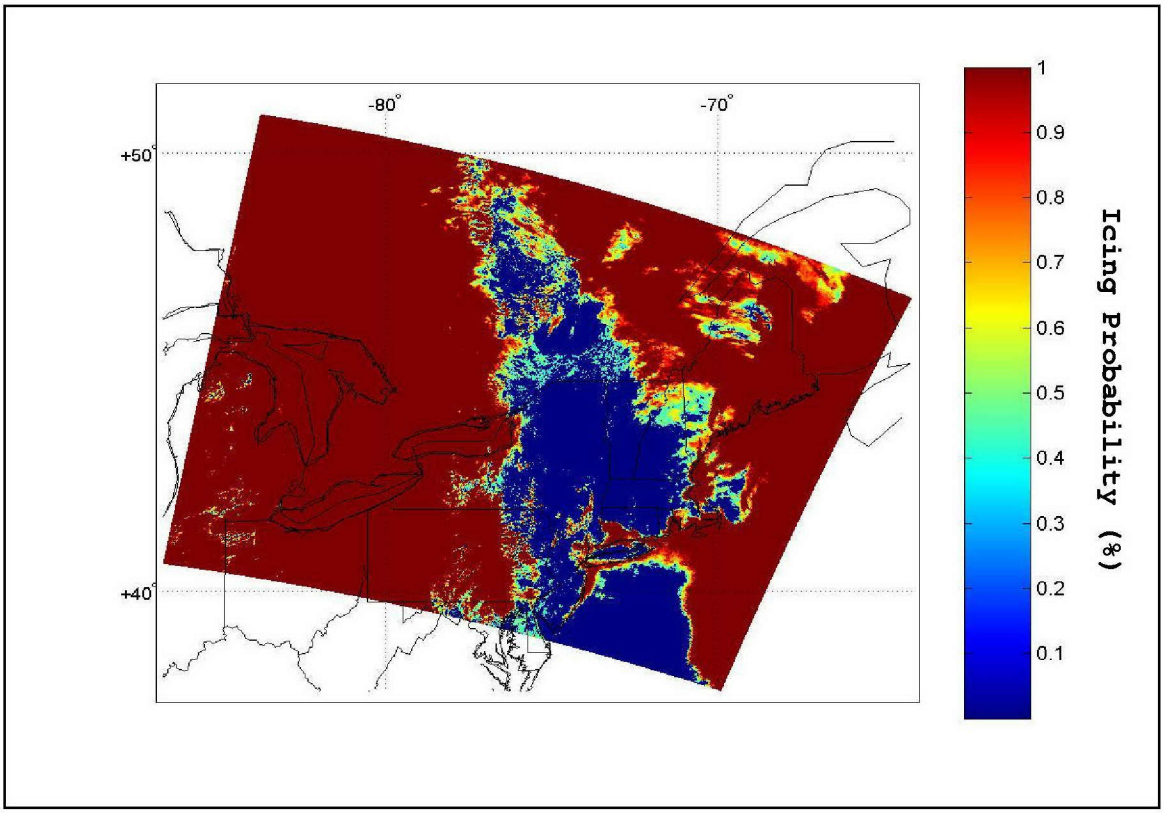

Figure 17. Icing potential probability test for Channel 1 reflectance (P01).

The Channel 6 reflectance (P06) test is one of many used to discriminate between SLD clouds and clouds composed

of ice crystals. Water clouds containing droplets of a given size will be more reflective than ice crystals of the same size. This causes water clouds to have higher values based on the P06 test. Notice in the P06 output image in Figure 18 that the cloud-free land over New England has a reflectance nearly identical to the cirrus in the scene. This would be problematic when using P06 alone, because non-cloud pixels could be misidentified as icing. However, the reflectance of the land surface remains weak when compared to water cloud regions, which have values at or above 50 percent. Also, other tests such as the P01 test successfully remove cloud-free pixels from the output.

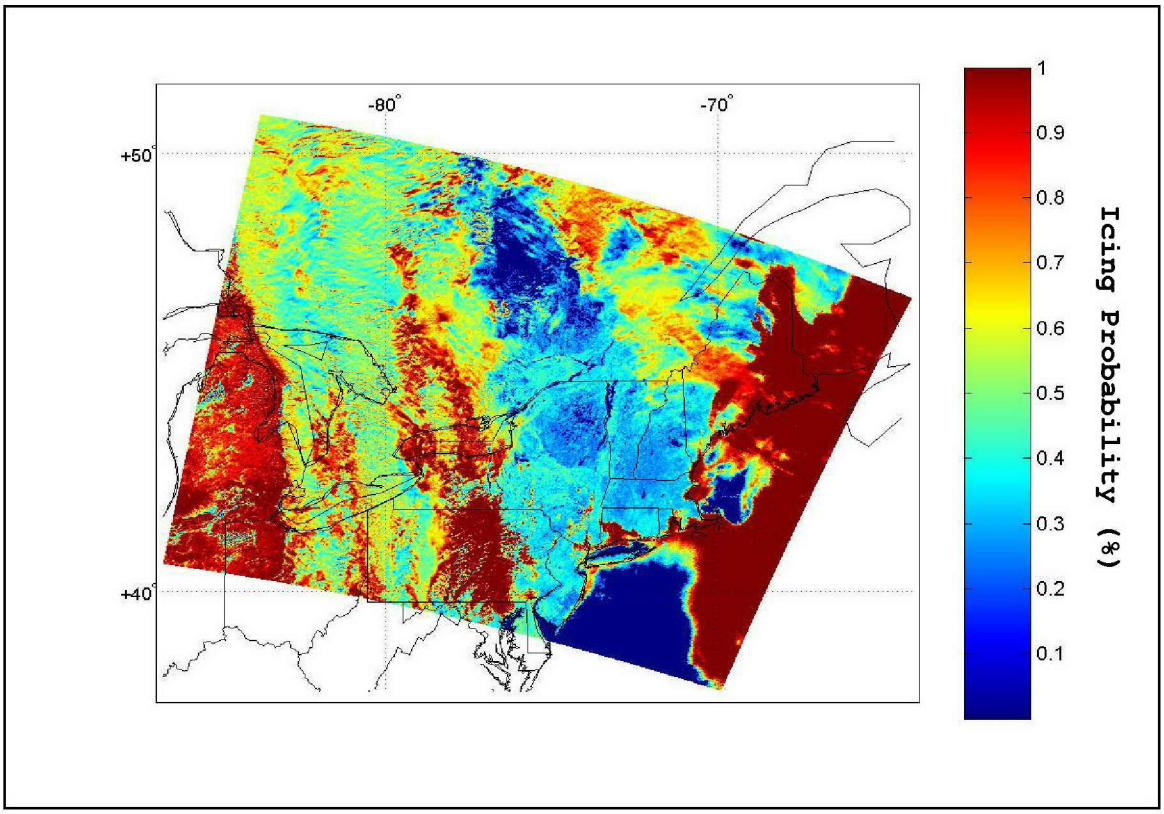

Figure 18. Icing probability for Channel 6 reflectance (P06) test.

The reflectance test for Channel 7 (P07) has results very similar to those of the P06 test. The threshold for water clouds is 40 percent due to increased absorption by

both water and ice clouds than for Channel 6. Water clouds are more reflective than ice clouds, and thus high reflectance regions will have a greater probability of icing. The mid-level clouds over Michigan, the low-level stratus over central Pennsylvania, and the coastal fog along the Atlantic coast all have high icing probabilities (Figure 19). The test also reveals ship tracks in fog off the coast of Massachusetts, which show up due to the presence of smaller cloud droplets formed on ship exhaust particles.

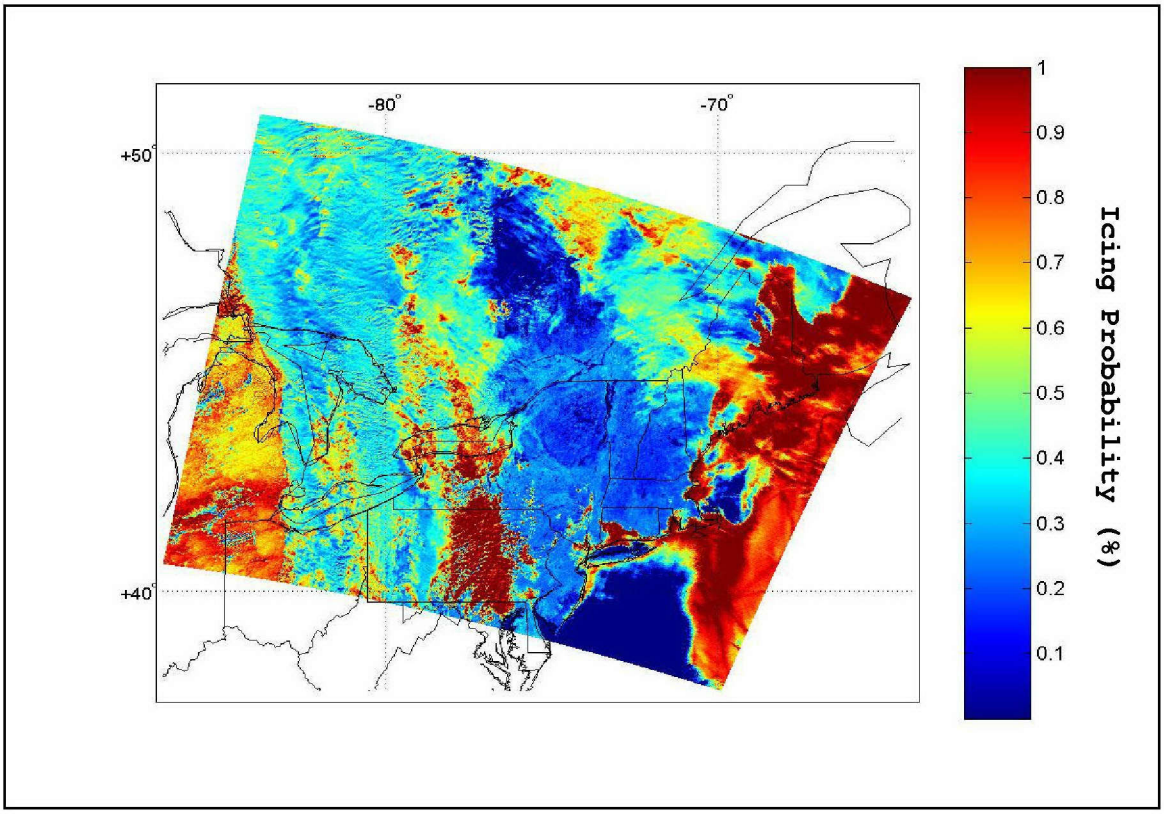

Figure 19. Icing probability for Channel 7 reflectance (P07) test.

The Channel 22 reflectance (P22) test uses the thresholds for the GOES algorithm. SLD clouds are more reflective at 3.9μm than ice clouds, so the P22 test gives higher icing probability scores to high reflectance areas associated with water, not ice, clouds (Fig. 20). This test

does not mask the cloud-free regions from the high icing probability regions due to a high surface reflectance greater than the 6 percent threshold. This is most evident over the Atlantic Ocean and central New England. This is similar to the P06 test; however, water clouds and cloud-free surface are both identified as icing. A higher threshold would likely eliminate most cloud-free surface pixels, since water clouds are more reflective than the surface at this wavelength.

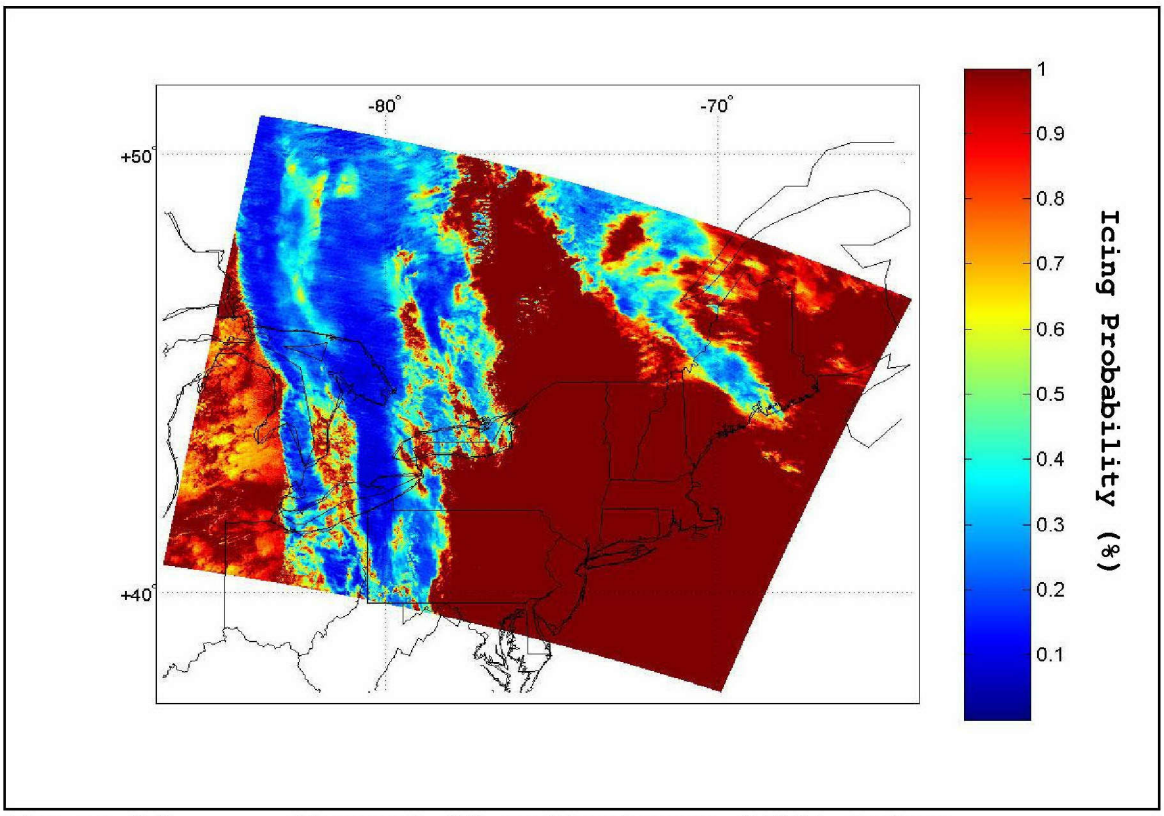

Figure 20. Channel 22 reflectance (P22) icing probability test.

The Channel 26 reflectance (P26) test is an inverse test when compared to the other 4 reflectance tests. Channel 26 reflectance will be high for clouds that reside higher in the atmosphere, which are most likely to consist of ice crystals. Therefore, low reflectance regions are given high values of icing probability, as opposed to the high reflectance regions in the other reflectance tests.

Like P22, this test does not separate low-level water clouds from the land surface, because water vapor absorption causes both surface and low-cloud features to have low reflectance. Shown in Figure 21, this test effectively reduces the icing probability for cirrus clouds.

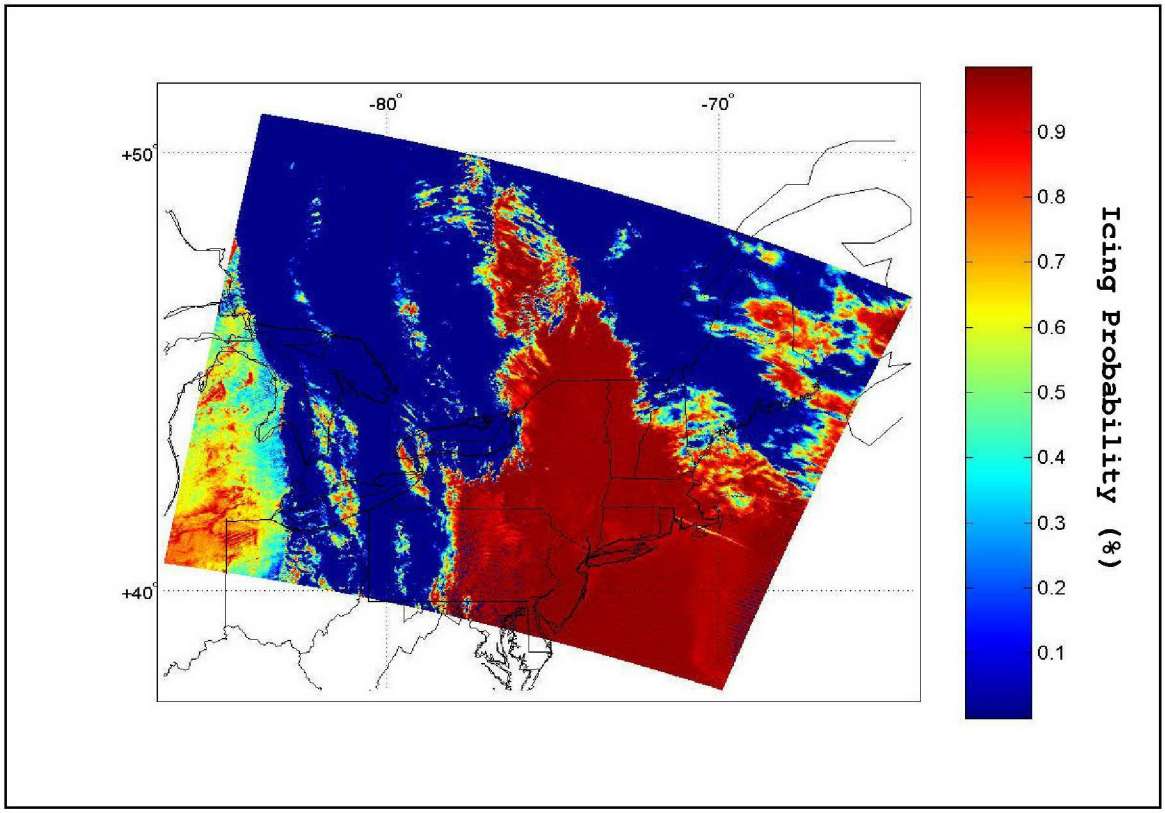

Figure 21. Channel 26 reflectance (P26) icing probability test.

When each pixel's maximum test score from the 5 reflectance tests is selected, the results of Group I indicate that as a whole, the reflectance tests do little to discriminate between water and ice clouds. This is due to the lack of an effective cloud screen, as well as the high reflectance of ice clouds in the Channel 1 test, as is obvious from Figure 22. It is expected that Group I would not need the Channel 1 test when placed in a sequence after an effective cloud mask such as the one developed by Ackerman et al (1998), since the P01 test is essentially a

weak cloud mask. If cloud-free regions and the Channel 1 test are eliminated, the Group I results would likely show better differentiation between water and ice clouds.

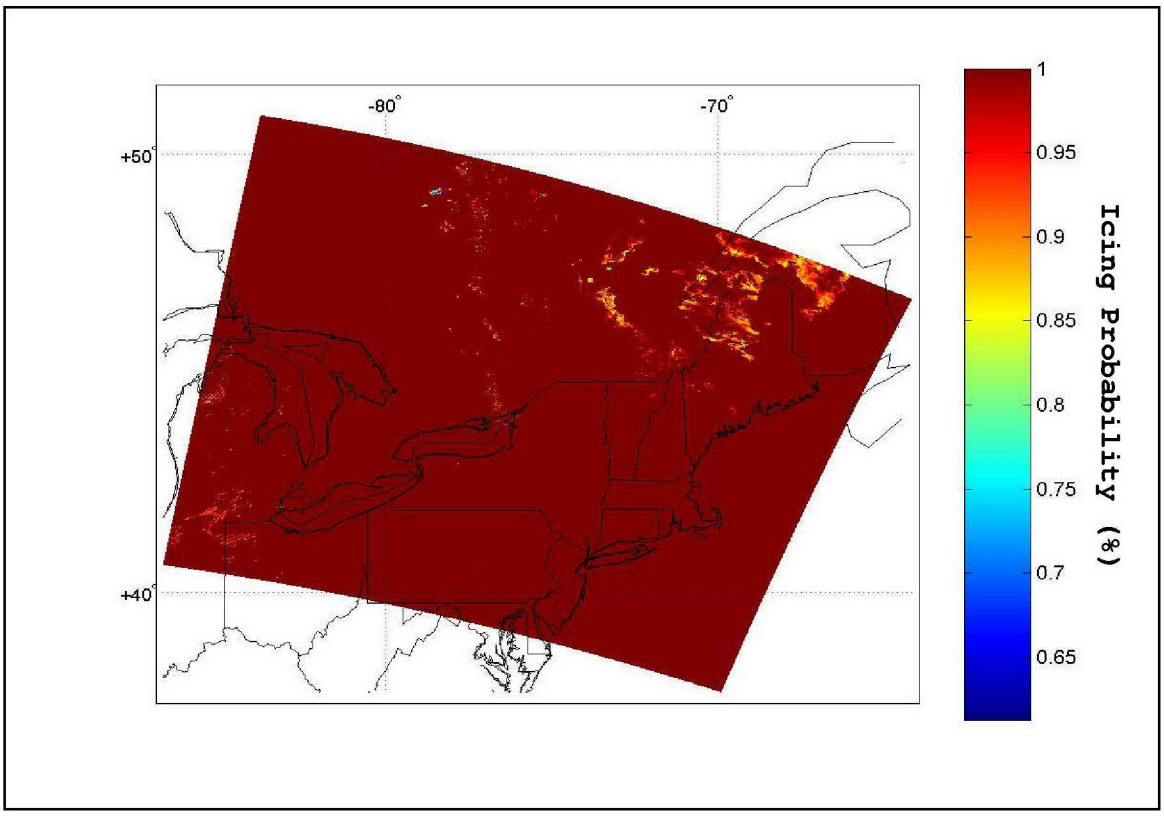

Figure 22. Group I results, indicating each pixel's maximum icing probability score for the 5 reflectance tests.

B. GROUP II RESULTS

The Channel 6/1 reflectance ratio (P61) test has results that are very similar to the P06 test. However, due to the lower reflectance ratio of land, the masking of cloud-free regions has improved dramatically over central New England. The icing probability difference between water and ice clouds has also increased. In Figure 23, the contrast between the low icing probability scores of the cirrus shield over the eastern Great Lakes and the high probability scores of the fog in the Atlantic Ocean is quite evident.

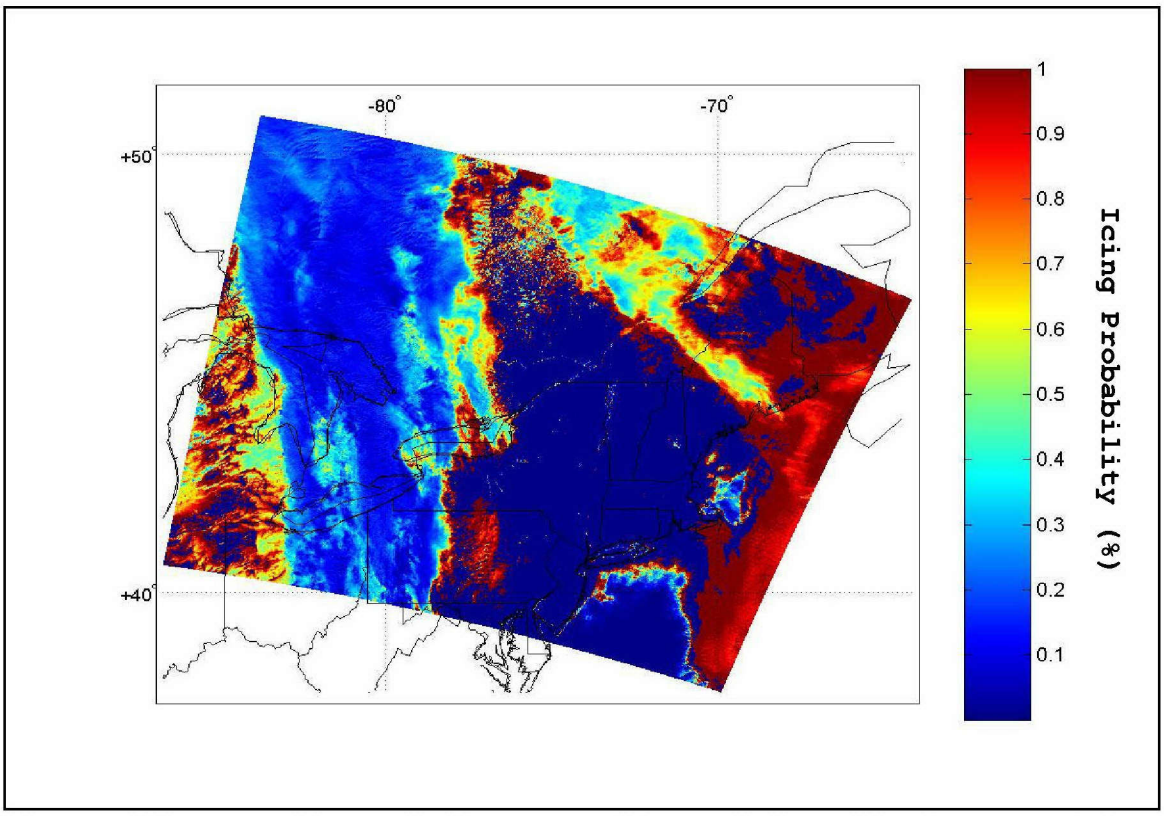

Figure 23. Channel 6 versus Channel 1 reflectance ratio (P61) test for icing probability.

Like the P61 test, the test of reflectance ratios between Channel 7 and Channel 1 reflectance (P71) is very effective at water versus ice cloud discrimination. The P71 test also allows more thin cloud or partly cloudy regions to be considered in the icing potential determination. While some of the thin fog over northeast New England and along Long Island is washed out in the P61 results, these regions are correctly identified as SLD clouds in the P71 results. As Figure 24 illustrates, this inclusion of thin and partly cloudy pixels is successful without diminishing the contrast between high and low icing probability regions discussed for the P61 test.

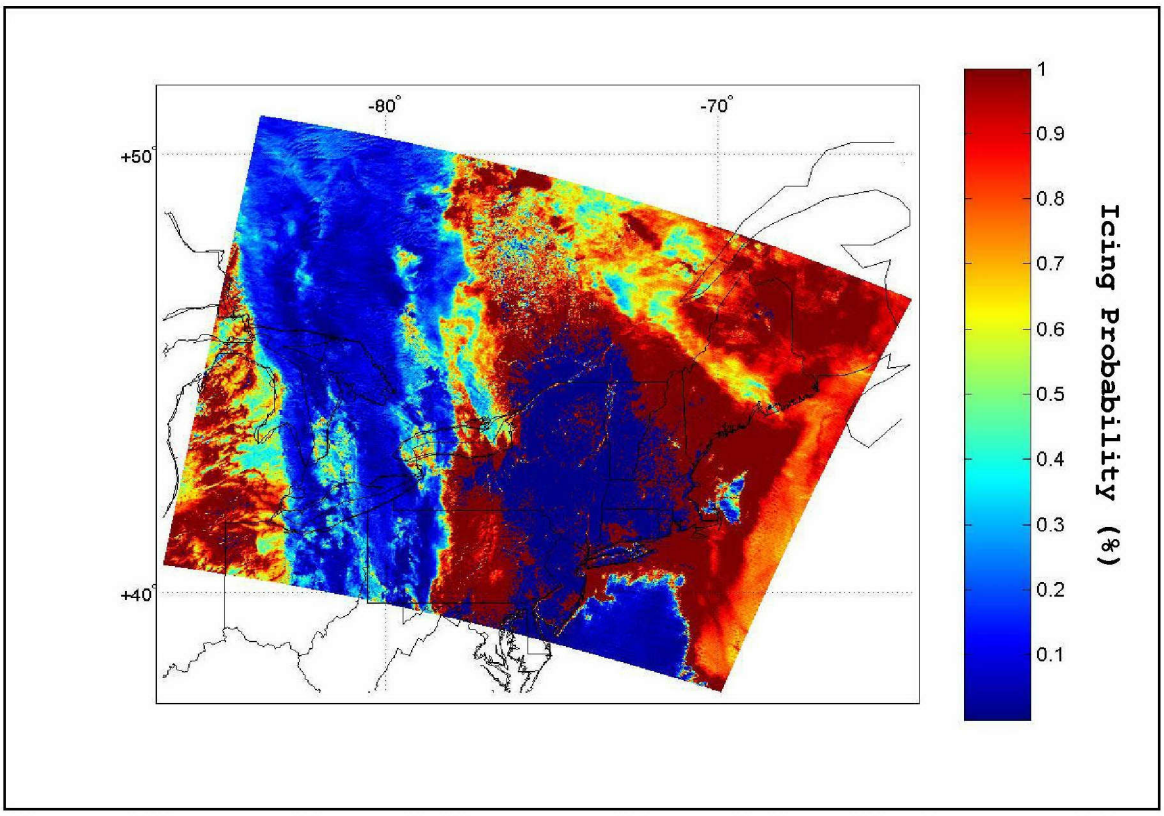

Figure 24. Channel 7 versus Channel 1 reflectance ratio (P71) test for icing probability.

The maximum scores from the 2 reflectance ratio tests indicate that Group II effectively screens out the majority of cloud free regions while allowing a sharper distinction between clouds with high and low icing potential. Figure 25 demonstrates the results of Group II. The inclusion of thin and partial cloud pixels by the P71 test is replicated in the final Group II scores.

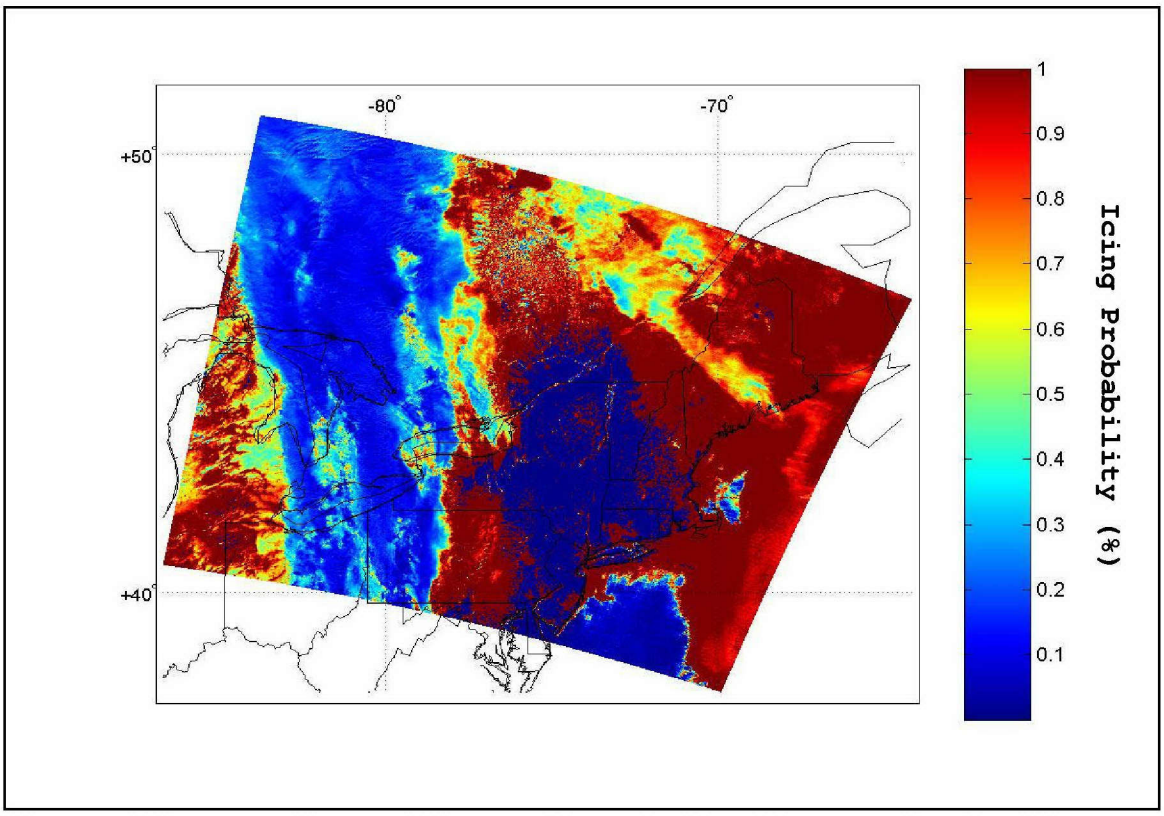

Figure 25. Group II results, indicating each pixel's maximum icing probability score for the 2 reflectance ratio tests.

C. GROUP III RESULTS

The lone test in Group III is the Channel 31 brightness temperature (T31) test. The importance of temperature to the determination of icing potential has been noted previously in Section II. The T31 test limits the potential icing region to cloud tops within the range of temperatures for which SLD clouds are possible. Figure 26 shows that while the water clouds found over Michigan fall within the SLD limits, the fog and stratus over central Pennsylvania and off the New England coast have cloud top temperatures above freezing. Although in this case the land surface temperature over central New England is above freezing, high latitude or mountainous regions with sub-zero surface temperatures can have anomalous icing

potential in other cases. This indicates that in future work the T31 test should be applied after the application of cloud mask to remove cloud-free pixels. Because Group III only contains the T31 test, the Group III icing probability results are identical to those for T31 (Figure 26).

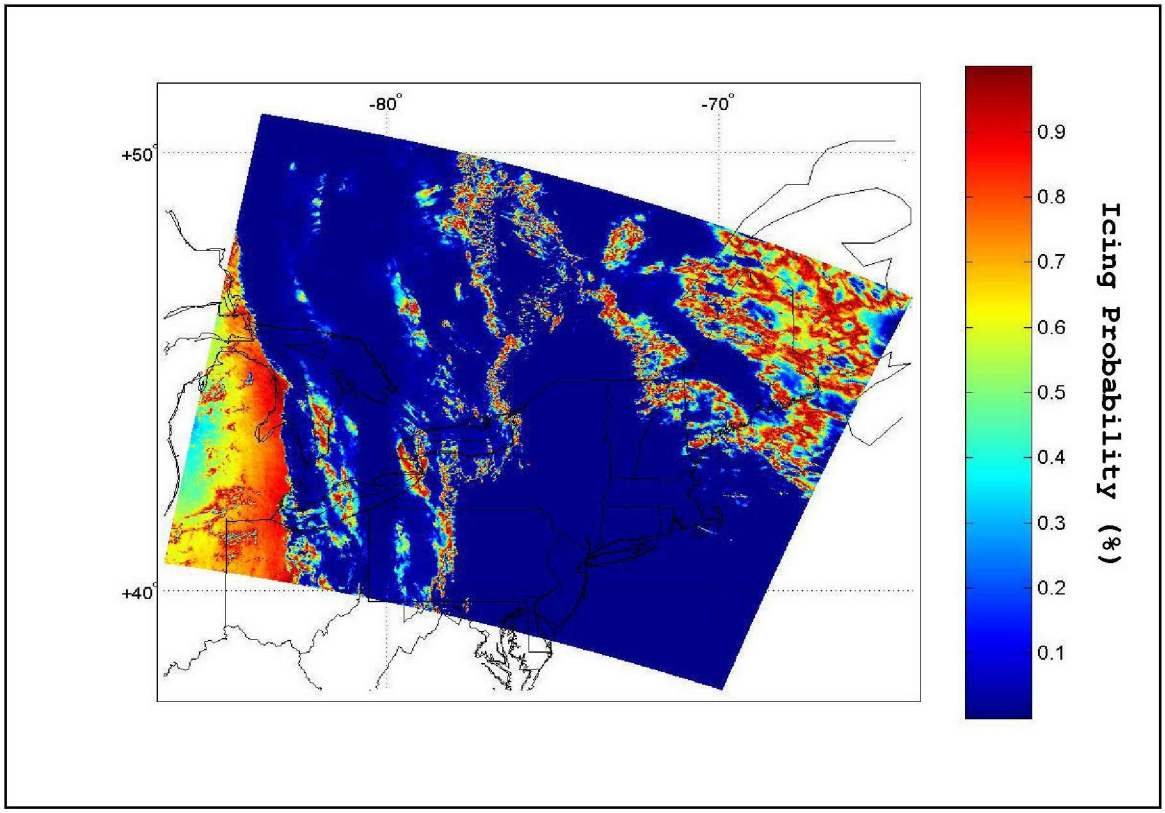

Figure 26. Channel 31 brightness temperature (T31) test for icing probability. Figure also represents Group III results.

D. GROUP IV RESULTS

The final group of tests is a series of brightness temperature difference tests to discriminate between water and ice clouds. The first such test is the Channel 22 – Channel 31 brightness temperature difference (BTD1) test. This test is one of the original GOES algorithm tests discussed in Section II. As shown by the P22 test, water

clouds reflect more incident solar energy than ice clouds. Pixels with BTD greater than 10°C will have high icing potential in the BTD1 test. This test is ineffective at eliminating regions of thin cirrus, as evident over Maine and eastern Canada in Figure 27. These are regions where reflected energy from possible water clouds below the cirrus causes higher icing potential than other tests have indicated. The BTD1 test successfully removes cloud-free regions.

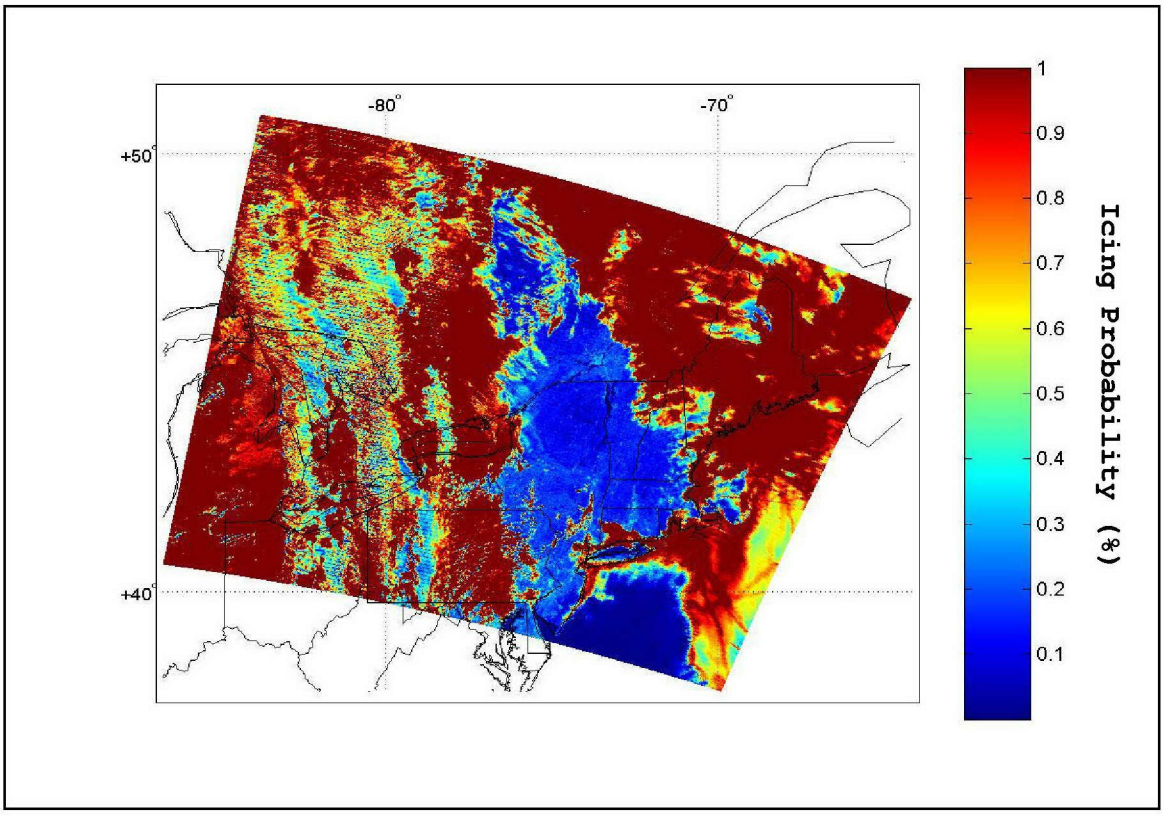

Figure 27. Channel 22 - Channel 31 brightness temperature difference (BTD1) test for icing probability.

The Channel 29 - Channel 31 brightness temperature difference (BTD2) test displays results that are somewhat opposite from those of the BTD1 test. In this case, distinct ice cloud regions have low icing probability, such as the cirrus over much of Quebec in Figure 28. Water

clouds are given much higher icing probabilities than the cirrus regions; however, the cloud-free regions are difficult to discriminate from water clouds. There is also some evidence of higher BTD values in regions of higher surface temperature (i.e. to the south). This effect bolsters the need for a cloud mask to remove cloud-free areas from the test region.

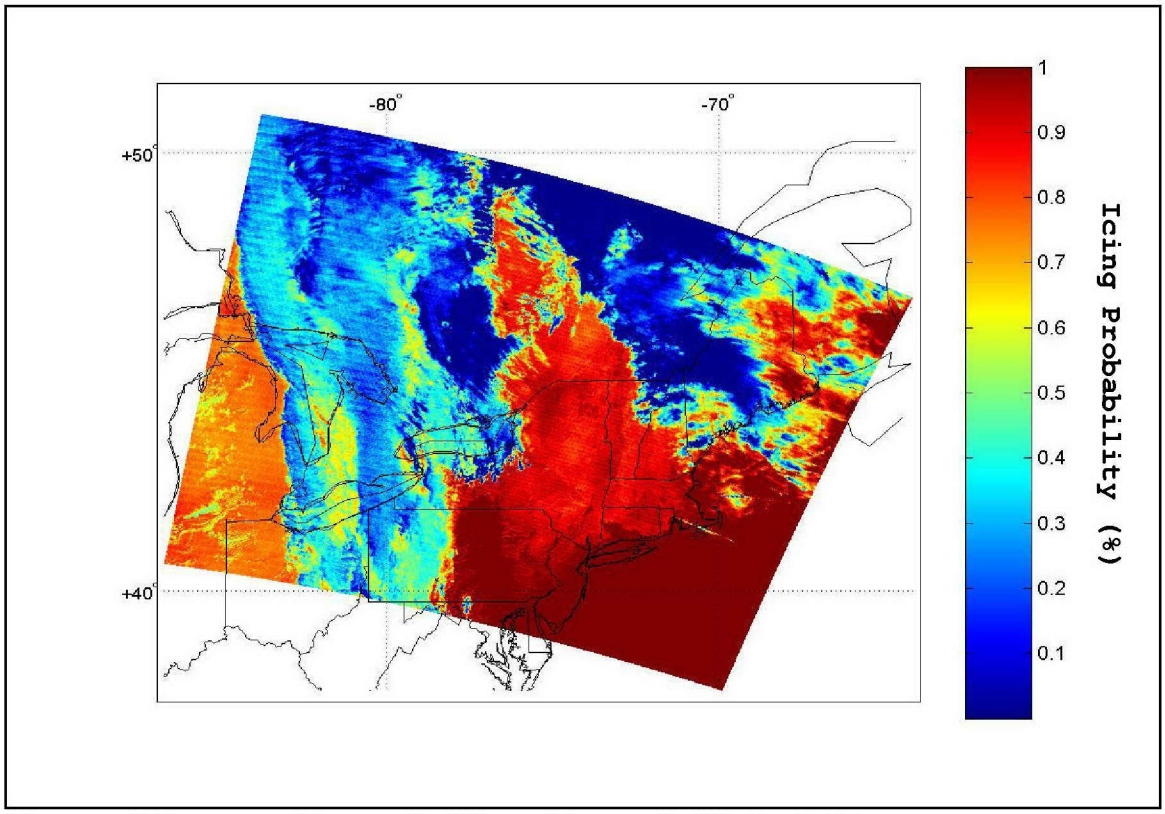

Figure 28. Channel 29 - Channel 31 brightness temperature difference (BTD2) test for icing probability.

The test for Channel 31 - Channel 32 brightness temperature differences (BTD3) was introduced as a thin cirrus test, however it is useful for delineating regions of water clouds, as well. Regions with low BTD values, as seen over Michigan, central Pennsylvania, and the fog deck in the Atlantic Ocean in Figure 29, have a high icing probability. Regions within +/- 1.5°C of a BTD value of 2°C will have low icing probability, as is evident in the

cirrus shield over the Great Lakes and eastern New England. Like the BTD2 test, land regions have comparable BTD values to water clouds, though the surface temperature change does not seem to modify the icing probability results. Also, the ocean surface BTD values for the BTD3 test result in low icing probability, which was not the case with the BTD2 test. Regions of thin water cloud, as seen along the edges of the stratus clouds over central Pennsylvania, have icing probabilities that are too low. This is expected to be nullified by the other BTD tests once the final Group IV test is run.

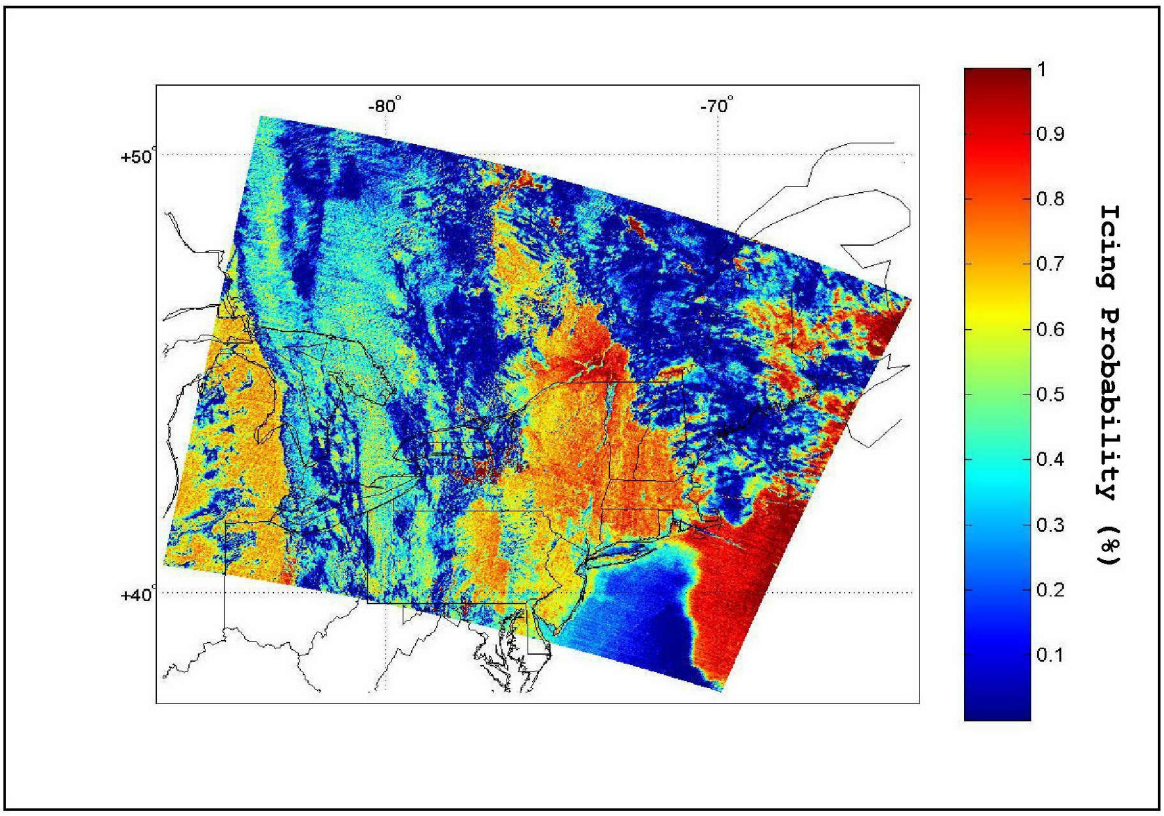

Figure 29. Channel 31 - Channel 32 brightness temperature difference (BTD3) test for icing probability.

The final test in Group IV is the trispectral brightness temperature difference (BTD4) test, which takes the difference between the Channel 29 - 31 BTD and the

Channel 31 - 32 BTD. The BTD4 test is heavily weighted by the results of the BTD2 test. There are slight increases in icing potential in regions of thin cirrus, where high icing potential clouds below the cirrus clouds are more likely to be visible and thus increase the BTD4 icing probability score. This is especially true over Maine as shown in Figure 30, where the cloud type varies across the state. As the BTD2 test indicated, land surfaces are difficult to discriminate from water clouds, and icing probability over cloud-free regions apparently increases with surface temperature.

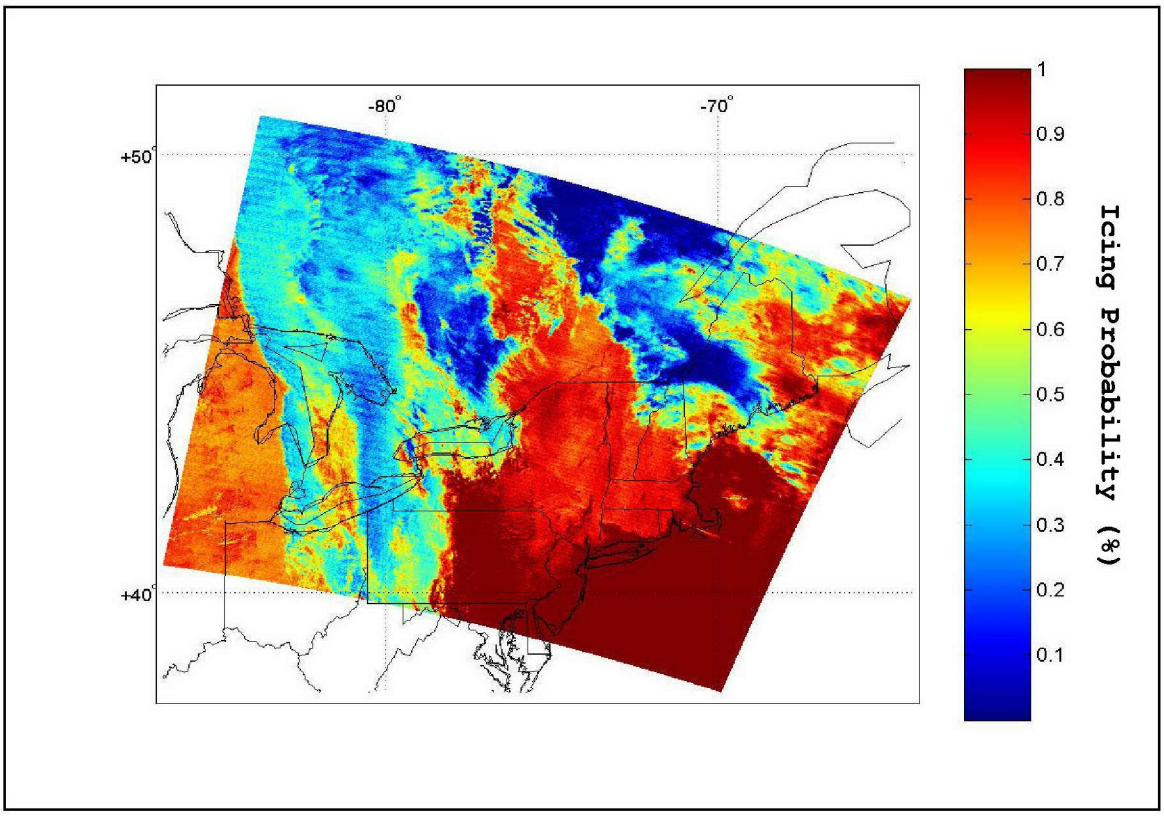

Figure 30. Trispectral brightness temperature difference (BTD4) test for icing probability.

The Group IV results reveal conclusively that a cloud mask will drastically improve the effectiveness and efficiency of the tests (not demonstrated here). The BTD2 and BTD4 tests severely inhibit the differentiation of

water clouds from surface features. As Figure 31 demonstrates, the BTD1 test results weaken the discrimination of ice and water clouds, though the thickest cirrus over the Great Lakes is correctly flagged as having low icing probability. This test's thresholds were based on the GOES algorithm, and should be re-evaluated for use with MODIS imagery to account for thin cirrus effects like those exhibited over Maine and southeastern Canada.

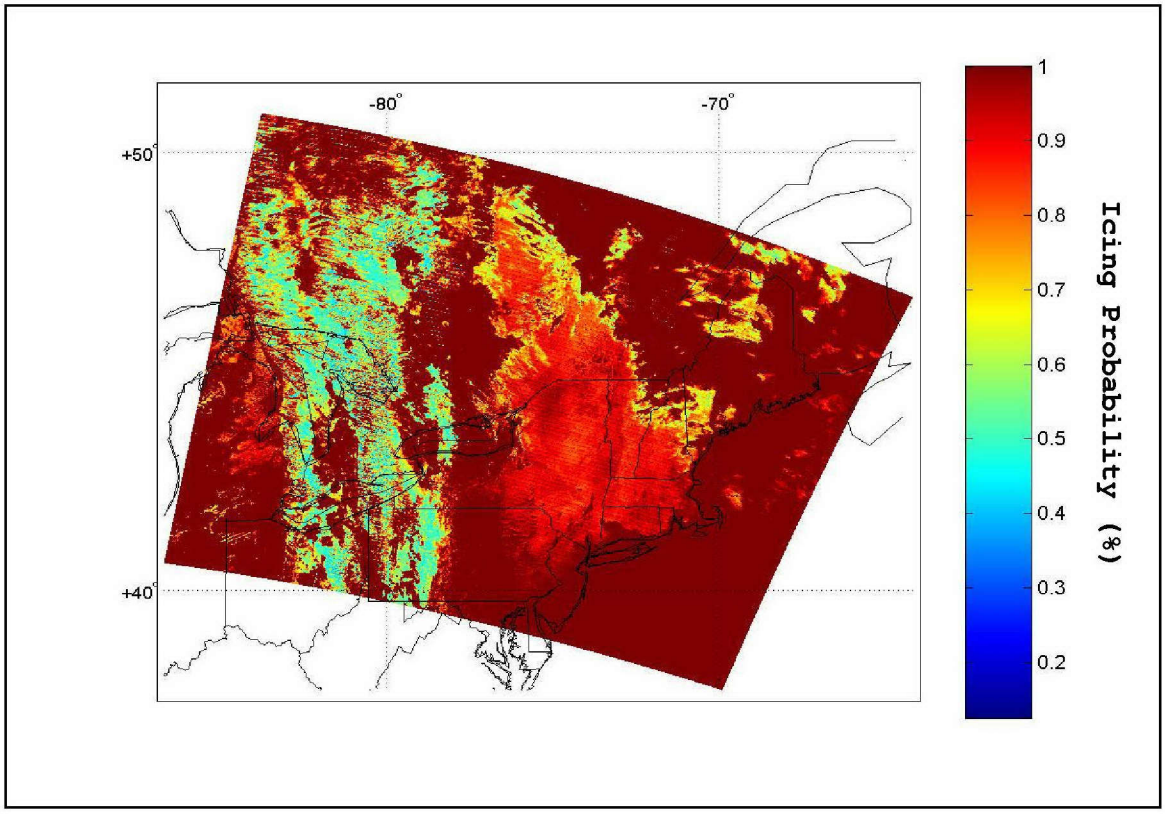

Figure 31. Group IV results, indicating each pixel's maximum icing probability score for the 4 reflectance ratio tests.

E. FINAL RESULTS

Despite the weaknesses indicated for several of the 12 tests used in the MODIS icing potential detection algorithm, the final icing probability product calculated with the maximum values from each group displays remarkable

accuracy. Regions of thick cirrus clouds, such as those stretching from the eastern Great Lakes northward into eastern Ontario have low icing probability scores in Figure 32. The SLD clouds over Michigan, northern Ohio, eastern Maine, and New Brunswick are given high icing probabilities, while the low-level water clouds over Pennsylvania and off the New England coast have low icing probabilities due to the lack of sub-zero cloud top temperatures. Regions of thin cirrus over water clouds and mixed cloud scenes are given icing probabilities between 30 and 70 percent.

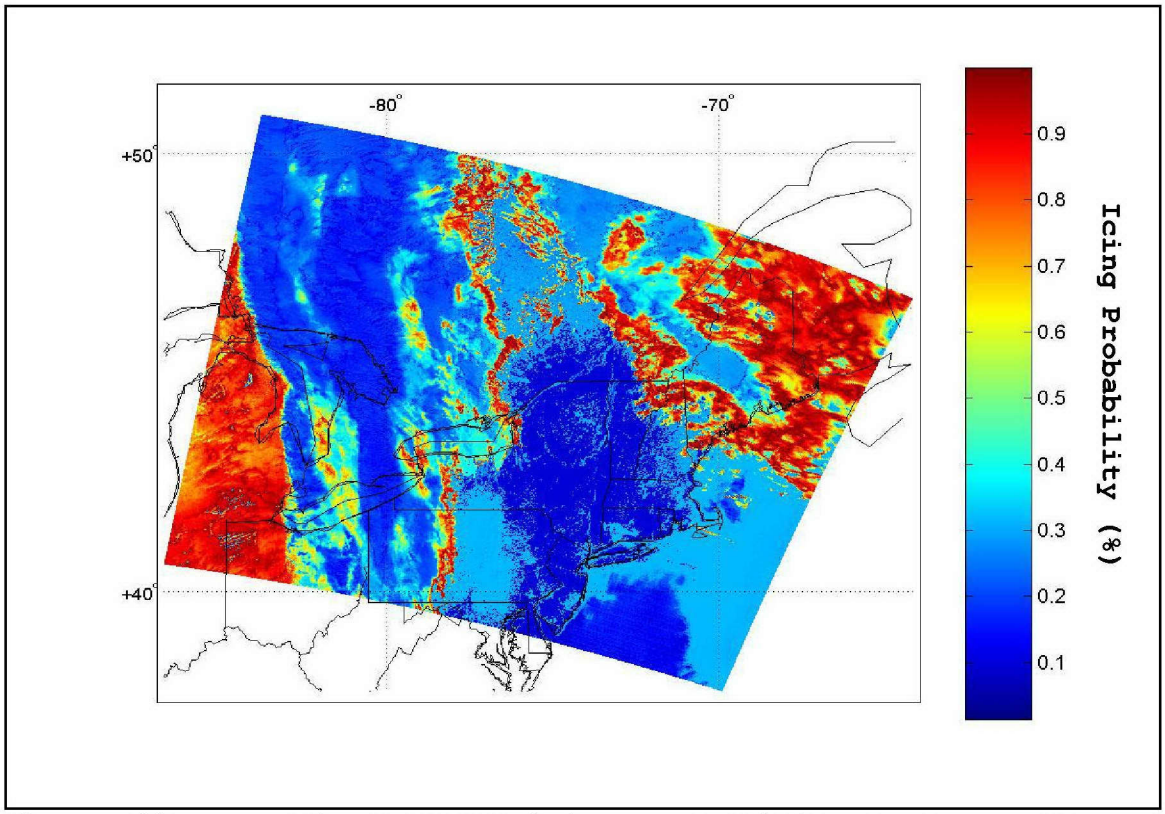

Figure 32. Final MODIS icing probability test results.

In comparison, the GOES algorithm's hard thresholds place spatial limitations on the regions that are considered to have high icing potential. Figure 33 depicts MODIS imagery processed with a GOES-equivalent icing potential detection algorithm exhibiting the same

thresholds and characteristics as the test used by NCAR. Pixels where the GOED algorithm detects icing potential are shaded white, while pixels with no icing potential are shaded based on false-color IR brightness temperature. While the region considered by the GOES test to have high icing potential roughly matches the region of high icing probability on the MODIS test, the area covered by the GOES icing potential flag is one-third the size of MODIS algorithm's high icing potential region for this case.

The November 11, 28, and 30, 2003, cases also have large coverage differences, allowing the MODIS algorithm to assign an icing probability to 2 to 3 times as much area as the GOES algorithm. The final results of the MODIS and GOES algorithms for these cases are shown in Figures 34–36.

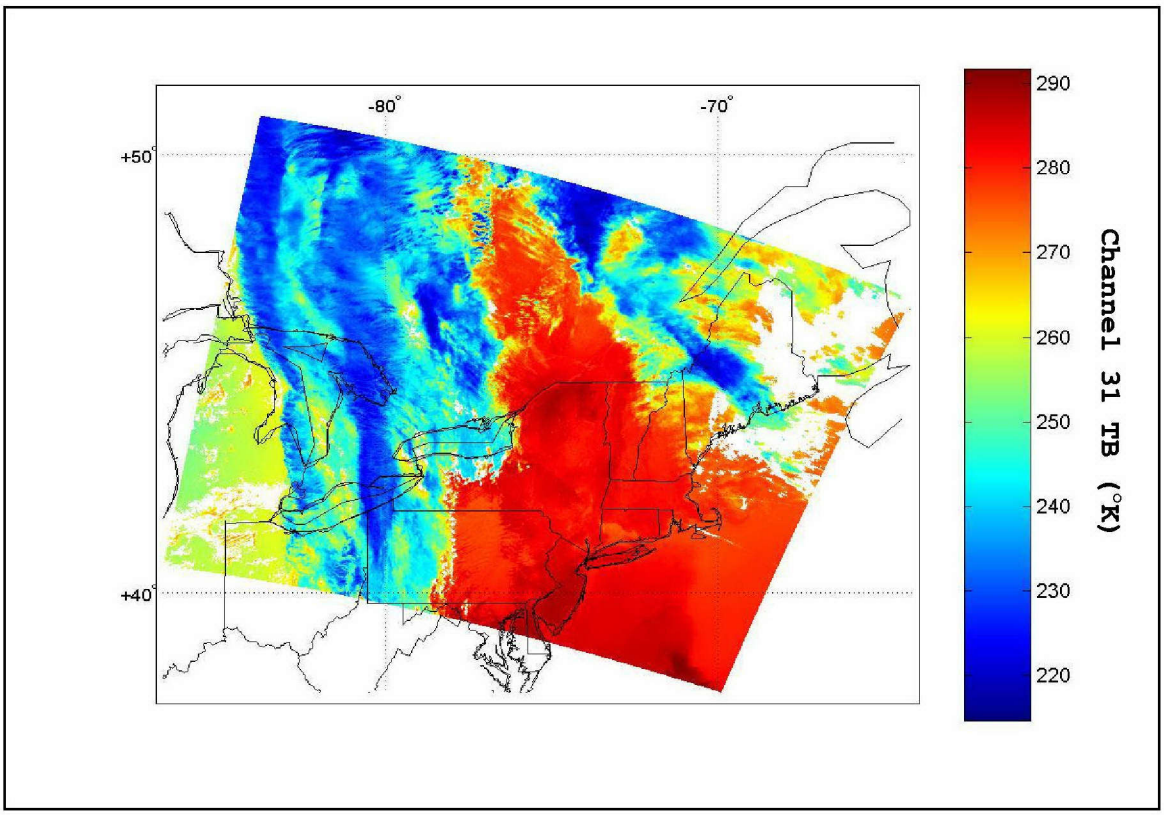

Figure 33. GOES icing potential algorithm results for November 24, 2003. Icing areas are shaded white; otherwise, Channel 31 brightness temperature is used.

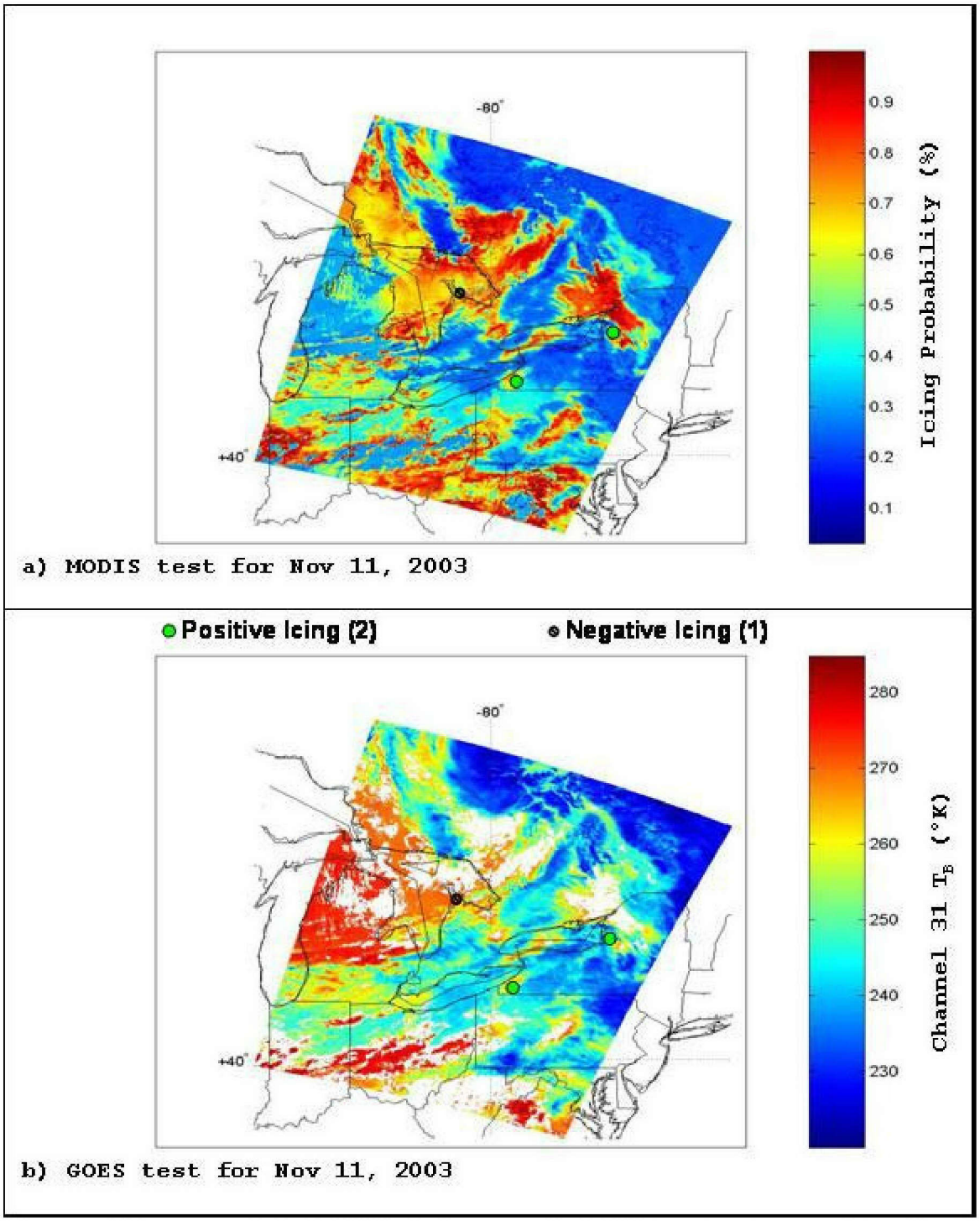

Figure 34. (a) MODIS icing probability test results for November 11, 2003. (b) GOES icing potential test results (icing areas in white) for November 11, 2003. Positive and negative icing PIREPS for November 11th are overlaid.

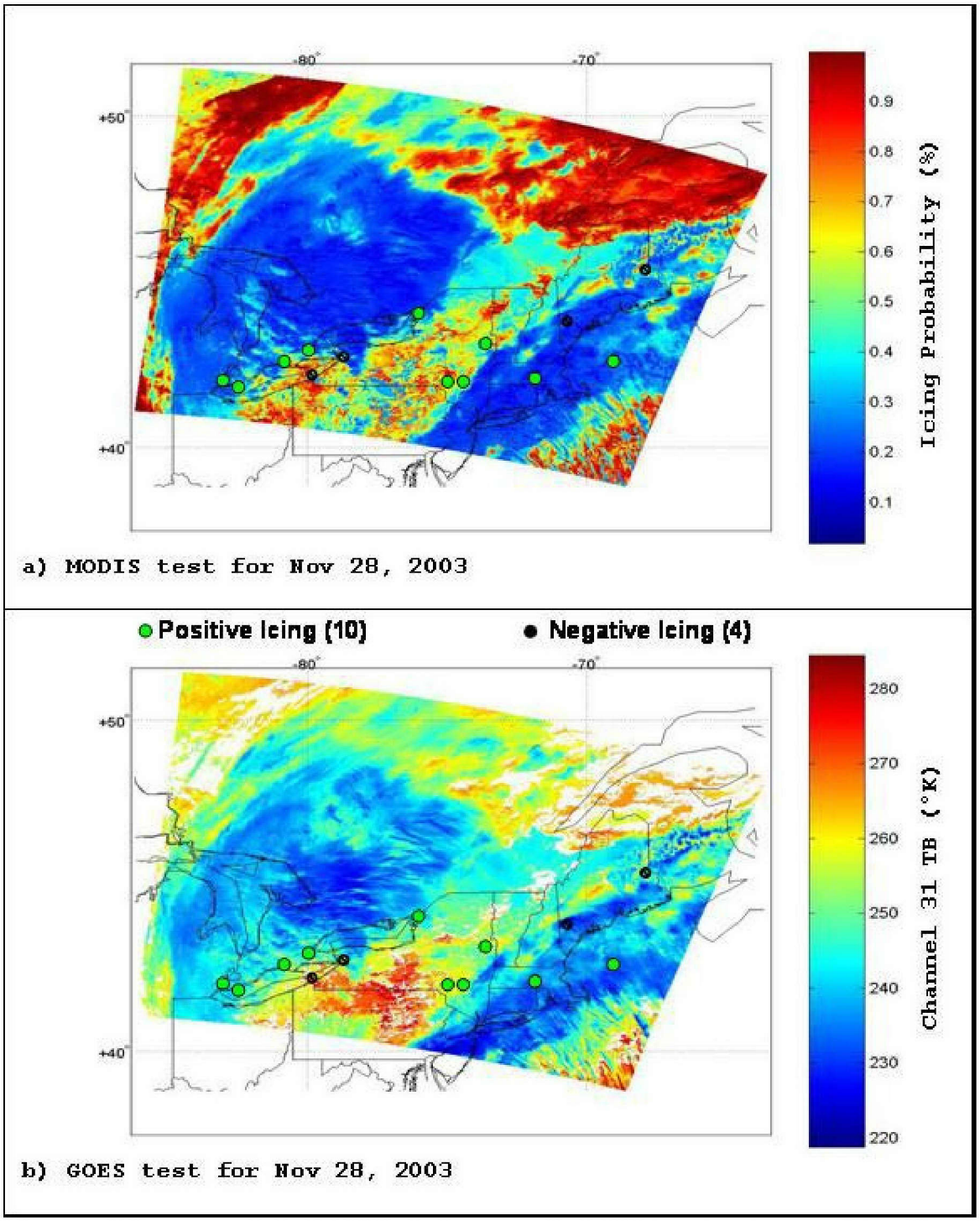

Figure 35. (a) MODIS icing probability test results for November 28, 2003. (b) GOES icing potential test results (icing areas in white) for November 28, 2003. Positive and negative icing PIREPS for November 28th are overlaid.

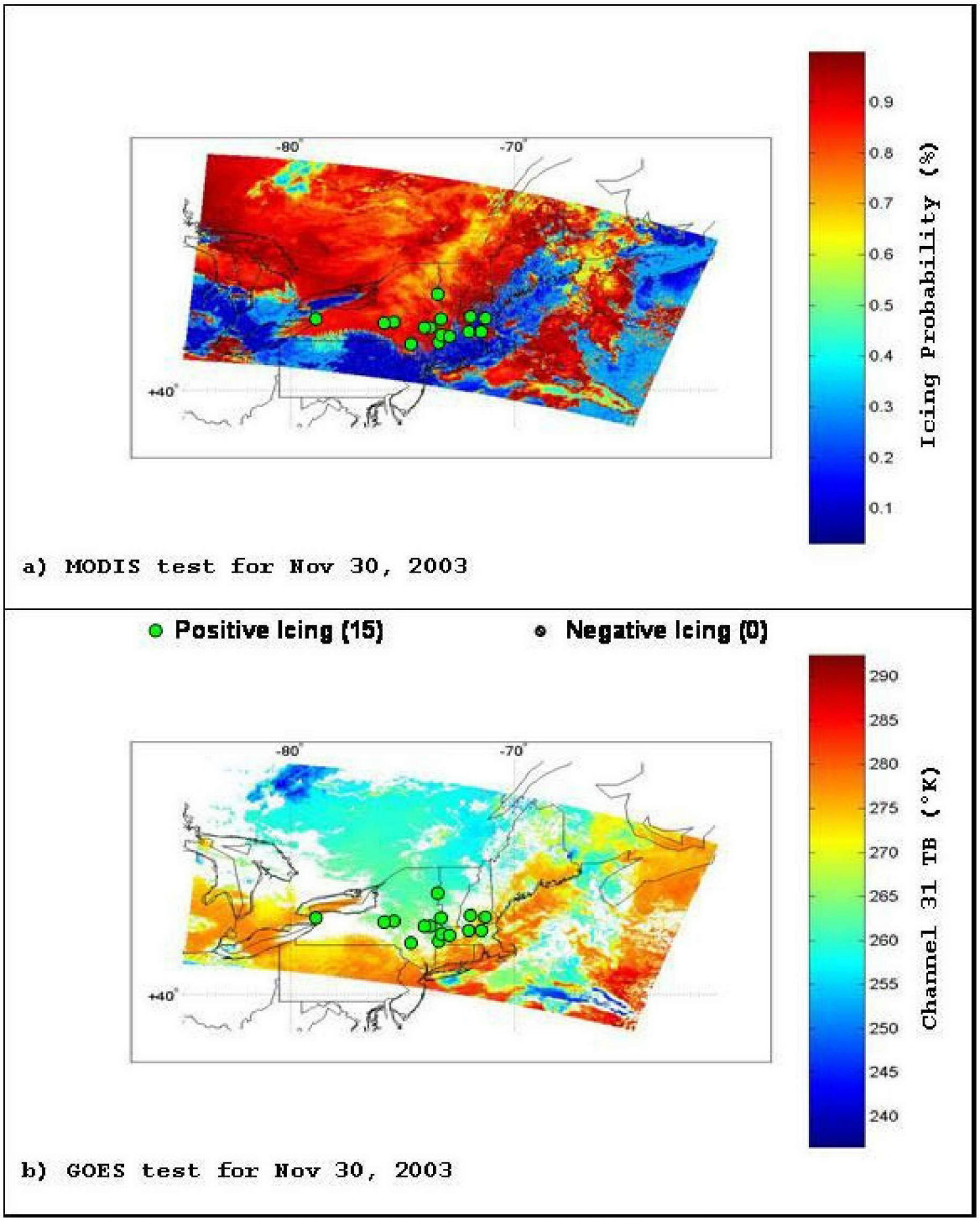

Figure 36. (a) MODIS icing probability test results for November 30, 2003. (b) GOES icing potential test results (icing areas in white) for November 30, 2003. Positive icing PIREPS for November 30th are overlaid.

F. STATISTICAL COMPARISON

Statistical results for the final MODIS and GOES icing potential algorithms were gathered for all 4 cases. The MODIS and GOES algorithm outputs were verified using PIREPs in the region to determine the probability of detection for positive icing PIREPS (POD), the POD for negative icing PIREPS (POD-no), and the area efficiency (AE) of both algorithms, defined as POD per unit area. These statistics were calculated within 25 miles of each PIREP. The results were grouped into 3 time ranges on each day: all PIREPS on the date of the MODIS image; PIREPS reported within 3 hours of the MODIS image valid time, and PIREPS reported within 1 hour of image valid time. The use of reports within 3 hours and 1 hours of image valid time is straightforward. The use of all PIREPS reported on the day of an image is sometimes appropriate given the low time resolution of Terra MODIS imagery (Two products per day are possible when the MODIS sensor onboard Aqua is included).

Table 7 shows the results of the GOES algorithm and the MODIS algorithm mean and median scores within 25 miles of all PIREPS on November 11, 24, 28, and 30, 2003. The MODIS algorithm detects icing potential within 25 miles of positive icing PIREPS throughout the day much better than the GOES algorithm. This is likely a result of the limited coverage allowed by the hard thresholds used in the GOES algorithm as discussed in Section III. The GOES algorithm correctly determines that all negative icing PIREPS are in regions of low icing potential, though the MODIS results for POD-no are higher than for POD. The MODIS algorithm is twice as efficient as the GOES algorithm in its detection of high icing probability areas. This result is the opposite of that found by Brown (1996), who indicated that generally algorithms with smaller POD values will have higher AE values. This discrepancy is likely due to POD for the GOES algorithm being sufficiently small to drive the GOES

algorithm's AE much lower than that of the MODIS algorithm. Small differences in POD and AE between the MODIS mean and median results indicate that the distribution of algorithm values is fairly normal for pixels within 25 miles of each PIREP. The POD-no score displays a wider difference of scores; however, this test is not as reliable as POD and AE due to the limited number of negative PIREPs available. The mean provides a more favorable score for all 3 tests despite the concerns with the sample size for POD-no.

Table 7. MODIS mean and median and GOES algorithm statistics for all PIREPS on November 11, 24, 28, and 30, 2003.

Test	POD (%)	POD-no (%)	AE (km^{-2})
MODIS Mean	46.2	71.4	0.1041
MODIS Median	41.0	57.1	0.0925
GOES	7.7	100.0	0.0453

The statistics for PIREPS reported within 3 hours of the MODIS image's valid time are displayed in Table 8. The POD for both algorithms increase substantially; however, the MODIS scores for POD-no dropped to 33.3 percent due to correctly identifying only one negative icing PIREP out of 3 that were reported. This small number of reported negative PIREPS renders the POD-no test statistically insignificant, and suggests that broader statistical comparison over a larger region and/or more dates be conducted to further check these results. While the number of positive PIREPS reported fell slightly below the accepted goal of 30 test cases, the POD results suggest a 2-to-1 ratio of correctly identified positive icing PIREPS to missed positive icing PIREPS. Again, the MODIS POD was more than twice that of the GOES algorithm. As a result of the increase in the GOES POD and the very small area flagged by the GOES algorithm as having icing potential, the AE of the GOES algorithm slightly surpasses that of the MODIS algorithm. This agrees with Brown's (1996) assessment of the trade-off between POD

and AE mentioned previously. At this point, MODIS mean and median values are equal, indicating an even distribution of MODIS icing algorithm scores around the PIREPS.

Table 8. MODIS mean and median and GOES test results for PIREPS on November 11, 24, 28, and 30, 2003, within 3 hours of MODIS image valid times.

Test	POD (%)	POD-no (%)	AE (km^{-2})
MODIS Mean	62.5	33.3	0.1409
MODIS Median	62.5	33.3	0.1409
GOES	25.0	100.0	0.1472

Though only 8 PIREPS were reported within 1 hour of the MODIS image valid times on the dates of the 4 cases, general trends can be identified from the results, which are depicted in Table 9. The POD for the MODIS mean and median values increased to 71.4 percent, while the MODIS algorithm incorrectly detected high icing probability for the one negative PIREP reported during this period. The GOES algorithm POD nearly doubled to 42.9 percent, causing a subsequent doubling of the GOES algorithm's AE. The AE for the GOES algorithm seems to continue to be higher than indicated by the POD due to the very small area covered by the icing potential flag.

Table 9. MODIS mean and median and GOES algorithm statistics for those PIREPS on November 11, 24, 28, and 30, 2003, reported within 1 hour of the MODIS image valid times.

Test	POD (%)	POD-no (%)	AE (m^{-2})
MODIS Mean	71.4	0.0	0.1611
MODIS Median	71.4	0.0	0.1611
GOES	7.7	100.0	0.2523

The overall statistical comparison of the MODIS and GOES algorithms indicates that the MODIS algorithm better identifies regions of high icing potential as indicated by positive icing PIREPS. This is expected since the use of

maximum values in each test group biases the algorithm toward finding more icing. The GOES algorithm's hard thresholds limited the area determined to have high icing potential, but this small detection region resulted in a much lower POD for GOES than MODIS and a very high POD of negative icing PIREPS. This indicates a bias of the GOES algorithm in finding regions of high icing potential, as the algorithm is much more likely to flag a pixel as having low icing potential. The POD for both algorithms increases as the difference between the PIREP reporting time and the image valid time decreases.

The AE of both algorithms increases as the time between the PIREP and image valid times decreases, as would be expected due to increasing POD. However, the substantial increase in the GOES algorithm's AE with decreasing time difference is easily attributed to the small area detected as having high icing potential. In theory, for every 50 percent drop in area covered, the AE would double given the same POD. In this case, the GOES algorithm's detected icing region is 1/3 of the size of the MODIS algorithm's high icing probability region, thus drastically inflating the AE for GOES. This adds emphasis to the restrictive nature of the hard thresholds used in the GOES algorithm.

V. CONCLUSION

A. SUMMARY

The 36 channels available on MODIS provide increased opportunity to study and measure terrestrial and atmospheric features. The high spatial and spectral resolution of MODIS' sensors allows for high quality, fine-scale analyses, though only once or twice per day for a given region. The current version of GOES icing potential detection algorithm allows for continual analysis of a given region, but with lower spatial resolution using only 5 wavelengths. Three of these GOES channels are used by NCAR to derive icing potential. However, 9 channels from the MODIS platform can be put to use to detect likely icing. In addition to providing an improved satellite-based icing potential detection algorithm, this research can support efforts ongoing efforts to determine which channels are employed on the next generation of GOES satellites.

Four MODIS scenes were investigated to compare a MODIS-based version of the 3-channel GOES icing potential detection algorithm with a new 9-channel MODIS icing probability detection algorithm. The MODIS algorithm contains 12 tests, placed in 4 test groups: reflectance tests, reflectance ratio tests, brightness temperature test, and brightness temperature difference tests. The tests were compared to positive and negative icing PIREPS.

While some of the individual tests appear to have inherent weaknesses in discriminating between SLD clouds other scenes (i.e. ice clouds, land or ocean backgrounds), the final MODIS algorithm outperformed the GOES in

detecting positive icing PIREPS. The GOES algorithm was better able to identify regions of negative icing. This was a combined result of its bias towards negative icing detection caused by the use of hard thresholds, as well as the very small areas flagged by the GOES algorithm as having high icing potential. These small icing potential areas also drove the area efficiency of the algorithm much higher than its POD suggests. Both algorithms improve as difference between PIREP valid time and imagery valid time decreases.

The MODIS algorithm's increased responsiveness to regions of high icing probability produces a more conservative approach, for potentially increased aircrew safety when compared to the GOES algorithm's output. However, by limiting high icing potential regions to clouds, the MODIS algorithm could easily diminish the diagnosed icing regions within spatially broad model output fields, allowing for better nowcast support.

B. RECOMMENDATIONS

Several of the tests that make up the MODIS algorithm fail to discriminate between clouds and cloud-free regions. While the end result of the MODIS algorithm shows favorable results, these results could be improved dramatically by running the imagery through the current MODIS cloud mask before the MODIS icing algorithm is processed. The then redundant Channel 1 test could then be removed from the MODIS icing probability algorithm. The thresholds for two of the tests transferred from the GOES algorithm caused weaker delineations between ice and water clouds for Groups I and IV than is possible without these tests. These therefore may require elimination or modification. Further research is needed for the Channel 22 reflectance and

Channel 22 – 31 BTD tests to establish more sensible thresholds for use with MODIS data.

While the results support initial the usefulness of MODIS icing detection, a broader statistical study could improve confidence in the algorithm output. Increasing the number of cases to acceptable statistical standards could help fine tune the MODIS algorithm. There are also other observation methods that would allow for better verification, such as using radiosonde observations, research aircraft measurements, and additional PIREP data such as flight level and temperature. Filtering the PIREP dataset to exclude PIREPS taken above or below cloud layers would purge problem validation data points.

While satellite-based icing potential detection is very accurate over regions of SLD cloud tops, cirrus contamination of SLD remains a problem. Until other remote sensing techniques are effectively applied to solve this problem, it may be useful to troubleshoot problematic pixels from the MODIS icing algorithm. A study into the use of the MODIS algorithm in multivariate techniques such as IIDA, especially for regions where observations are sparse, would likely produce excellent results based on the statistics presented here.

Finally, there may be some merit to investigating whether the restricted spatial coverage of the GEOS algorithm can be improved by replacing the hard thresholds with a set of fuzzy tests as demonstrated here. Based on the increased coverage allowed by using fuzzy set theory for the MODIS algorithm, it could also improve the GOES algorithm's POD and AE.

THIS PAGE INTENTIONALLY LEFT BLANK

APPENDIX

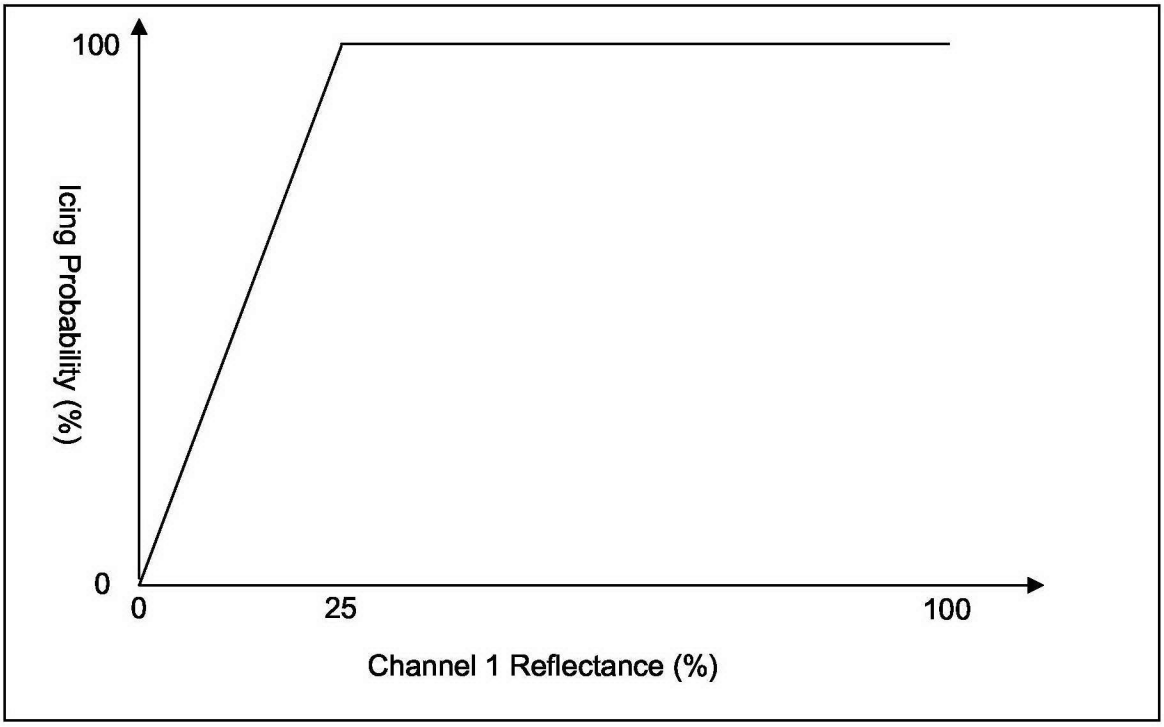

Figure 37. Icing probability test for Channel 1 reflectance.

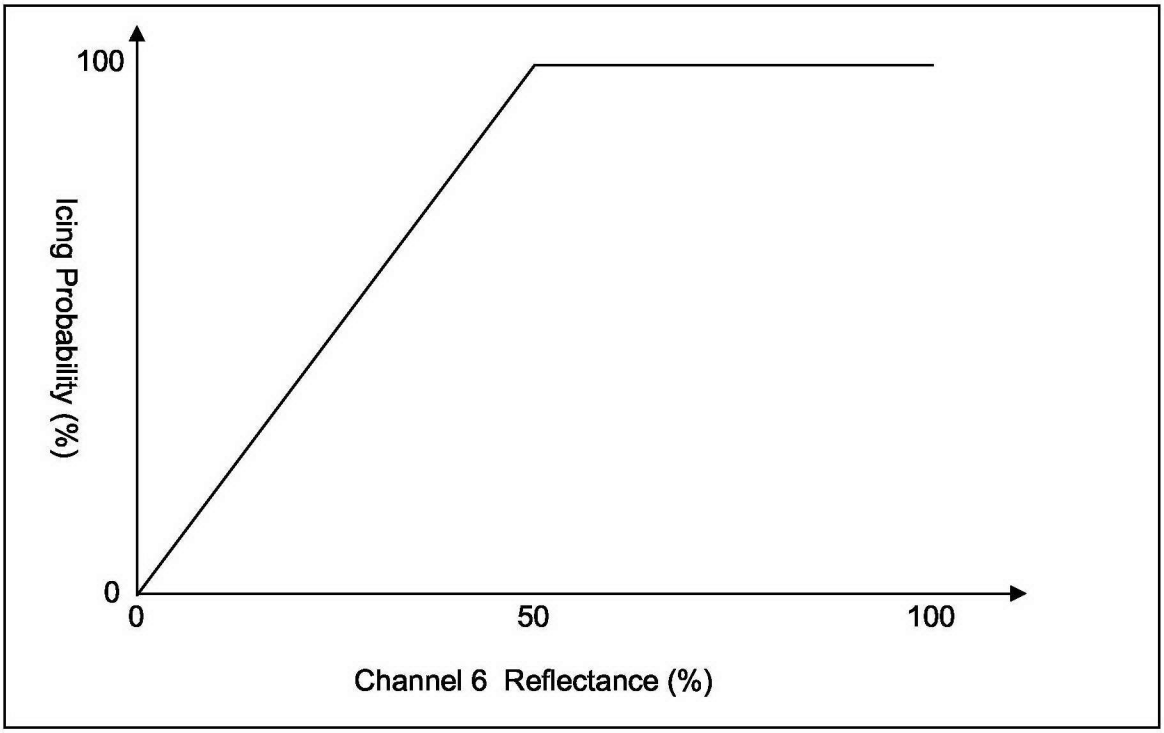

Figure 38. Icing probability test, Chan. 6 reflectance.

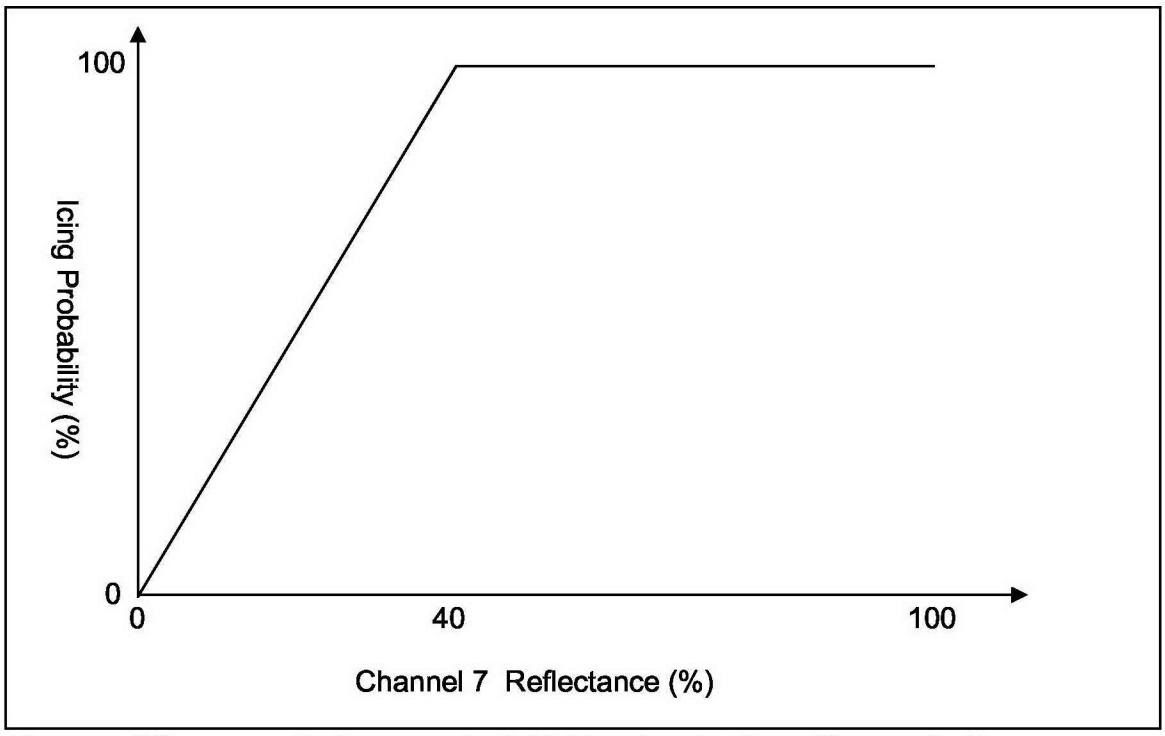

Figure 39. Icing probability test for Channel 7 reflectance.

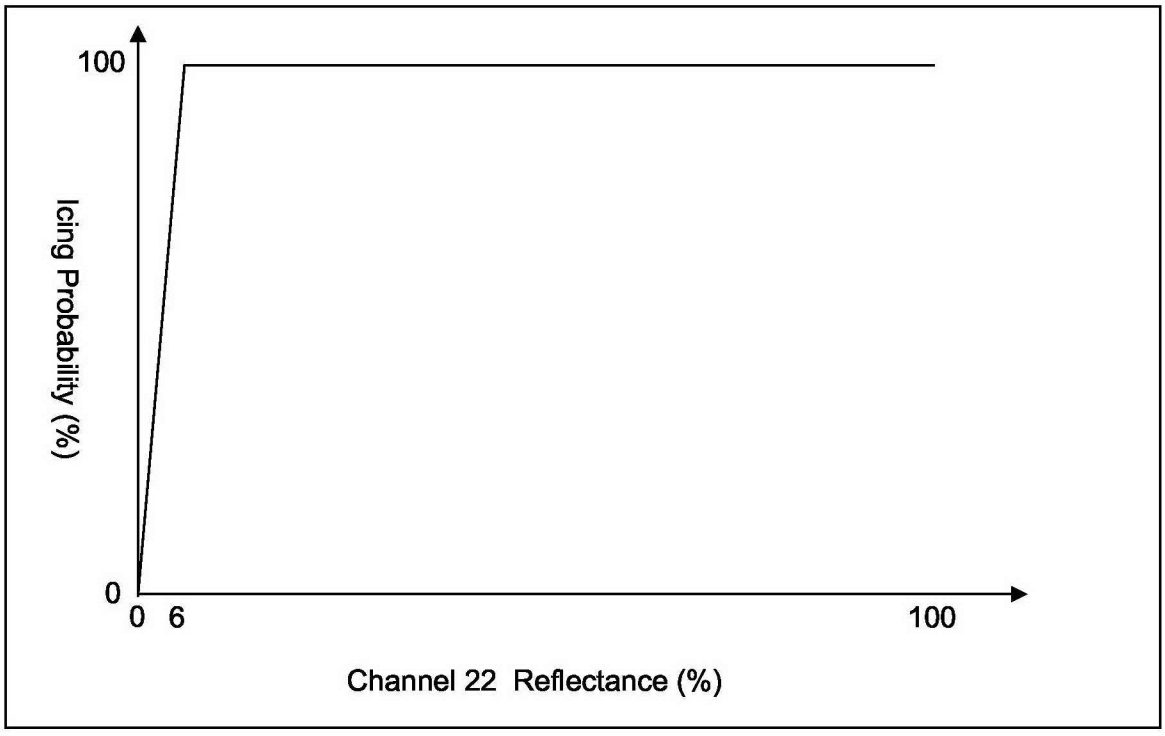

Figure 40. Icing probability test for Channel 22 reflectance.

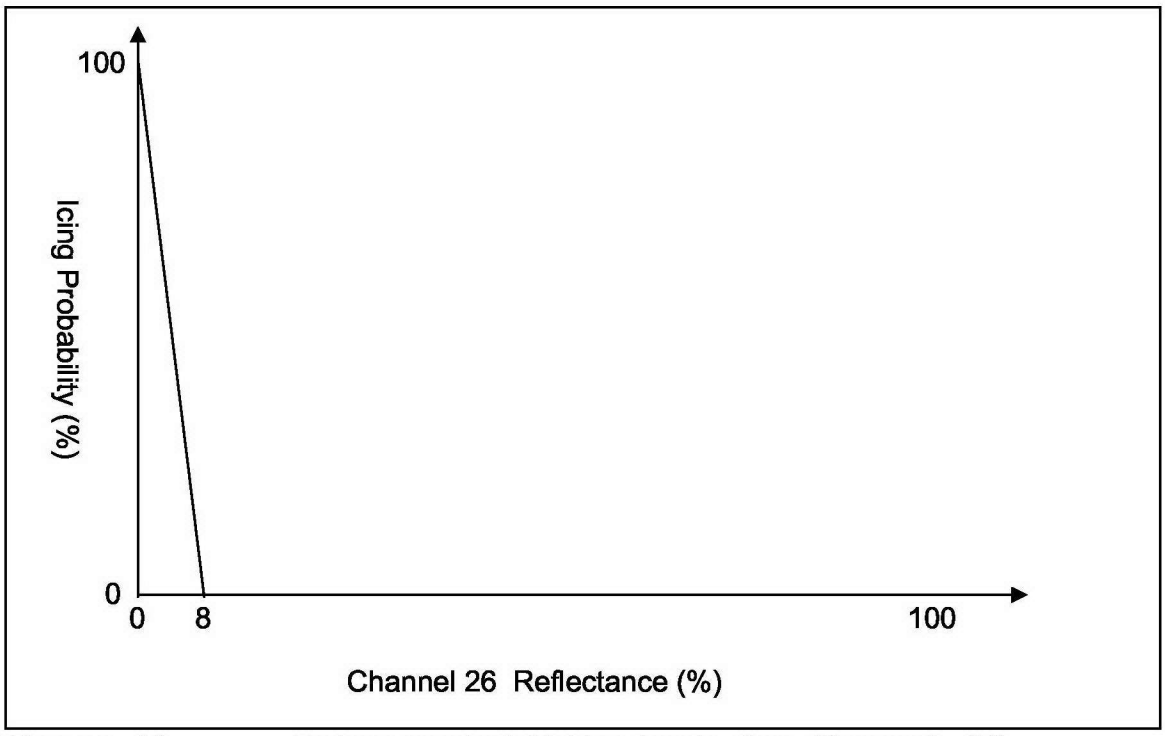

Figure 41. Icing probability test for Channel 26 reflectance.

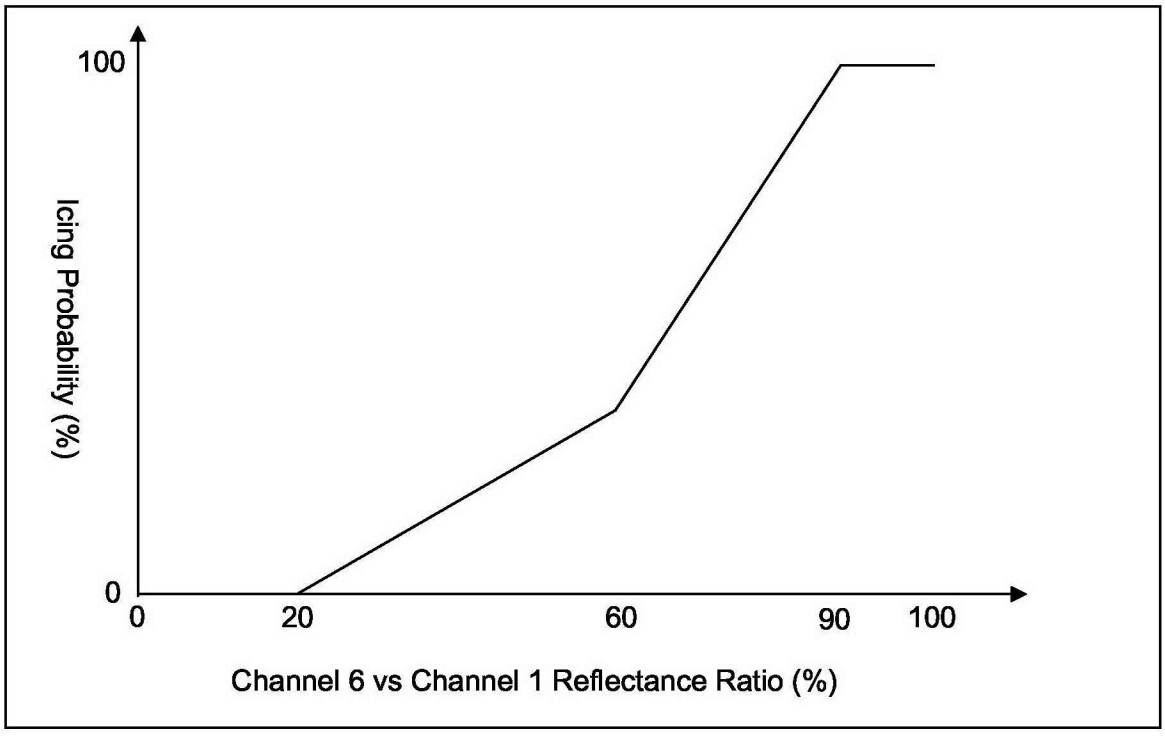

Figure 42. Icing probability test for Channel 6 vs. Channel 1 reflectance ratio.

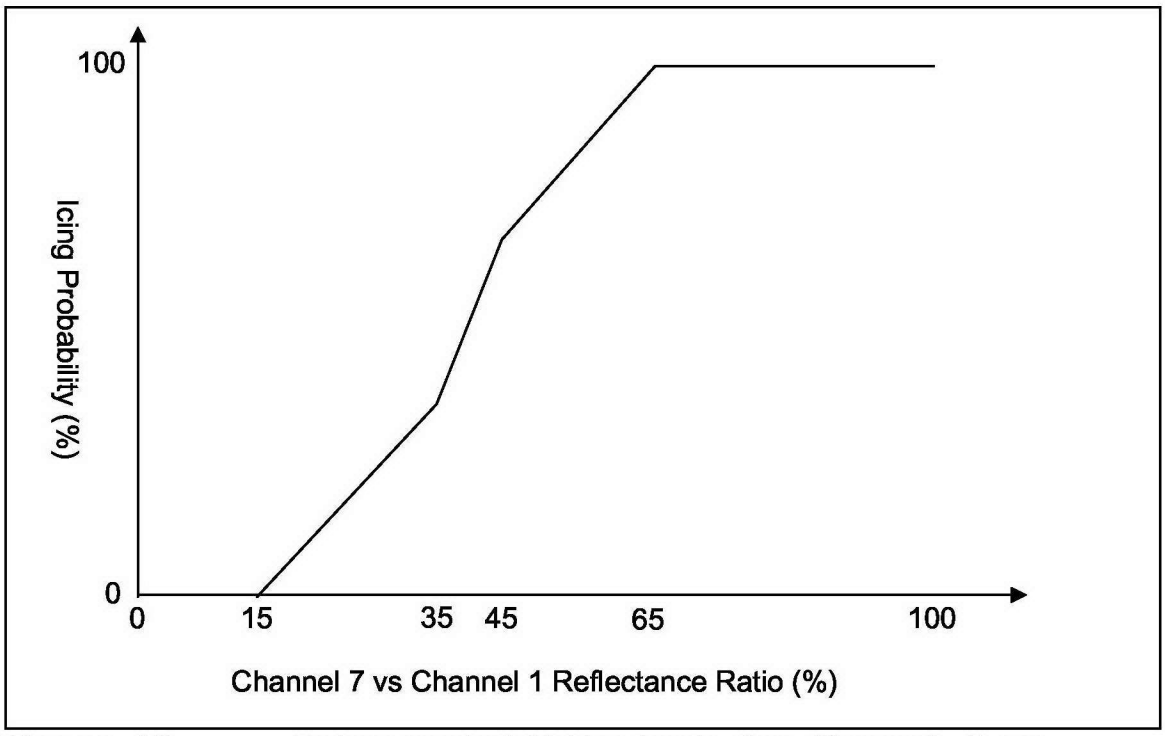

Figure 43. Icing probability test for Channel 7 vs. Channel 1 reflectance ratio.

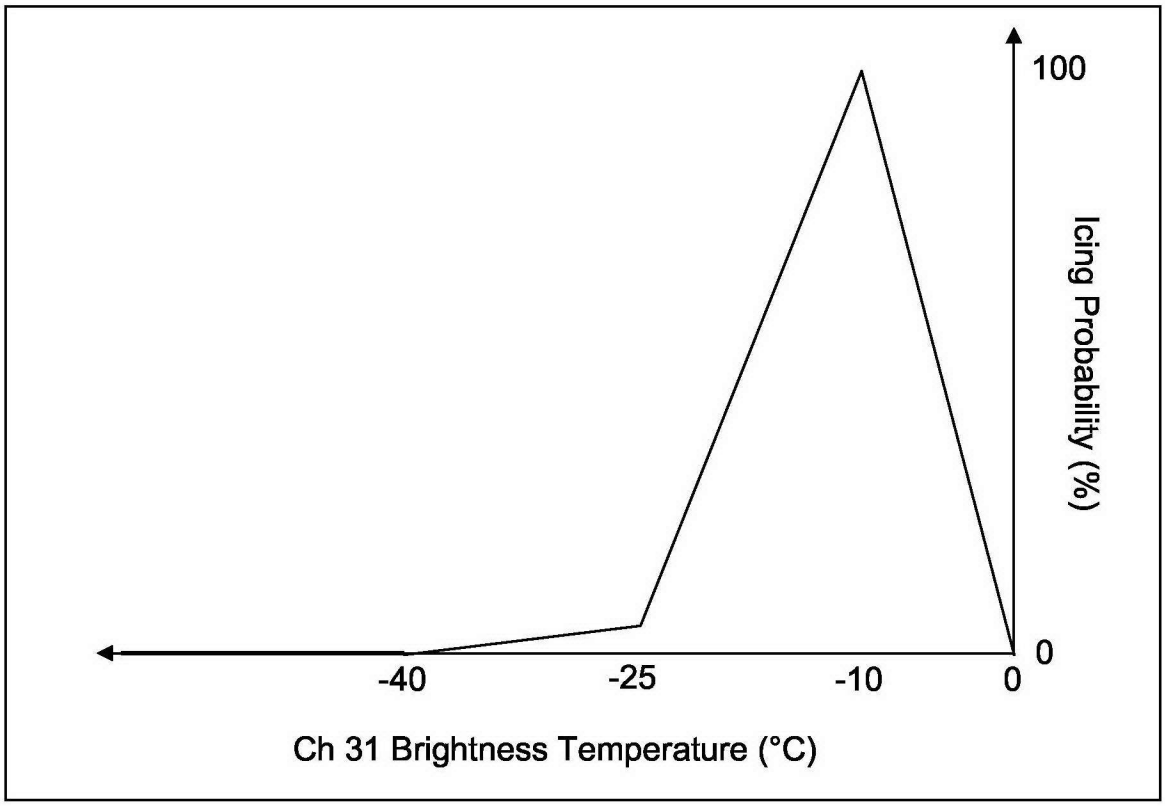

Figure 44. Icing probability test for Channel 31 brightness temperature.

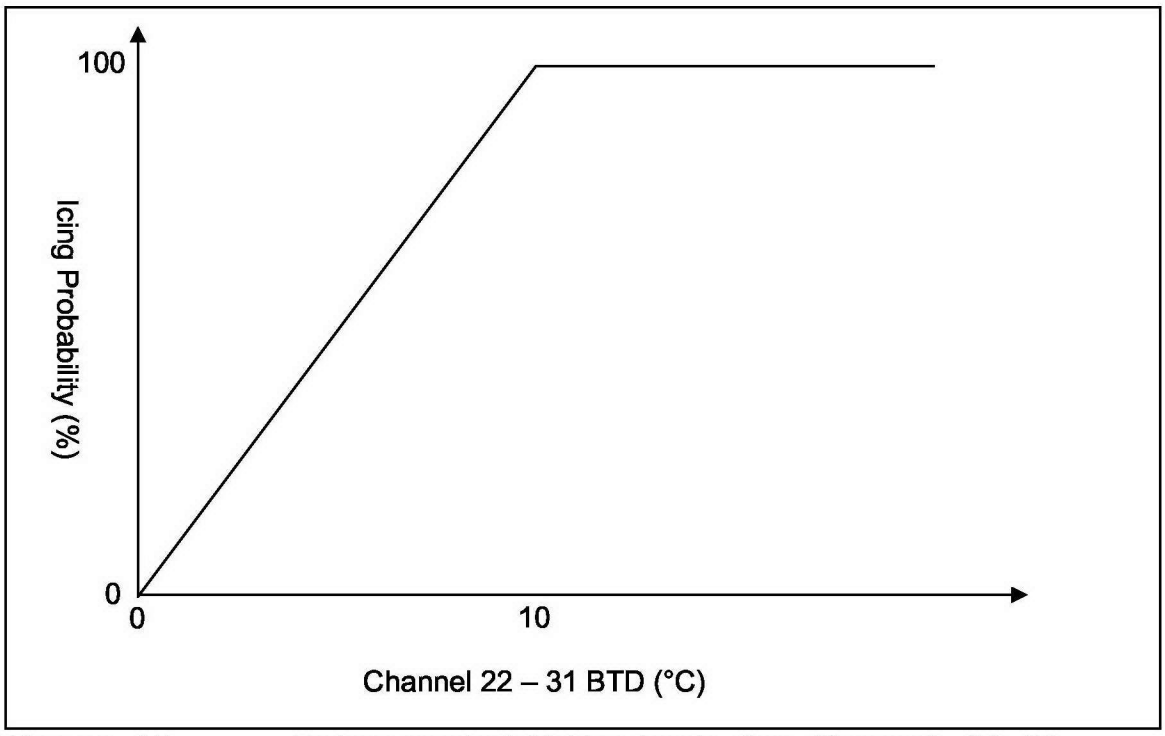

Figure 45. Icing probability test for Channel 22-31 brightness temperature difference.

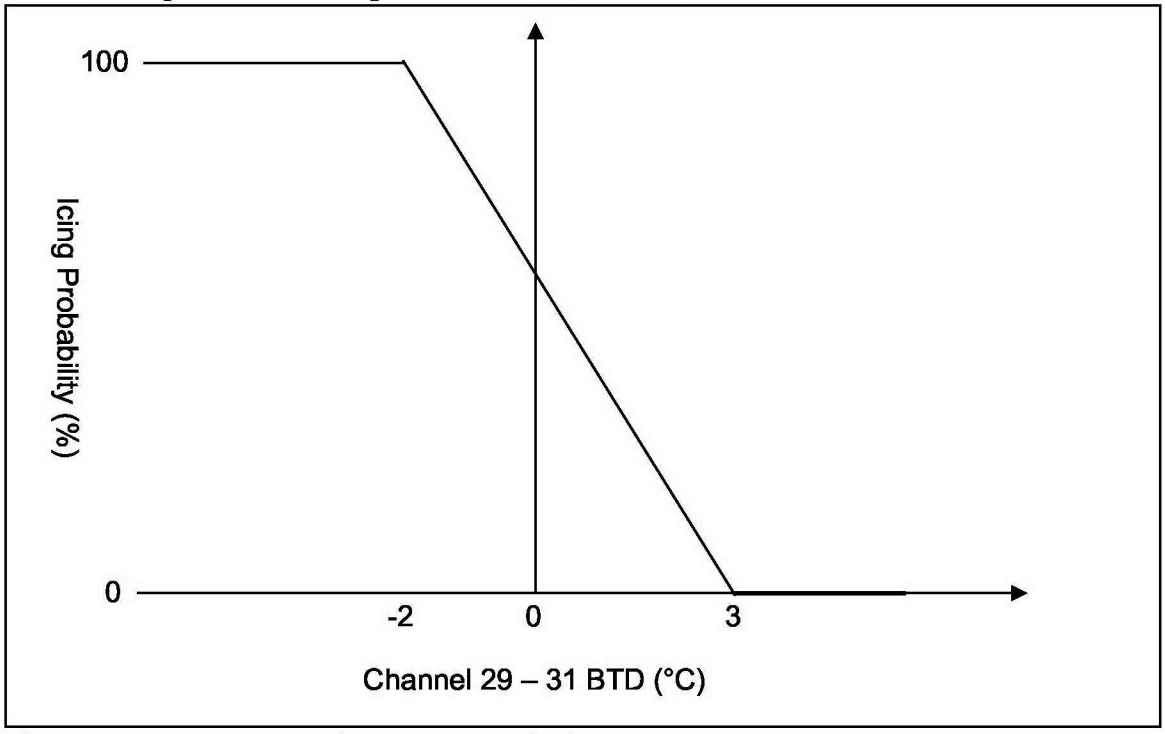

Figure 46. Icing probability test for Channel 29-31 brightness temperature difference.

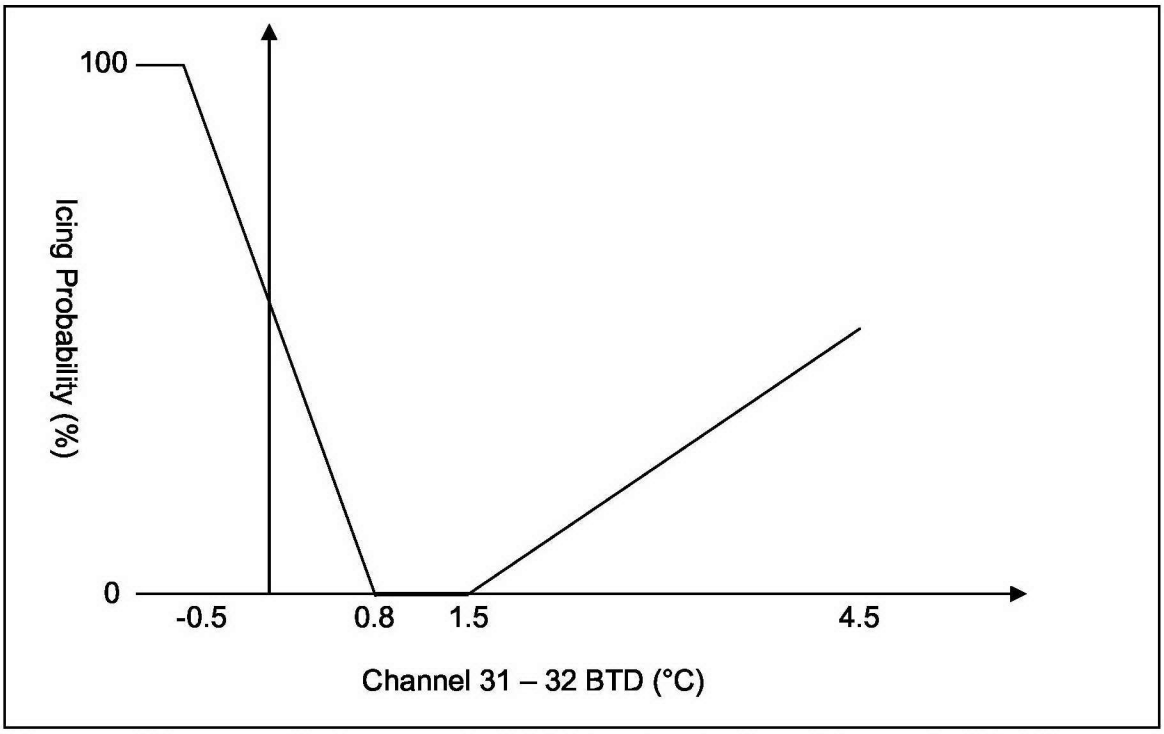

Figure 47. Icing probability test for Channel 31-32 brightness temperature difference.

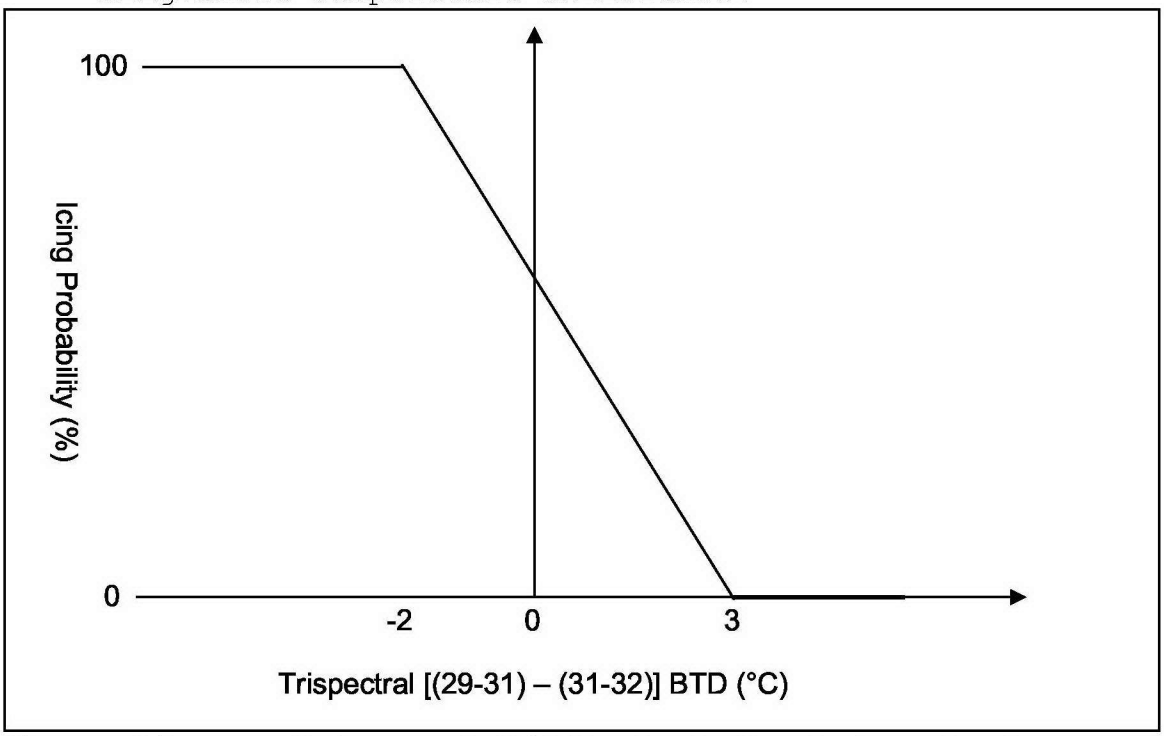

Figure 48. Icing probability test for trispectral brightness temperature difference.

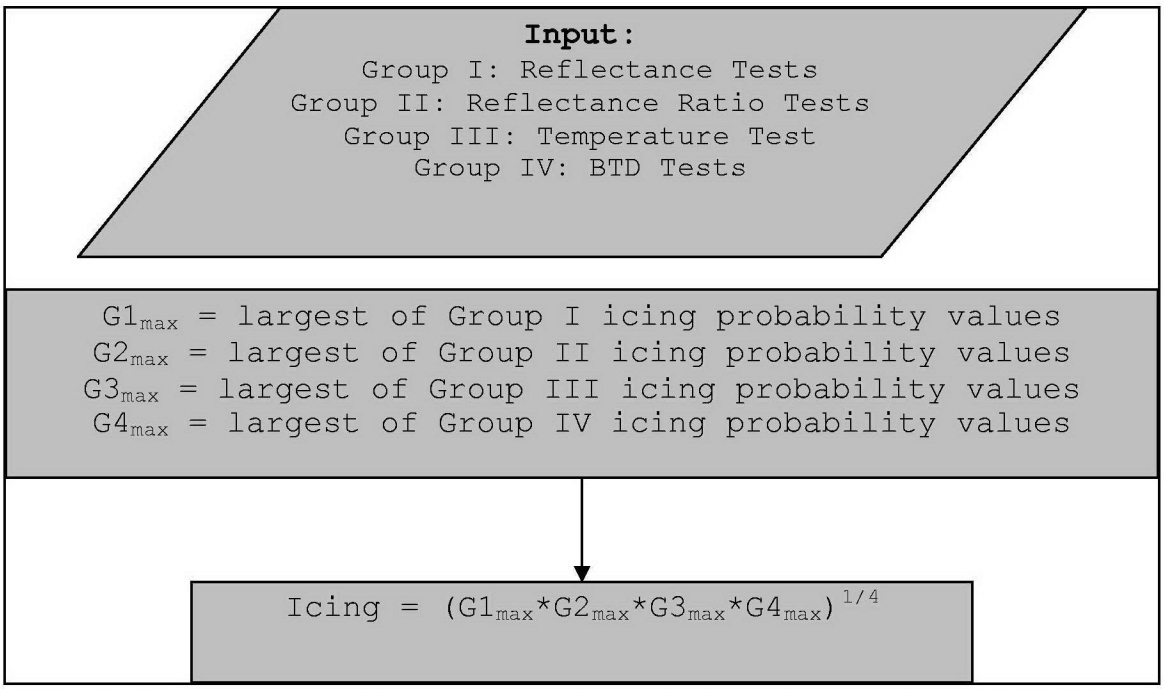

Figure 49. Final icing probability determination test.

THIS PAGE INTENTIONALLY LEFT BLANK

LIST OF REFERENCES

Ackerman, S., K. Strabala, W. Menzel, R. Frey, C. Moeller, L. Gumley, 1998: Discriminating Clear Sky from Clouds With MODIS. *J. Geophys. Res.*, **103, No. D24**, 23141 - 32157.

Air Force Safety Center, 2004: Aircraft Mishap database.

Air Safety Foundation, 2002: Safety Advisor, Weather No. 1: Aircraft Icing. Federal Aviation Administration.

Allen, R., 1987: Automated Cloud Analysis: A Multispectral Approach to the Problem of Snow/Cloud Discrimination. M.S. thesis, Dept. of Oceanographic Studies, Naval Postgraduate School, 114 pp. [Available from Dudley-Knox Library, Naval Postgraduate School, 411 Dyer Rd., Monterey, CA 93943.]

Atlantic THORpex Regional Campaign / Alliance Icing Research Study II, cited 2005: NASA Langley ATReC & AIRS-II Satellite Page. [Available online at http://angler.larc.nasa.gov/bangor/], accessed 25 Sept, 2004.

AWS, 1980: Forecaster's Guide on Aircraft Icing. AWS Tech. Rep. 80/001, 2-1 - 2-3.

Baum, B., P. Soulen, K. Strabala, M. King, S. Ackerman, W. Menzel, and P. Yang, 2000: Remote sensing of cloud properties using MODIS airborne simulator imagery during SUCCESS 2. Cloud thermodynamic phase. *J. Geophys. Res.*, **105, No. D9**, 11781 - 11792.

B.C. Berstein, F. McDonough, M.K. Politovich, and B.G. Brown, 2000: A Research aircraft verification of the Integrated Icing Diagnostic Algorithm (IIDA). *Preprints: 9th Conf. on Aviation, Range and Aerospace Meteor.*, Orlando, FL, Amer. Meteor. Soc., CD-ROM, P4.12.

Brown, B., 1996: Verification of In-Flight Icing Forecasts: Methods and Issues. *Proc. Of the FAA Int'l. Conf. On Aircraft In-flight Icing, Vol. 2 - Working Group Papers.* Springfield, VA, U.S. Dept. of Trans., 319-330.

Brown, B., G. Thompson, R. Bruintjes, R. Bullock, and T. Kane, 1997: Intercomparison of In-Flight Icing Algorithms. Part II: Statistical Verification Results. *Wea. Forecasting*. **12**, 890-914.

Bunting, J. and K. Hardy, 1984: Cloud identification and characterization from satellites. *Satellite Sensing of a Cloudy Atmosphere - Observing the Third Planet*. A. Henderson-Sellers, Ed., Taylor and Francis, 203 - 240.

Chavez, P., D. Mackinnon, R. Reynolds, M. Velasco, 2002: Monitoring dust storms and mapping landscape vulnerability to wind erosion using satellite and ground-based digital images. *Arid Lands Newsletter*, **51**, 6-1 - 6-9.

Cooperative Institute for Research in the Atmosphere (CIRA) - Colorado State University (CSU), cited 2005: GOES 3.9μm Tutorial. [Available online at http://www.cira.colostate.edu/ramm/goes39/cover.htm.]

Curry, J. and G. Liu, 1992: Assessment of Aircraft Icing Potential Using Satellite Data. *J. Appl. Meteor.*, **31**, 605-621.

Ellrod, G. P., and S. Bachmaier, 2003: Inter-comparison of GOES and MODIS Imagery in the Analysis of Fog and Stratus. Preprints, *12th Conf on Satellite Meteorology and Oceanography,* Long Beach, CA, Amer. Meteor. Soc., CD-ROM, P1.15.

Encyclopaedia Britannica Premium Service, cited 2005: Electromagnetic Radiation. [Available online at http://www.britannica.com/eb/article?tocId=11360&query=planck-brit&ct=.]

Erickson, S. (1997) Air line pilots. *NASA-LeRC/ CRREL/FAA Inflight Remote Sensing Icing Avoidance Workshop, Summaries and Presentations,* 1-2 April, Ohio Aerospace Institute, Cleveland, Ohio.

Heymsfield, A. and C. Platt, 1984: A parameterization of the particle size spectrum of ice clouds in terms of the ambient temperature of the ice water content. *J. Atmos. Sci.*, **41**, 846-855.

Hobbs, P.V. and A. Deepak, 1981: *Clouds: Their Formation, Optical Properties, and Effects*. Academic Press, 497 pp.

Inoue, T., 1987: A Cloud Type Classification with NOAA-7 split-window measurements. *J. Geophys. Res.*, **92**, 3991-3999.

Kidder, S.Q. and T.H. Vonder Haar, 1995: *Satellite Meteorology: An Introduction*. Academic Press, 466 pp.

King, M., S. Platnick, and J. Reidi, 2005: MODIS Cloud Thermodynamic Phase Flowchart - Products: 06_L2, 08_D3, 08_E3, 08_M3, cited 2005. [Received by personal e-mail on Feb 9, 2005, from Dr. Michael King.]

Lai, Y. and C. Hwang, 1992: *Fuzzy Mathematical Programming - Methods and Applications*. Lecture Notes in Economics and Mathematical Systems, Vol. 394. Springer-Verlag, 301 pp.

Liou, K.N., 1992: *Radiation and Cloud Processes in the Atmosphere*. Oxford Press, 486 pp.

Memmen, S., 2000: *Optimization of MAS and MODIS Polar Ocean Cloud Mask*. M.S. thesis, Dept. of Meteorology, Naval Postgraduate School, 58pp.

MODIS Web - NASA/Goddard Space Flight Center, cited 2005: MODIS Web: About MODIS. [Available online at http://modis.gsfc.nasa.gov/about/specs.html], accessed 16 May 2004.

Nasiri, S., cited 2005: MODIS FILE READERS AND ACCESSORIES, Shaima Nasiri Ph.D. Research Page. [Available online at: http://www.ssec.wisc.edu/~shaima/Matlab/MfilesOther/index.html], accessed 25 February 2005.

National Aeronautics and Space Administration, *Terra: Flagship of the Earth Observing System*; Press Kit, November 1999, Release No. 99-120, NASA/Goddard Space Flight Center, Greenbelt, MD, 1999a.

National Center for Atmospheric Research – Research Application Laboratory, 1994: GOES-based Icing Potential Detection Algorithm. NCAR-RAL.

National Center for Atmospheric Research – Research Application Laboratory, cited 2005: RAL Real-time Weather Data: About NCAR-RAL multi-spectral satellite products [Available online at http://www.rap.ucar.edu/weather/satellite/multispectral.html.], accessed 16 March 2005.

Pavolonis, M. and A. Heidinger, 2004: Daytime Cloud Overlap Detection from AVHRR and VIIRS. *J. Appl. Met.*, **43**, 762-778.

Platnick, S., M. King, S. Ackerman, W. Menzel, B. Baum, J. Riedi, and R. Frey, 2003: The MODIS Cloud Products: Algorithms and Examples from Terra. *IEEE Trans. Geosci. Remote Sens.*, **41**, 459-473.

Pruppacher, H.R., 1995: A New Look at Homogeneous Ice Nucleation in Supercooled Water Drops. *J. Atmos. Sci.*, **52**, 1924-1933.

Rogers, R.R. and M.K. Yau, 1989, *A Short Course in Cloud Physics*, 290 pp.

Ryerson, C.C., 2000: Remote Sensing of In-Flight Icing Conditions. *Monogr., ERDC-CRREL M-00-1*, US Army Corps of Engineers Research and Development Center, Cold Regions Research and Engineering Lab, 76 pp.

Sand, W., W. Cooper, M. Politovich, and D. Veal, 1984: Icing conditions encountered by a research aircraft. *J. Climate Appl. Meteor.*, **23**, 1427-1440.

Strabala, K., S. Ackerman, and W. Menzel, 1994: Cloud Properties Inferred from 8-12μm Data. *J. Appl. Meteor.*, **33**, 212-229.

Thompson, G., R. Bullock, and T. Lee, 1997: Using Satellite Data to Reduce Spatial Extent of Diagnosed Icing. *Wea. Forecasting*, **12**, 185-186.

United States Air Force, 1997: *AF Handbook 11-203*, Volume 1: Weather for Aircrews, AF Publishing Center, 111-121.

USAF, 2004: *AF Manual 15-129*, Air and Space Weather Operations - Processes and Procedures, AF Publishing Center, 75-76.

Wieman, S., 1990: *Multiple Channel Satellite Analysis of Cirrus*. M.S. thesis, Dept. of Meteorology, Naval Postgraduate School, 60pp.

Welch, R., S. Cox, J. Davis, 1980: Solar Radiation and Clouds. *Meteorol. Monogr.*, **17**, 96 pp.

Young, S., C. Platt, R. Austin, and G. Patterson, 2000: Optical Properties and Phase of Some Midlatitude, Midlevel Clouds in ECLIPS. *J. Appl. Meteor.*, **39**, 135-152.

THIS PAGE INTENTIONALLY LEFT BLANK

INITIAL DISTRIBUTION LIST

1. Defense Technical Information Center
   Ft. Belvoir, Virginia

2. Dudley Knox Library
   Naval Postgraduate School
   Monterey, California

3. Thomas Lee
   Naval Research Laboratory
   Monterey, California

4. Leanne Siedlarz
   Air Force Combat Weather Center
   Hurlburt Field, Florida

5. Joe Turk
   Naval Research Laboratory
   Monterey, California

6. Steve Miller
   Naval Research Laboratory
   Monterey, California

7. Greg Thompson
   National Center for Atmospheric Research
   Boulder, Colorado

8. Julie Haggerty
   National Center for Atmospheric Research
   Boulder, Colorado

9. Marcia Politovich
   National Center for Atmospheric Research
   Boulder, Colorado

10. Jothiram Vivekanandan
    National Center for Atmospheric Research
    Boulder, Colorado

11. Barbara Brown
    National Center for Atmospheric Research
    Boulder, Colorado

12. Shaima Nasiri
Cooperative Inst. for Meteorological Satellite Studies
Madison, Wisconsin